A-TRAIN ANALYSIS OF LOW CLOUD STRUCTURE, ORGANIZATION, AND WARM RAIN

A Dissertation

by

KEVIN M. SMALLEY

Submitted to the Office of Graduate and Professional Studies of
Texas A&M University
in partial fulfillment of the requirements for the degree of

DOCTOR OF PHILOSOPHY

Chair of Committee,	Anita D. Rapp
Committee Members,	Andrew Dessler
	Christopher Nowotarski
	Steven Dimarco
Head of Department,	Ramalingam Saravanan

December 2020

Major Subject: Atmospheric Sciences

ABSTRACT

Low-cloud cover continues to be a dominant source of uncertainty in climate models and past observational-based studies to help constrain this uncertainty have typically been limited in both space and time or by measurements sensitivities. To address this, satellite observations with sensitivities to both cloud and rain are used to analyze the influence of thermodynamics, the environment, and organization on precipitating low clouds. This provides an avenue to sample low clouds both globally and over a longer time period. This analysis shows that both the likelihood of shallow cumulus rainfall and the efficiency of rain production increase as cloud size, environmental moisture, and sea-surface temperature increase. While aerosols hamper rainfall production and require larger clouds than in a clean environment for a similar rain likelihood, they have little influence on rain efficiency once rain begins. This implies that cloud size distributions may be important for improving the simulation of warm rain in climate models. Focusing on the influence of mesoscale organization in raining cells across the transition of stratocumulus to shallow cumulus over the southeast Pacific, analysis shows that cloud fraction is generally lower over the transition region when patches of raining stratocumulus are larger. We attribute this to larger raining patches being more likely to produce more intense rainfall, which may result in stronger cold pools that could drive transitions. This implies that mesoscale organization in precipitation may need to be better captured within climate models to better capture low cloud fraction transitions over the sub-tropical oceans.

DEDICATION

This dissertation is dedicated to my family who have supported my dreams in everyway possible for the first thirty years of my life.

ACKNOWLEDGEMENTS

I would like to thank my advisor, Dr. Anita Rapp for giving me this wonderful opportunity, always helping me along the way, and all the advice that she has given me. Her sheer understanding of shallow cumulus, precipitation, how to examine them using satellites, and passion for the subject inspire me every day to be better. Finally, if it was not for her, I would not be in the position I'm in today. I would also like to thank my committee, Dr. Andrew Dessler, Dr. Chris Nowotarski, and Dr. Steven Dimarco for critiquing my work.

A big thanks goes out to my group members and friends here at A&M. It would have been impossible to make it through the difficult classes without you. In particular, thank you Kyle Wodzicki for helping me with code, answering any stupid question that I possibly had, and critiquing my work.

Additionally, I thank my Masters advisor Dr. Andrew Dessler for giving me the my initial opportunity at Texas A&M University to conduct my graduate studies. Specifically, thanks for the life advice, help with coding, and critiques of my writing and presentation style that you gave along the way.

Finally, I would not be here today if it were not for my family. Thank you for always being there for me.

CONTRIBUTORS AND FUNDING SOURCES

Contributors

This work was supported by a dissertation committee consisting of Professor Anita Rapp and Andrew Dessler and Chris Nowotarski of the Department of Atmospheric Sciences and Professor(s) Steven Dimarco of the Department of Oceanography.

The data analyzed for Chapters 1,2, and 3 was acquired from the CloudSat Data Processing Center and can be accessed at `http://www.cloudsat.cira.colostate.edu`. The analyses depicted in Chapters 1,2, and 3 were conducted by Kevin Smalley, and the analyses depicted in Chapters 1 and 2 were published in 2020.

All other work conducted for this dissertation was completed by the student independently.

Funding Sources

Graduate study was supported by NASA grant NNX14AO72G.

NOMENCLATURE

AOD	aerosol optical depth
A-Train	Afternoon Constellation
CCN	cloud condensation nuclei
CPR	Cloud Profiling Radar
W_C	cloud water path
extent	along-track extent
GPM	Global Precipitation Measurements
ITCZ	Intertropical Convergence Zone
LES	large-eddy simulation
LTS	Lower-Tropospheric Stability
MAD	mean absolute deviation
MODIS	Moderate Resolution Imaging Spectroradiometer
RH	relative humidity
W_P	precipitation water path
spacing	nearest-neighbor distance between raining patches
ITCZ	South Pacific Convergence Zone
SST	sea-surface temperature
TRMM	Tropical Rainfall Measuring Mission
VGZ	vertical reflectivity gradient

VGZ_{CP}	VGZ at cloud object center pixel
VGZ_{CP}	VGZ at cloud object edge pixel
VOCALS	VAMOS Ocean-Cloud-Atmosphere-Land Study
WRE	warm rain efficiency

TABLE OF CONTENTS

Page

LIST OF FIGURES

FIGURE Page

LIST OF TABLES

TABLE Page

1. INTRODUCTION

Low cloud cover continues to be a dominant source of uncertainty in projecting future climate (e.g. Bony and Dufresne, 2005; Dufresne and Bony, 2008; Vial et al., 2013) with variations in shallow cumulus distributions explaining much of the differences in climate model-derived estimates of climate sensitivity (e.g. Wyant et al., 2006; Medeiros and Stevens, 2011; Nam et al., 2012). This stems from climate models' inability to simulate shallow cumulus and their impacts, due in part to the low temporal and spatial resolution of these models (e.g. Stevens et al., 2002), as well as the fact that small-scale processes important for cloud development, including turbulence and convection, must be parameterized (e.g. Tiedtke, 1989; Zhang and McFarlane, 1995; Bretherton et al., 2004; Park and Bretherton, 2009). For instance, Nam et al. (2012) found climate models produce shallow clouds that are too reflective due to poorly simulating environmental impacts on the vertical structure of low clouds. They hypothesize that model precipitation efficiencies are too weak and could play a role in the overestimation of model shortwave cloud radiative effects. Before parameterizations can be improved, a better physical understanding of these cloud processes and their influence on warm rain production is needed. The overall goal of this research is to use satellite observations to better understand the relationship between shallow cumulus cloud structure, organization, and warm rain production/likelihood.

Observations show that 20% - 40% of marine shallow cumulus produce rainfall, although usually light with intensities < 1 mm day-1 (Nuijens et al., 2017). For warm rain to occur, shallow cumulus must have sufficient updraft strength, droplet size, and duration for the collision-coalescence process to result in rainfall (Wood et al., 2009). Factors that may influence warm rain production include the thermodynamic environment (e.g. Heus and Jonker, 2008; Schmeissner et al., 2015), entrainment (e.g. Korolev et al., 2016), aerosols (e.g. Dagan et al., 2016, 2018), and convective organization (e.g. Zuidema et al., 2012).

Entrainment of dry air into a cloud can have competing effects on potential rainfall. It may enhance the potential of warm rain by broadening the drop size distribution (e.g. Beard and Ochs,

1993; Derksen et al., 2009), and mixing a few large droplets that could initiate collision-coalescence (Cooper et al., 2013). However, mixing may introduce new aerosols into a cloud, potentially increasing the number of cloud condensation nuclei which would generally suppress warm rain production by increasing the number of small droplets (e.g. Derksen et al., 2009).

The evaporative cooling at cloud edges induced by entraining ambient air may also have competing effects on warm rain production. First, the cooling at a cloud's lateral edges creates a humid barrier between the cloud and the environment (e.g. Heus and Jonker, 2008). Schmeissner et al. (2015) showed that this barrier helps protect the cloud core from the negative impacts of entrainment on cloud microphysics, reducing negative impacts on warm rain production. However, mixing dry air into a cloud may also cool the cloud core, resulting in the in-cloud air becoming less buoyant. As a result, weakened updrafts (Hernandez-Deckers and Sherwood, 2018) within a cloud do not transport as much humid air to higher altitudes within the cloud inhibiting warm rain production.

Several studies have used cloud models or limited field campaign observations to analyze the impact of entrainment on shallow cumulus and subsequently precipitation. Lu et al. (2012) used field campaign data to find that entrainment rates decrease as the distance from cloud core increases, which implies that the impact of entrainment on precipitation may decrease as shallow cumulus increases in size. Using a large-eddy simulation (LES), Heus and Jonker (2008) showed negative buoyancy is most likely to occur within a cloud's core for the smallest shallow cumulus clouds due to mixing at cloud edges. As a result, cloud cores simulated by LES models and identified from limited field campaign observations are wider for shallow cumulus clouds (e.g. Kirshbaum and Grant, 2012; Watson et al., 2015) and have larger liquid water content. Similarly, Tian and Kuang (2016) used an LES to show the influence of entrainment on cloud updraft velocity decreases as clouds become larger.

Other LES studies have found larger shallow cumulus clouds are more likely to rain because their updrafts are more protected from entrainment (Kirshbaum and Grant, 2012; JÃ¤hn et al., 2016). Watson et al. (2015) referred to this phenomenon as a "cloud size mechanism." Burnet and

Brenguier (2010) compared the life cycle of three different oceanic clouds and found one cloud larger and with a higher liquid water content than the other two. They conclude that the smaller clouds' updraft cores were most affected by mixing, which resulted in those clouds collapsing on themselves before they could grow tall enough to produce precipitation. The larger cloud was able to sustain its updraft despite the influence of entrainment, allowing it to grow tall enough and sustain a high enough liquid water content to produce precipitation. One would also expect that a drier environment would negatively impact a cloudy updraft more than a humid environment, because dry air would dilute cloudy air more (Li et al., 2014; Lamer et al., 2015), stabilizing the updraft. LES results from Hernandez-Deckers and Sherwood (2018) recently found that buoyancy within a cloud's core decreases faster in a drier environment than a humid environment. *Following these prior modeling studies, this research uses global satellite observations to test the hypothesis that larger marine shallow cumulus and/or shallow cumulus occurring in a wetter environment are more likely to produce warm rain.*

In an ideal shallow cumulus cloud, liquid water content increases adiabatically from cloud-base to top. Unfortunately, liquid water content is generally only 50% - 80% of the adiabatic values due to entrainment (Gerber et al., 2008). Evaporation induced by cloud-edge mixing not only impacts shallow cumulus updraft strength, but also the number and size of droplets within a cloud (Lu et al., 2012), with increased evaporation potentially reducing the number and size of available droplets. Using an LES, Moser and Lasher-Trapp (2017) found the influence of entrainment decreases from cloud-edge to center of individual shallow cumulus, resulting in increased liquid water content at cloud center because fewer droplets will potentially evaporate away at cloud-center. This implies that the collision-coalescence process is more efficient at cloud center because there is more cloud water available to be collected by large droplets. At cloud edge, there are not only fewer droplets but also smaller droplets, potentially reducing collision-coalescence efficiencies there. Given LES results showing that shallow cumulus updrafts are more protected as clouds grow in size and/or environmental moisture increases, the number of cloud droplets and large droplets at cloud center should be largest within the largest shallow cumulus and/or those that develop in the most humid

environments. While not as important as organization (Minor et al., 2011) or cloud size (Jiang and Feingold, 2006), it is also widely understood that aerosol concentrations act to suppress warm rain production (Albrecht, 1989) by increasing the cloud droplet concentration but reducing cloud droplet sizes (Squires, 1958). This should reduce the number of large droplets able to fall at sufficient terminal velocities to initiate collision-coalescence and continue growing to large enough sizes to fall out as rain (e.g. Twomey, 1974), which would reduce warm rain efficiency (WRE). This implies that changes in cloud size, environmental moisture, and aerosol concentration can influence the amount of cloud water converted to rain water, which is a measure of WRE. *This study uses global satellite observations to test the hypothesis that WRE is higher in larger shallow cumulus and is modulated by environmental moisture and aerosol loading.*

The relationship between warm rain, cloud properties, and the environment discussed above are primarily thermodynamic and microphysical. Prior literature found outflow induced by precipitation may also promote stratocumulus breakup (e.g. Stevens et al., 1998). Modeling studies have shown the evaporation of drizzle induces cold pools that help break apart closed-cell stratocumulus into open-cell shallow cumulus (Feingold et al., 2010). Using aircraft observations, Terai and Wood (2013) found that these cold pools typically range in size from 10-100 km. Once open pockets of organized shallow cumulus appear, colliding cold pools may initiate new convection that is more likely to both rain and produce more intense precipitation and further break apart the stratocumulus. Using a model, Yamaguchi and Feingold (2015) found the distance between raining patches important in determining if a transition to open-cell shallow cumulus will occur. They showed stratocumulus are more likely to break apart if raining patches are located closer together because the resulting cold pools can easily interact. Yamaguchi and Feingold (2015) concluded that rain rate alone is insufficient in driving transitions and that raining patches must be both large enough and producing heavy enough rain rates for transitions to occur if the distance between raining patches is large. Rapp (2016) used observations to show cloud fraction changes faster around raining clouds than non-raining clouds within the southeast Pacific transition region. This suggests that these raining patches are close enough together, large enough, and producing a sufficient rain

rate to allow their cold pools to interact, promoting stratocumulus breakup (Feingold et al., 2010). *Based on these studies, this research hypothesizes that raining cell spacing minima, raining patch size maxima, or rain intensity maxima are present across a stratocumulus to shallow cumulus cloud fraction transition over the southeast Pacific.*

The prior literature presented here depends primarily on a few clouds during field campaign observations (Rauber et al., 2007; Zhou et al., 2015), or cloud models (e.g. Nuijens et al., 2017; Dagan et al., 2018) to analyze the relationship between cloud microphysics, macrophysics, and organization to rainfall and the environment. This limits analyses of low clouds characteristics to regional studies over short time frames. While these case and model studies provide insight into the physical processes, it is unclear how well they represent the shallow cumulus clouds observed globally. Satellites can observe a large enough sample size of low clouds over different regions and during different stages of their lifecycle to gain a more holistic view of this relationship. Previous studies using satellite observations have utilized the Tropical Rainfall Measuring Mission (TRMM) and/or the Global Precipitation Measurements (GPM) to investigate warm rain (e.g. Lau and Wu, 2003; Liu and Zipser, 2009); unfortunately, TRMM and GPM are precipitation radars operating at the Ku- and Ka-bands not capable of observing the non-raining portions of clouds or light precipitation. This research uses the higher sensitivity CloudSat and CALIPSO observations to determine the relationship between cloud size and rain likelihood, cloud size and WRE, and cloud organization and rain intensity.

The overall goal of this research is to use satellite observations to better understand the relationship between shallow cumulus cloud structure, organization, and warm rain production/likelihood. To address this, CloudSat, CALIPSO, and Aqua satellite observations will be used to analyze the microphysical, macrophysical, and organizational characteristics of raining shallow cumulus globally, and the three *hypotheses* identified above will be discussed in the next three chapters. Note that these satellites are part of the Afternoon Constellation (A-Train) which contain a set of sun-synchronous polar orbiting satellites that observe clouds, aerosols, and other atmospheric conditions (Schoeberl, 2002).

The rest of this dissertation has been organized with the following 3 chapters presented as separate papers with their own introduction, data and methodology, results, and conclusions sections. Chapter 2 addresses the first hypothesis and has been published in the Journal of Applied Meteorology and Climatology. Chapter 3 addresses the second hypothesis and is in review at Atmospheric Chemistry and Physics. Chapter 4 addresses the third hypothesis and is currently in preparation for submission. Finally, Chapter 5 briefly ties all three hypotheses together and gives some overall implications.

2. THE ROLE OF CLOUD SIZE AND ENVIRONMENTAL MOISTURE IN SHALLOW CUMULUS PRECIPITATION*

2.1 Abstract

Cloud models show that precipitation is more likely to occur in larger shallow clouds and/or in an environment with more moisture, in part due to decreasing the impacts of entrainment mixing on the updrafts. However, the role of cloud size in shallow cloud precipitation onset from global satellite observations has mostly been examined with precipitation proxies from imagers and not been systematically examined in active sensors primarily due to sensitivity limitations of previous spaceborne active instruments. Here we use the more sensitive CloudSat/CALIPSO observations to identify and characterize the properties of individual contiguous shallow cumulus cloud objects. The objects are conditionally sampled by cloud top height to determine the changes in precipitation likelihood with increasing cloud size and column water vapor. On average, raining shallow cumulus clouds are typically twice as tall and have a greater horizontal extent than their non-raining counterparts. Results show that for a fixed cloud top height, the likelihood of precipitation increases with increasing cloud size, and generally follows a double power-law distribution. This suggests that the smallest cloud objects being able to grow freely within the boundary layer, but the largest cloud objects are limited by environmental moisture. This is supported by our results showing, for a fixed cloud top height and cloud size, the precipitation likelihood also increases as environmental moisture increases. These results are consistent with the hypothesis that larger clouds occurring in a wetter environment may be better able to protect their updrafts from entrainment effects, increasing their chances of raining.

*Reprinted with permission from "The role of cloud size and environmental moisture in shallow cumulus precipitation" by Kevin M. Smalley and Anita D. Rapp, 2020. *Journal of Applied Meteorology and Climatology*, 59, 535–550,

2.2 Introduction

Shallow cumulus clouds occur over all ocean basins; however, they are most prominent over the trade wind regions of the central ocean basins (Norris, 1998; Eastman et al., 2011). These clouds impact both the atmospheric radiation budget (e.g., Zeng, 2018), as well as the precipitation budget. As noted by Nuijens et al. (2017), observations reveal 20 - 40% of oceanic shallow cumulus clouds produce rain, although, warm rain is usually light, with typical intensities less than 1 mm day^{-1}.

Unfortunately, climate models struggle to accurately simulate shallow cumulus clouds and their impacts, primarily resulting from coarse model temporal and spatial resolution (e.g., Stevens et al., 2002). The small-scale processes important for the development of these clouds, including turbulence and convection, must be parameterized to adequately represent the impact of shallow cumulus clouds on climate (e.g. Tiedtke, 1989; Zhang and McFarlane, 1995; Bretherton et al., 2004; Park and Bretherton, 2009). For instance, Nam et al. (2012) found that climate models tend to underestimate low cloud cover, but produce shallow clouds that are too reflective, as a result of poorly simulating the impact of the environment on the vertical structure of low clouds. They hypothesize that precipitation efficiencies that are too weak could play a role in the overestimation of model shortwave cloud radiative effects.

For warm rain to occur, shallow cumulus clouds must have sufficient updraft strength, liquid water, and duration for the collision-coalescence process to produce rain droplets (e.g., Wood et al., 2009). Additionally, the drop size distribution is an important factor that influences warm rain production. Factors that may impact the drop size distribution include aerosols (e.g., Dagan et al., 2016; Jung et al., 2016b,a), convective organization (e.g. Zuidema et al., 2012) and entrainment (e.g., Korolev et al., 2016; Pinsky et al., 2016b,a). While entrainment can enhance the potential of warm rain production by broadening the drop size distribution (e.g., Beard and Ochs, 1993; Derksen et al., 2009), mixing may also introduce new particles into a cloud that could act as cloud condensation nuclei (CCN). While the introduction of a few large particles may help warm rain production (Cooper et al., 2013), overall an increase in CCN would suppress warm rain production by increasing the cloud droplet concentration (e.g., Derksen et al., 2009). However, Minor et al.

(2011) analyzed the relationship between warm rain production and giant CCN concentration; they found that giant CCN concentrations are not as important as the spatial organization of shallow convection to warm rain production.

Entrainment mixing and the resulting evaporative cooling may also have competing effects at cloud edges. First, the cooling at a cloud's lateral edges creates a humid barrier between the cloud and the environment (e.g., Heus and Jonker, 2008; Heus et al., 2009). Schmeissner et al. (2015) showed that this barrier helps protect the cloud core from the negative impacts of entrainment on cloud microphysics and reduces the suppression of warm rain production. However, the mixing of dry air into a cloud may also cool the cloud core resulting in the in-cloud air becoming less buoyant. As a result, weakened updrafts (e.g. Hernandez-Deckers and Sherwood, 2018) within a cloud do not transport as much humid air to higher levels of the cloud inhibiting warm rain production.

Several studies have used cloud models to analyze the impact of entrainment on a cloud core and subsequent precipitation. Lu et al. (2012) used field campaign data to find that entrainment rates decrease as the distance from cloud core increases, which implies that the impact of entrainment on precipitation may decrease as shallow cumulus clouds increase in size (e.g., Jiang and Feingold, 2006). Using a LES, Heus and Jonker (2008) showed negative buoyancy is most likely to occur within a cloud's core for the smallest shallow cumulus clouds due to mixing at cloud edges. As a result, cloud cores simulated by LES models and identified from limited field campaign observations are wider for larger shallow cumulus clouds (Kirshbaum and Grant, 2012; Watson et al., 2015) and have a larger liquid water content. Similarly, Tian and Kuang (2016) found the influence of entrainment on cloud updraft velocity decreases as clouds become larger in an LES.

Other LES studies have found that larger shallow cumulus clouds are more likely to rain because their updrafts are more protected from entrainment (e.g., Kirshbaum and Grant, 2012; JÃ¤hn et al., 2016). Watson et al. (2015) referred to this phenomenon as a "cloud size mechanism". Burnet and Brenguier (2010) compared the life cycle of three different oceanic clouds and found one cloud larger and with a higher liquid water content than the other two. They conclude that the smaller clouds' updraft cores were most affected by mixing which resulted in those clouds collapsing on

themselves before they could grow tall enough to produce precipitation. The larger cloud was able to sustain its updraft in spite of the influence of entrainment, allowing it to grow tall enough and sustain a high enough liquid water content to produce precipitation. Similarly, LES results from Jiang et al. (2010) showed that as clouds become larger, they are more likely to produce precipitation, regardless of aerosol loading.

It is well understood that developing convection requires a moist environment. One would expect that a dryer environment would impact a cloudy updraft more than humid environmental air because dry environmental air would dilute cloudy air more (e.g., Li et al., 2014; Lamer et al., 2015), and stabilize the updraft. LES results from Hernandez-Deckers and Sherwood (2018) recently found that buoyancy within a cloud core decreases faster for drier environments than for a more humid environment. Thus, it can be expected that a larger shallow cumulus cloud occurring in a moister environment has a higher likelihood of producing warm rain.

Most of the aforementioned studies are based on field campaign (e.g., Rauber et al., 2007; Zhou et al., 2015) or LES models (e.g., Nuijens et al., 2017; Dagan et al., 2018), which are limited to a small spatial domain for a short period. This limits the conditions over which clouds can be sampled and the effects of cloud size on precipitation can be examined. However, satellite observations provide a large sample of shallow cumulus clouds both occurring over different regions and in different stages of their life cycle. Previous satellite studies have used TRMM and/or Global Precipitation Measurement observations to investigate warm rain (e.g., Lau and Wu, 2003; Liu and Zipser, 2009), however these precipitation radars that operate at Ku- and Ka-bands are not sensitive to the cloud-sized particles in the non-raining portion of a cloud and, as a result, cannot be used to analyze cloud size. While direct measurements of the entrainment impact on cloud updrafts are not possible, the higher sensitivity to clouds and light precipitation of CloudSat and CALIPSO instruments can be used to examine the relationship between cloud size and rain likelihood. Over a long enough time period, satellite observations provide a large cloud population to constrain this relationship and infer the likelihood of a cloud size mechanism and the role of the local moisture environment. We expect that larger clouds will have a higher likelihood of producing rain and the

relationship between cloud size and rain likelihood is modulated by the surrounding moisture environment. To test this, we identify individual warm shallow cumulus clouds for 4.5 years of global CloudSat observations and analyze their characteristics to investigate the relationship between rain likelihood and cloud size in various environments.

2.3 Data and Methods

CloudSat and CALIPSO satellite data are used to identify individual contiguous shallow cumulus cloud objects. The CloudSat and CALIPSO missions both carry instruments capable of identifying the vertical distribution of cloud particles. Cloud Profiling Radar (CPR) (Tanelli et al., 2008) on CloudSat is a near nadir pointing 94-GHz radar that measures backscattered radiation from cloud particles and has a 1.7 x 1.4 km horizontal resolution and 480 m pulse length oversampled by a factor of 2 giving 240 m vertical resolution. The CPR has two main limitations (Tanelli et al., 2008): attenuation in intense precipitation and ground clutter in the lowest three bins.
CALIPSO carries a lidar that measures backscatter from both cloud and aerosol particles. It is a non-scanning instrument, and in the lowest 8 km of the atmosphere, it is highly sensitive to small particles. It also has a high resolution of 333 m horizontally and 60 m vertically (Anselmo et al., 2007). CALIPSO also allows us to see cloudy pixels in the lowest part of the atmosphere otherwise obscured by ground clutter or that are too small to detect using CPR.

To identify cloud objects we use 2B-GEOPROF-LIDAR (Mace and Zhang, 2014) layer base and top height variables. This product utilizes both CPR and lidar data to identify cloudy pixels, making it ideal for identifying individual cloud objects. A binary mask is then applied with all pixels having a cloud fraction greater than zero assigned a value of one. At least two cloudy pixels must be touching either vertically or horizontally for cloudy pixels to be considered contiguous. Additionally, a single cloudy bin that is not touching any other cloudy pixels is not considered contiguous and removed from this analysis. Each contiguous cloudy region is then stored as individual cloud objects and the median cloud-top height and along-track extent (extent) for each cloud object. We only include ocean measurements and use the Navigation Land Sea Flag from 2B-GEOPROF

(Marchand et al., 2008) to remove cloud objects occurring over land.

For this analysis, warm cloud objects are defined as any cloud object with cloud-top heights entirely below the freezing level designated in the 2C-PRECIP-COLUMN (Haynes et al., 2009) product. Figure 2.1 shows a sample cloud object distribution for one orbit seen by CloudSat and CALIPSO.

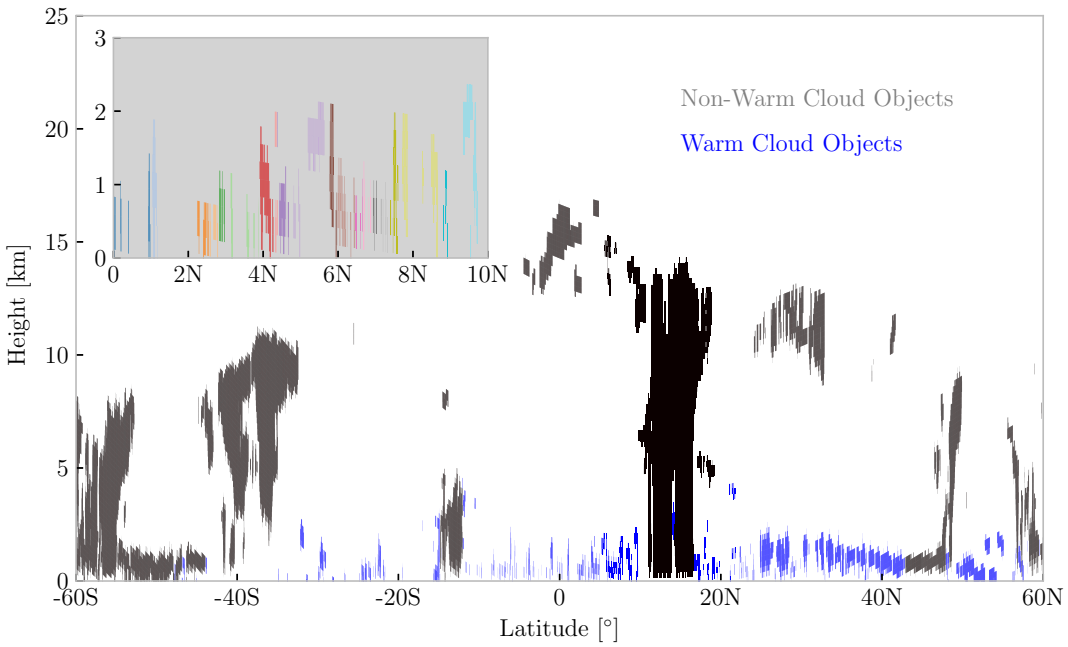

Figure 2.1: A snapshot of the clouds along CloudSat's orbit on 12 August 2006 over the Pacific Ocean . The zoomed in region more clearly shows a subset of color-coded individual warm cloud objects. Reprinted from Smalley and Rapp (2020b).

Over the ocean, there are two primary warm cloud types: stratocumulus and shallow cumulus. Both cloud types generally form under different environmental conditions. Studies have found that shallow cumulus tends to develop in regions with a more unstable boundary layer than stratocumulus (e.g., Wood and Bretherton, 2004a). We use ECMWF-AUX (P. Partain, Cloudsat ECMWF-AUX Auxiliary Data Process Description and Interface Control Document, 2007, `http://www.`

cloudsat.cira.colostate.edu/dataICDlist.php?go=list&path=/ECMWF-AUX) matched vertical temperature profiles to identify regions of weaker stability associated with shallow cumulus cloud objects. Lower-Tropospheric Stability (LTS), $LTS = \theta_{700hPa} - \theta_{surface}$ (e.g., Slingo, 2007; Klein and Hartmann, 1993), is often used to quantify the strength of the stable boundary layer and has been widely used by the scientific community (e.g., Nam et al., 2012; Medeiros et al., 2014) to separate stratocumulus and shallow cumulus cloud regimes. To accomplish this, the maximum LTS value is taken for each warm cloud object. First established by Klein and Hartmann (1993), we use an LTS threshold of 18.55 K to classify shallow cumulus cloud objects.

Figure 2.2 shows a violin plot for both the shallow cumulus and stratocumulus cloud object extent distributions, determined using the threshold LTS. Note, the white dots represent the median extent, thick black regions represent the interquartile region, and shaded regions represent the proportion of cloud objects at a given extent. We see a noticeable separation between both distributions, with the stratocumulus cloud object subset containing larger cloud objects than the shallow cumulus cloud object subset. This implies that our environment separation scheme is generally correctly identifying conditions associated with shallow cumulus cloud objects. Unfortunately, our environmental separation scheme does not remove all large warm cloud objects. To remove these objects that are unlikely to be shallow cumulus, we remove warm cloud objects with a maximum extent exceeding the 95^{th} percentile (shown in Figure 2.2) of shallow cumulus cloud objects identified by the environmental separation scheme to finalize our shallow cumulus cloud object dataset. This results in the shallow cumulus cloud objects identified here having a maximum extent of 29.20 km.

Given the main goal of analyzing the impact of cloud extent and environmental moisture on the likelihood of rain, the precipitation flag product from 2C-PRECIP-COLUMN is used to separate raining and non-raining clouds. To identify raining shallow cumulus cloud objects, we tested three different combinations of flags (rain certain, certain and probable, and certain, probable, and possible) to determine if rain is occurring within a CloudSat pixel within any shallow cumulus cloud object. All three flags are used to identify raining shallow cumulus cloud objects, with any cloud object containing at least one raining pixel being considered a raining cloud object. However, the

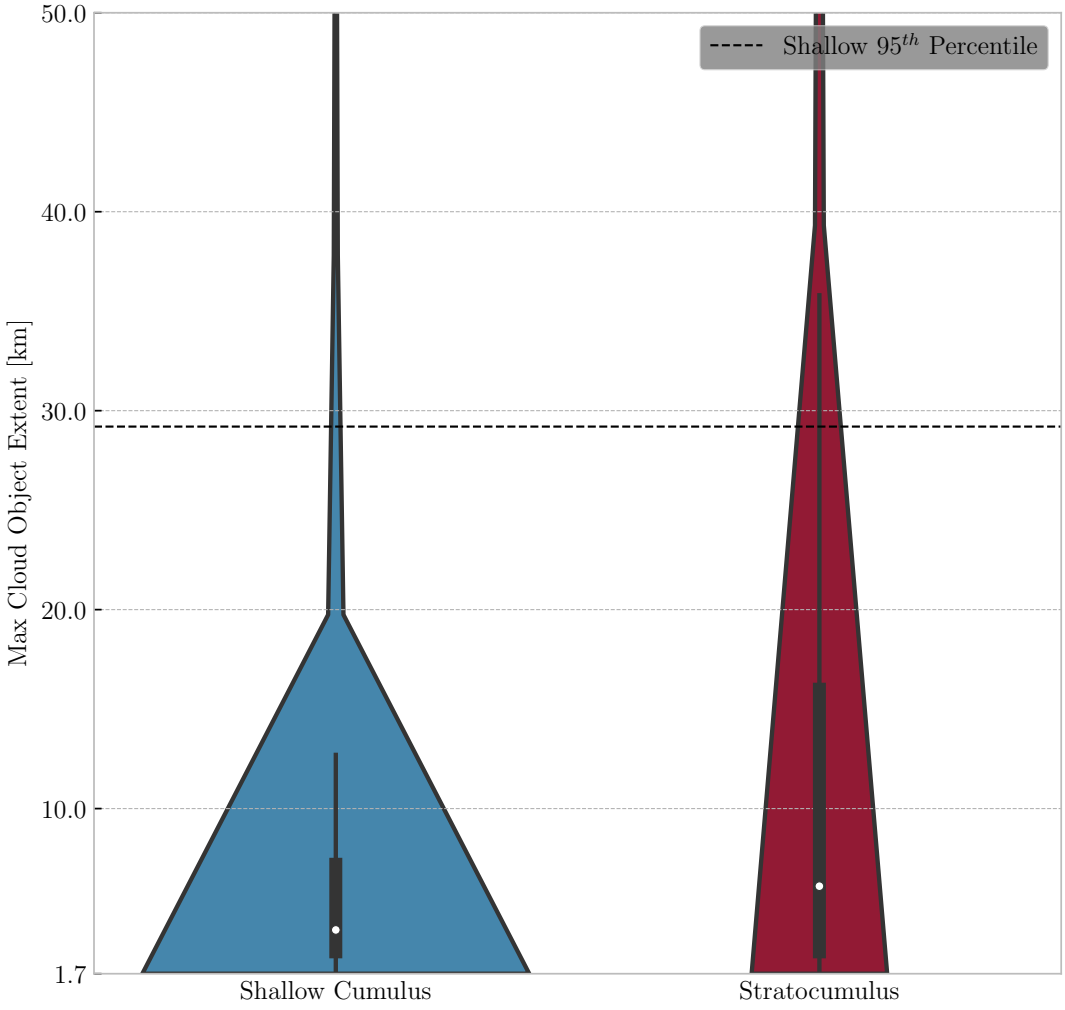

Figure 2.2: Shallow cumulus and stratocumulus cloud object along-track extent defined using a lower-tropospheric stability threshold of 18.55 K are presented as boxplots, indicating the median (white dots) and quartiles (thick black areas) with whiskers (thin black areas reaching up to 1.5 times the interquartile range. The violin plot outlines illustrate kernel probability density, i.e. the width of the shaded area represents the proportion of the data located at that cloud object extent.

overall findings of this study are similar no matter the combination of rain flags used.

Both this analysis (see Figure 2.3) and others (e.g., Wood and Field, 2011; Medeiros and Nuijens, 2016) show most warm shallow cumulus clouds occur within the subtropical and tropical

ocean basins. For this reason, we further constrain our sample region to the global ocean basins confined within 60 S and 60 N. Measurements are also restricted to between August 2006 and December 2010 when both instruments recorded observations during both the day and nighttime satellite overpasses. To classify environmental moisture, we use the average RH below 3 km derived from ECMWF-AUX. Both cloud-top height and RH are used as control variables when determining the relationship between rain likelihood and cloud extent.

2.4 Results

We first analyze the spatial distribution of raining and non-raining shallow cumulus cloud objects by binning them to a 2.5°x2.5° global grid. A similar binning method is applied to cloud-top height and cloud extent, and these results are discussed in detail below.

Figure 2.3a depicts the distribution of shallow cumulus objects over the global ocean basins and shows that a majority of these cloud objects are found within the trade regions of the central ocean basins, in particular, the Intertropical Convergence Zone (ITCZ), South Pacific Convergence Zone (ITCZ), and the west Pacific warm pool. Previous studies have found similar results using different satellite (Wood and Field, 2011) and field campaign (Medeiros and Nuijens, 2016) observations.

Figure 2.3b shows the spatial distribution of raining shallow cumulus cloud objects over the global ocean basins. Similar to the distribution of all shallow cumulus cloud objects, most raining shallow cumulus cloud objects occur over the trade regions of the central ocean. In these regions, shallow convection tends to organize at cold pool boundaries (e.g., Seifert and Heus, 2013) into cloud sheets, clusters, and arcs (e.g., Warner et al., 1979; Rauber et al., 2007), and produce rainfall (e.g., Lau and Wu, 2003; Schumacher and Houze, 2003).

Figure 2.3c shows the likelihood of rain occurrence of shallow cumulus cloud objects within a given grid box. As implied in Figure 2.3b, these results explicitly show a relatively small fraction of shallow cumulus cloud objects identified by CloudSat produce rain with the largest fraction of raining shallow cumulus cloud objects occurring over the central ocean basins, especially in large-scale convergence zones. Over this area, at most 15% of all shallow cumulus cloud objects within

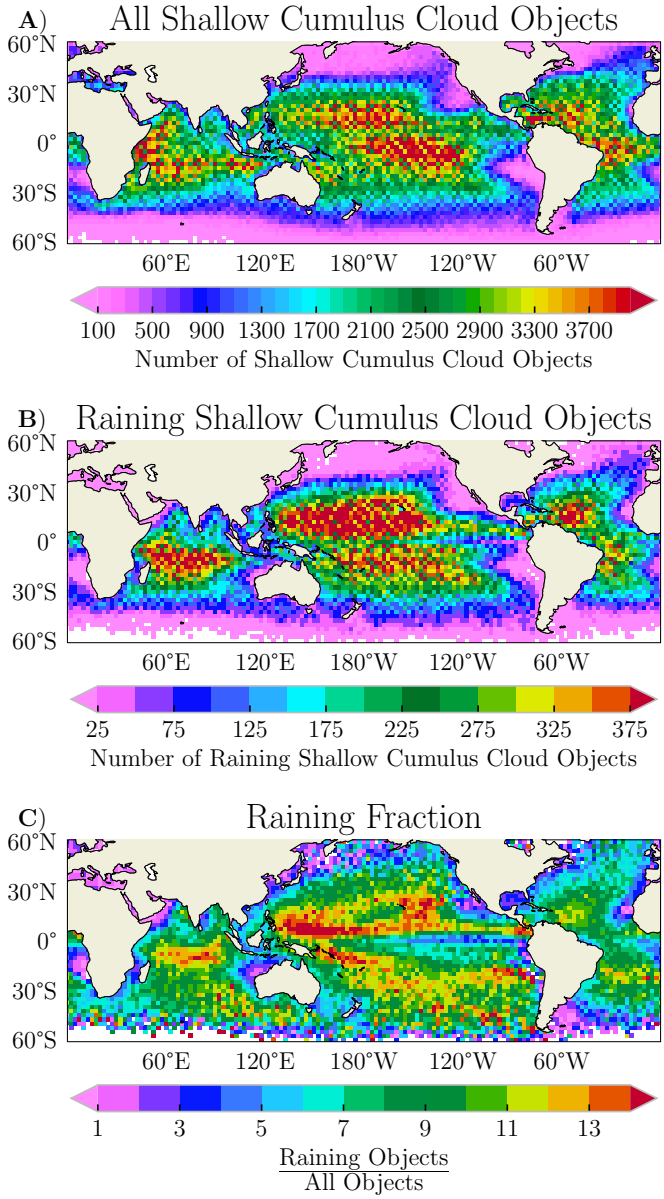

Figure 2.3: The spatial distribution in number of shallow cumulus cloud objects for both (A) all and (B) raining shallow cumulus cloud objects gridded to a 2.5° x 2.5° spatial grid. Grid boxes containing no data are white. Also shown is the (C) fraction of raining shallow cumulus cloud objects occurring within any grid box. Reprinted from Smalley and Rapp (2020b).

a given grid box produce rain, while only 5-10% of shallow cumulus cloud objects in all other regions produce rainfall. Nuijens et al. (2017) found similar results, showing only 5-10% of warm clouds produce rainfall globally. However, it should be noted that CloudSat only takes a snapshot

of shallow convection at two times of the day. As a result, we may be oversampling raining shallow cumulus cloud objects if the two times of day that happen to coincide with CloudSat's orbit are also peaks in the diurnal cycle. However, this is not likely to be a large problem given the diurnal cycle in warm rain over oceans is weak (Liu and Zipser, 2009).

It has long been established that shallow cumulus producing rainfall typically have top heights of 2 km or more (e.g., Short and Nakamura, 2000). This study analyzes the impact of cloud-top height on the rain likelihood of shallow cumulus cloud objects using both the univariate and spatial distributions of all, raining, and non-raining shallow cumulus cloud objects. Table 2.1 shows shallow cumulus cloud object statistics for all, raining, and non-raining cloud objects respectively. To assume a normal univariate distribution, skewness values between -2 and +2 are considered acceptable (George and Mallery, 2009). This criterion is used to analyze the overall characteristics of each distribution. In this paper, we use the median and mean absolute deviation (MAD) to describe the data, however MAD and standard deviation is similar in cases where the data can be assumed to be normal.

Table 2.1: Shallow Cumulus Cloud Object Cloud-Top Statistics. Reprinted from Smalley and Rapp (2020b).

	All	**Raining**	**Non-Raining**
Mean (km)	1.26	2.07	1.19
Median (km)	1.06	1.96	1.01
STD (km)	0.71	0.68	0.67
MAD (km)	0.49	0.63	0.42
Skewness	1.87	0.78	2.23
Num. Samples	$7.89e^6$	$6.65e^5$	$7.23e^6$

Figure 2.4a shows the cloud-top height univariate distribution for all shallow cumulus cloud objects peaks at approximately 750 m and has a median shallow cumulus cloud object-top height of 1.26 ± 0.49 km (see Table 2.1). Similar to our results, Rauber et al. (2007) found shallow cumulus cloud-top heights are generally below 1 km using a combination of radar, aircraft, ground, and ship-based measurements.

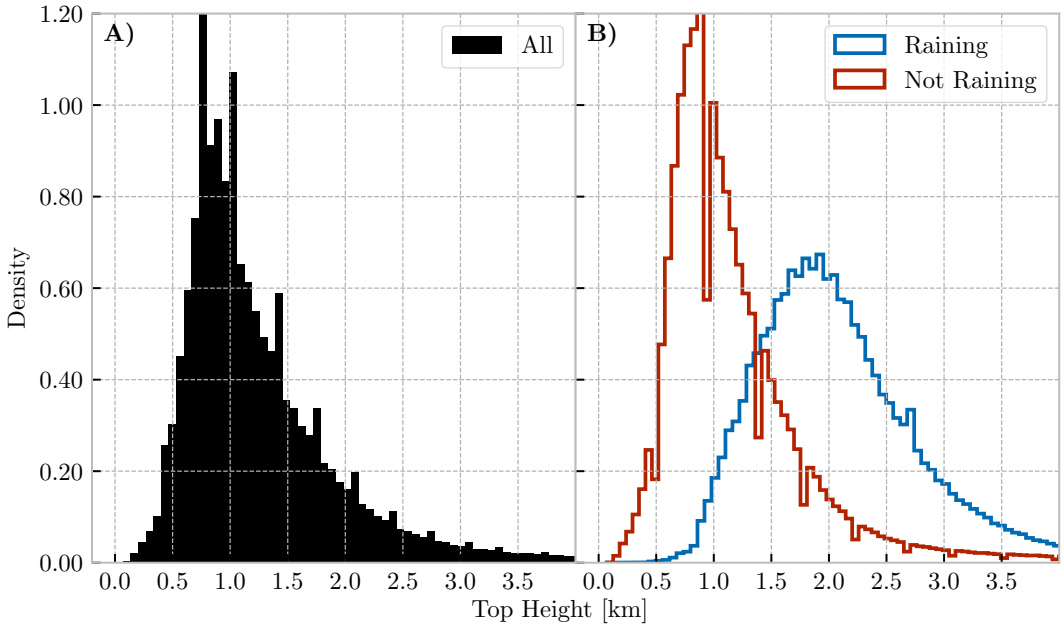

Figure 2.4: The probability density function of cloud-top height for (A) all shallow cumulus cloud objects and (B) a comparison between the raining and non-raining cloud-top height probability density functions is shown. Reprinted from Smalley and Rapp (2020b).

Figure 2.4b shows the distributions of both raining and non-raining shallow cumulus cloud object cloud-top height with Table 2.1 showing that raining shallow cumulus cloud objects have a median cloud-top height of 2.07 $\pm$ 0.63 km, while non-raining shallow cumulus cloud objects are approximately two times shallower, having a median of 1.19 $\pm$ 0.42 km. As shallow cumulus clouds grow deeper, it is well known that both the chance and intensity of warm rain increases (e.g., Short and Nakamura, 2000; Rauber et al., 2007). Within the Caribbean and Atlantic, Snodgrass et al. (2009) found detectable rainfall was most likely for clouds with tops between 2.25 - 2.75 km. Considering our definition of raining cloud objects is dependent on the rain possible flag which has a reflectivity threshold of -15 dBZ (Haynes et al., 2009), we may be sampling cloud objects producing very light rain and light drizzle that evaporates before hitting the surface otherwise not included by the Snodgrass et al. (2009) 7 dBZ threshold used to identify precipitation.

Figure 2.5a shows the median cloud-top height spatial distribution for all shallow cumulus cloud

objects. The tallest shallow cumulus cloud objects tend to cluster into two longitudinal zones, one centered at 30 N and the other at 30 S with top heights reaching 1-1.5 km, while shallow cumulus cloud objects in other regions rarely exceed 1 km in altitude.

Figure 2.5b shows the median cloud-top height spatial distribution for raining shallow cumulus cloud objects are taller and peak in different locations than the total spatial distribution of shallow cumulus cloud objects. The median raining shallow cumulus cloud-top height increase latitudinally towards the equator, with raining shallow cumulus cloud-top heights approaching 2.5 km in the ITCZ, tropical Indian Ocean, and west Pacific warm pool regions. This supports the hypothesis that shallow convection tend to organize in regions of high near-surface humidity and over regions with SSTs above 27°C (Chen and Liu, 2016), where there is enough moisture and instability available for shallow cumulus cloud objects to grow deep enough to produce rainfall.

To test the importance of cloud object depth to the likelihood of rain, we analyze the spatial distribution of top height (hereby top-height threshold) where at least 25% of cloud objects contained within an individual 2.5°x2.5° grid box are raining. Figure 2.5c shows top-height thresholds are smallest (< 2.0 km) over the ITCZ and west Pacific warm pool regions. Outside these regions, the top-height threshold generally increases. This is most noticeable over the south pacific trade region, where the top-height threshold to produce rainfall is > 2 km. Outside the ITCZ and west Pacific warm pool regions environmental moisture tends to decrease. This implies that mixing is not as harmful to clouds occurring in the humid environments allowing shallower cumulus to sustain rainfall, whereas shallow cumulus in drier environments must grow deeper to sufficiently protect themselves from dry air mixing at cloud boundaries (e.g., Lu et al., 2012).

Another region of interest is the global coastlines, particularly the east coast of North America and the east coast of Asia. Over these regions, the top-height threshold required for at least 25% of cloud objects to rain is > 2 km (Figure 2.5c). Given the high density of populated and industrial regions over eastern Asia and North America coupled with typically westerly atmospheric flow, the transport of polluted air from these regions over the ocean leads to a higher CCN concentrations (Rosenfeld, 2000), which can increase the number of small droplets and decrease variability in the

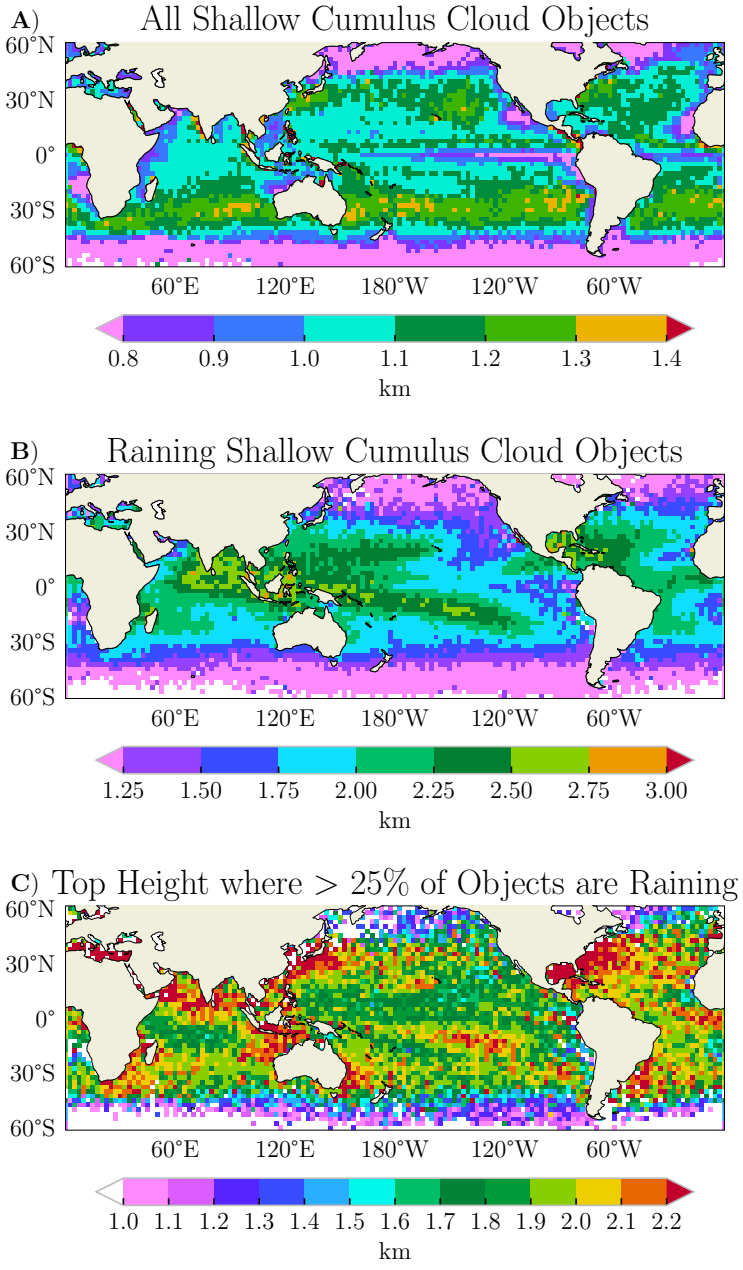

Figure 2.5: The spatial distribution of median cloud-top height for (A) all, (B) raining shallow cumulus cloud objects, and (C) the cloud-top height where at least 25% of cloud objects produce rain. Cloud objects are binned onto a 2.5° x 2.5° degree spatial grid, and any grid box containing no data is white. Reprinted from Smalley and Rapp (2020b).

drop size distribution (e.g., Squires, 1958). Both of these impacts reduce the chance of growing droplets large enough to fall out as rain (e.g., Albrecht, 1989). A similar pattern exists west of

the North African continent and southeast of Saudi Arabia, where dust has a similar impact (e.g., Koren et al., 2014).

If cloud depth was the main factor in determining precipitation likelihood, Figure 2.5c would show little regional variability. From Figure 2.5c, it is clear that rain likelihood is not entirely dependent on cloud depth, and that other processes such as aerosols, cloud extent, and environmental moisture are important. To determine the importance of cloud extent, we analyze the cloud extent distributions of all, raining, and non-raining shallow cumulus cloud objects. Table 2.2 shows the overall statistics of each cloud extent distribution to determine how cloud size impacts the likelihood of precipitation.

Table 2.2: Shallow Cumulus Cloud Object Cloud Extent Statistics. Reprinted from Smalley and Rapp (2020b).

	All	**Raining**	**Non-Raining**
Mean (km)	4.45	9.92	3.95
Median (km)	2.80	8.85	2.80
STD (km)	3.47	4.73	2.85
MAD (km)	1.63	4.08	1.63
Skewness	2.46	0.86	2.93

Figure 2.6a shows the univariate cloud extent for all shallow cumulus cloud objects. Most cloud objects are small with a median cloud extent of 4.45 $\pm$ 1.63 km (Table 2.2). Recently, Guillaume et al. (2018) investigated the differences in the horizontal cloud length scale for different cloud types using CPR data and found shallow cumulus clouds smaller than those identified by our study. These differences are likely due to their inclusion of single bin cloud objects and their use of the 2B-CLDCLASS product (Sassen and Wang, 2008), rather than the regime separation used here, to classify cumulus cloud objects.

Figure 2.6b shows the univariate cloud extent distribution for both raining and non-raining shallow cumulus cloud objects, with raining shallow cumulus cloud objects on the order of two to three times larger than non-raining cloud objects with a median cloud extent of 9.92 $\pm$ 4.08 km

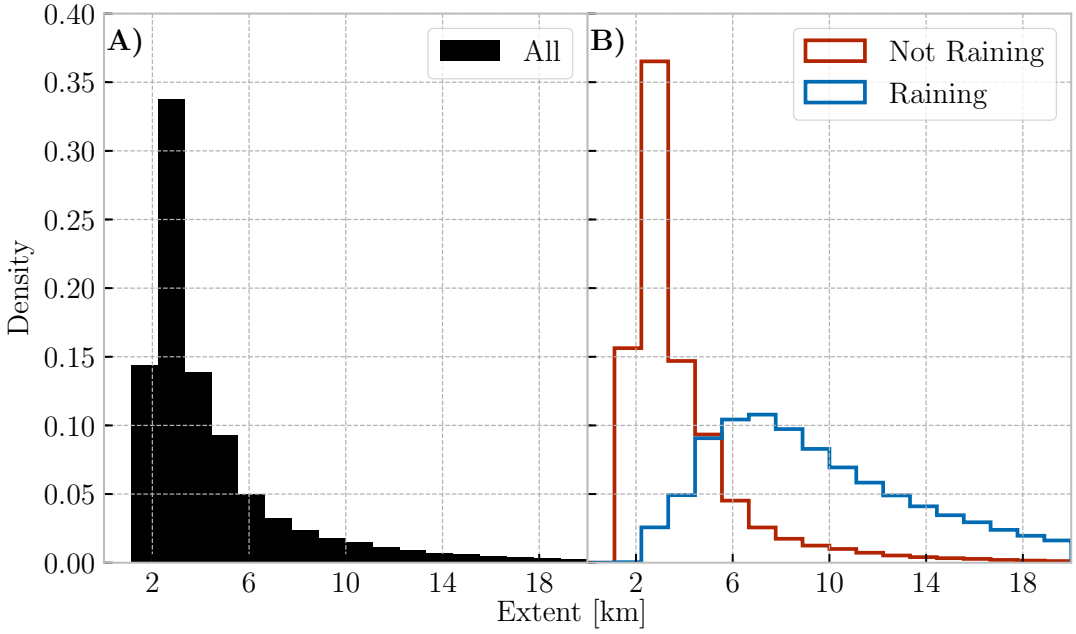

Figure 2.6: The probability density function of cloud extent for (A) all shallow cumulus cloud objects and (B) a comparison between the raining and non-raining cloud extent probability density functions is shown.

(Table 2.2). This suggests that the cloud size mechanism may be detected in observations, with larger clouds being less effected by lateral entrainment and better able to maintain their updrafts longer, grow taller, and produce more intense rainfall. Liu and Zipser (2009) used the TRMM Precipitation Radar (PR) to show that 90% of all raining shallow cumulus typically have an area < 100 km^2. If we define the diameter of each cloud object using extent, then we find that 90% of all raining shallow cumulus cloud objects have an equivalent circular area that is < 226 km^2, which are larger than those found by Liu and Zipser (2009). This discrepancy is expected due to the higher sensitivity and resolution of CloudSat/CALIPSO, with both CloudSat/CALIPSO able to identify cloudy area associated with small cloud particles (e.g., You et al., 2006) and CPR being better able to identify very light rainfall (e.g., Leon et al., 2008; Behrangi et al., 2014), neither of which can be detected by TRMM PR.

Figure 2.7a shows the spatial distribution of median cloud extent for all shallow cumulus cloud objects. These results show that cloud extent does not vary much across the global ocean basins,

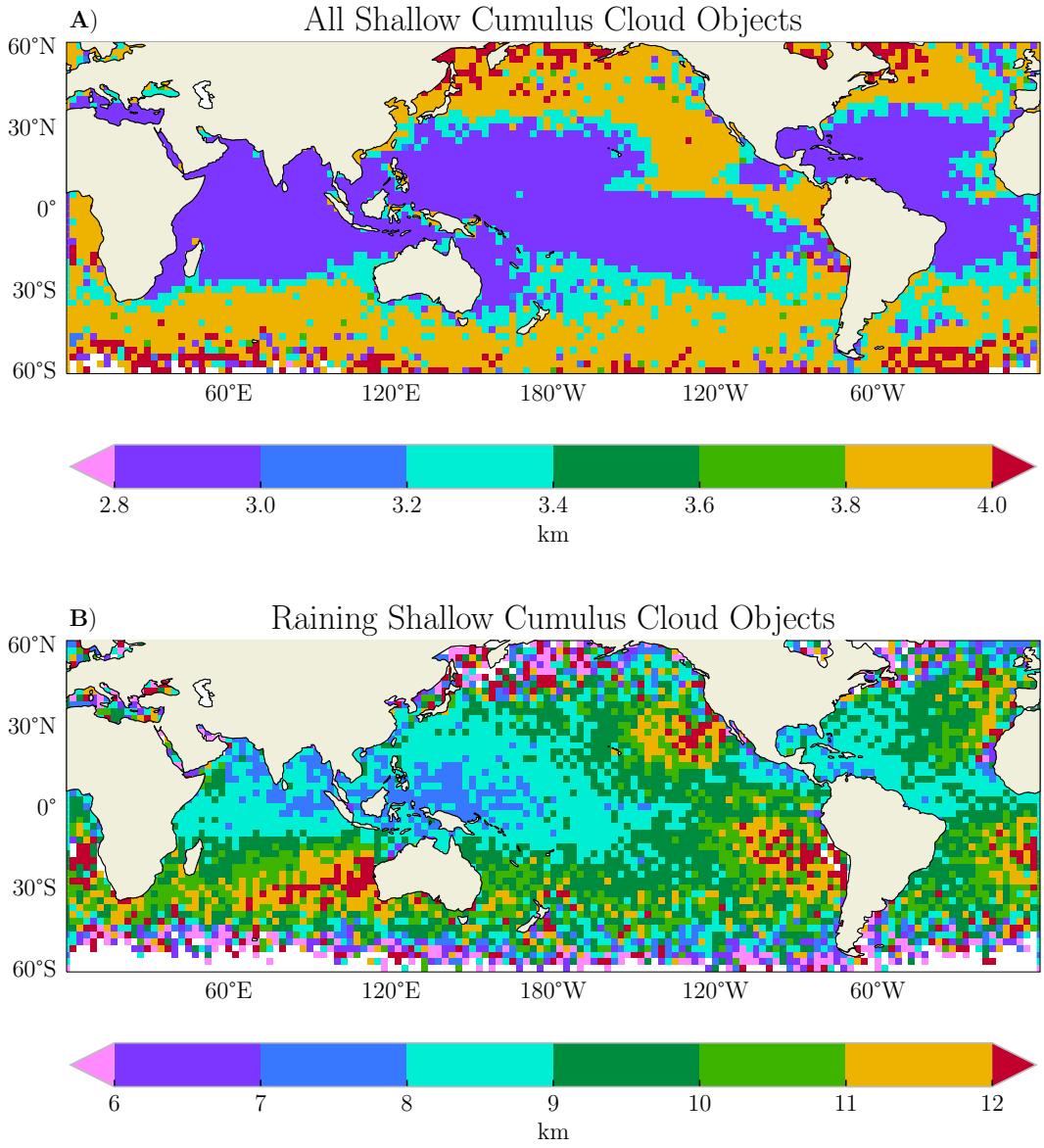

Figure 2.7: The spatial distribution of median cloud extent for both (A) all and (B) raining shallow cumulus cloud objects gridded to a 2.5° x 2.5° spatial grid. Grid boxes containing no data are white. Reprinted from Smalley and Rapp (2020b).

with an extent typically between 2 and 4 km. By comparing the spatial distribution of median raining shallow cumulus cloud object extent to the spatial distribution of median cloud extent for all shallow cumulus cloud objects, Figure 2.7b implies there is more variability in extent among raining cloud objects than non-raining cloud objects. Among raining cloud objects, Figure 2.7b.

shows that extent increases from both poles to the equator and from the west to east over the global oceans. This can be attributed to a deepening boundary layer (Wood and Field, 2011) resulting in the boundary layer decoupling from the surface (Bretherton and Wyant, 1997) and smaller clouds (Wood and Bretherton, 2006).

So far, our results identify two key characteristics of raining shallow cumulus cloud objects:

1. They are usually taller than non-raining shallow cumulus cloud objects.

2. They usually have a larger extent than non-raining shallow cumulus cloud objects.

Both of these conclusions support the overall hypothesis of this study; however, we have not explicitly shown if larger clouds in a wetter environment are more likely to rain. Next, we investigate the impact of both environmental moisture, cloud-top height, and cloud size on the likelihood of shallow rain by conditioning our shallow cumulus cloud object data set using cloud-top height and RH.

Figure 2.8 shows the likelihood of warm rain as a function of environmental moisture, cloud-top height, and extent. Focusing first on environmental moisture, Figure 8 shows that shallow cumulus cloud objects that develop in a wetter environment are the most likely cloud objects to produce rainfall. This pattern is consistent among all shallow cumulus cloud objects and not dependent on cloud-top height. The dependence of rain likelihood on environmental moisture is largest for the shallowest cloud objects, with rain likelihood approximately 30% higher in the wettest environments for the largest cloud objects.

Now focusing on shallow cumulus cloud top height, the change in rain likelihood is approximately linear and increases slower than rain likelihood of objects with top heights < 2 km. This may be because cloud objects shallower than 1.5 km never reach the trade inversion, which can limit shallow cumulus growth (Wood and Field, 2011). By limiting cloud top heights to < 1.5 km, we could also be heavily sampling clouds in the earliest development stages which are less likely to rain. For top heights > 1.5 km, the relationship between rain likelihood shifts, with one power-law scaling distribution for cloud extents < 7 - 8 km breaking down to another power-law scaling

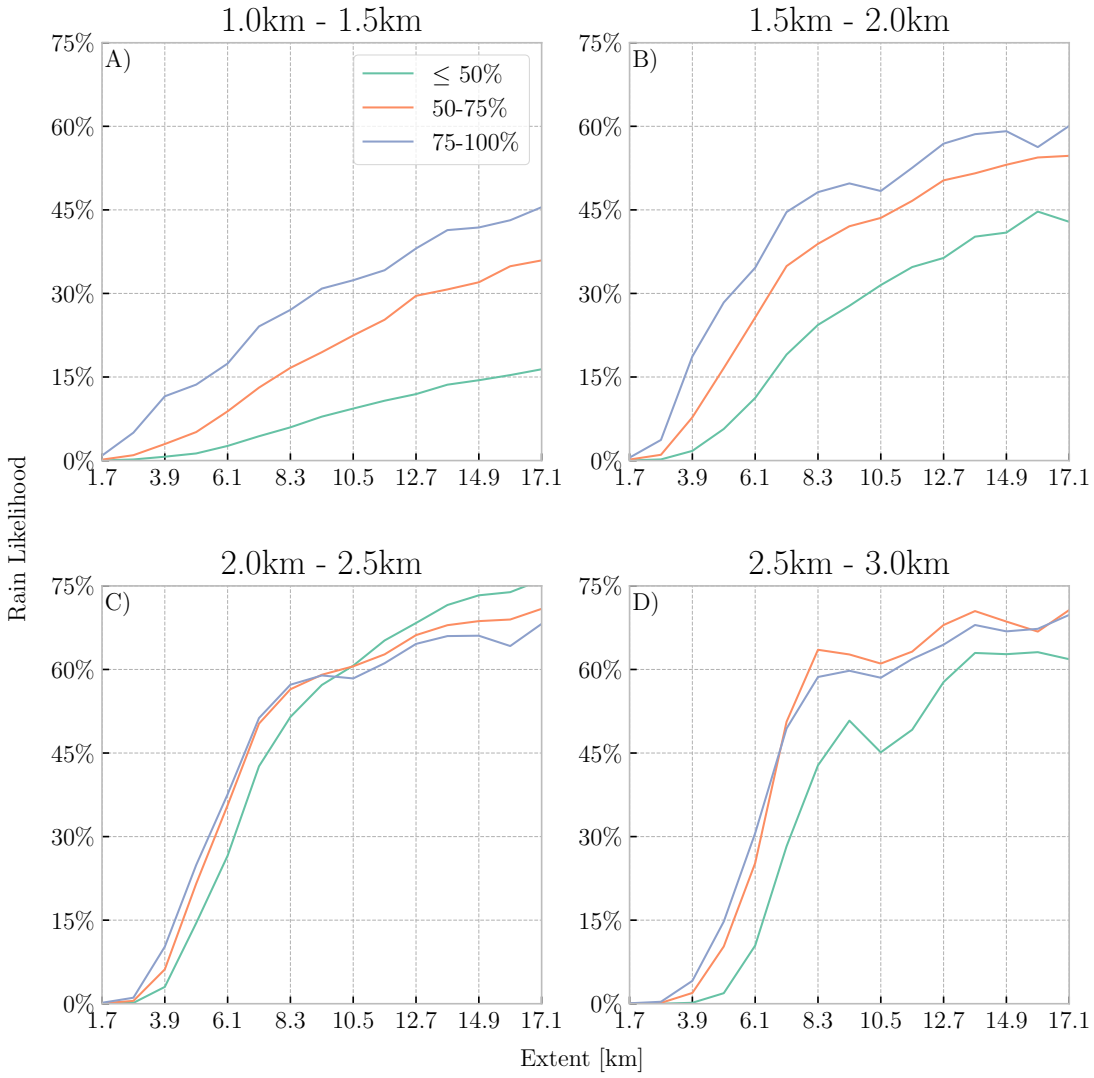

Figure 2.8: The relationship between cloud along-track extent and rain likelihood for clouds with top heights between A) 1-1.5 km, B) 1.5-2 km, C) 2-2.5 km, and D) 2.5-3 km. The line color corresponds to the different RH regimes (see legend in panel A). Reprinted from Smalley and Rapp (2020b).

distribution for cloud extents above 8 km, consistent with past literature (e.g., Kuo et al., 1993; Benner and Curry, 1998; Neggers et al., 2003; Trivej and Stevens, 2010; Neggers et al., 2019), of a double power-law scaling for cloud size distributions. Trivej and Stevens (2010) show similar behavior for the size of precipitating shallow cumuli with a break in the scaling at approximately

10 km^2. Assuming that half of the along-track extent represents the cloud radius, these data show a break in rain likelihood occurs in the range of 9 - 17 km^2. Prior studies attribute the double power-law behavior to different regimes, where below the scale break small shallow cumulus can grow quickly up to the trade inversion where they become limited. Above the break, cloud objects are limited by environmental moisture conditions.

Examination of the cloud top height and extent distribution for precipitating shallow cumulus in Figure 2.9 further supports the idea that the double power-law relationship exists between top height and extent, consistent with previous tropical shallow cumulus work by Benner and Curry (1998). Below the break, top height and extent scale at approximately the 2:1 aspect ratio shown in previous studies (Benner and Curry, 1998; Kuo et al., 1993) although slightly slower in the driest environments. Cloud objects in the driest environments rarely exceeding 1.7 km, while cloud objects occurring in the wettest environments can reach $\geq$ 2.4 km. Since boundary layer depth increases while trade inversion strength decreases as environmental moisture increases, this allows shallow cumulus that form in a more humid environment to grow larger and support more robust updrafts, increasing the chance of warm rain. Above the break, the relationship between height and extent depends strongly on the moisture environment. Trivej and Stevens (2010) found that environmental moisture is a key contributor to large shallow cumulus development. Combining Figures 2.8 - 2.9 suggests that the general precipitating cloud size distribution follows scaling shown in previous studies; however, for a fixed cloud depth, the likelihood of precipitation depends on the size of the cloud and/or the moisture environment. For clouds with a similar depth, a larger cloud or a cloud in a more moist environment is more likely to rain.

Figure 2.10 shows the median fraction of raining pixels within each cloud object conditioned on environmental moisture. It also shows a scale break and supports the idea that precipitation likelihood increases with environmental moisture, especially after the scale break where Trivej and Stevens (2010) suggest that cloud objects are limited by environmental moisture regime. For a fixed cloud extent greater than 7 - 8 km, the fraction of the cloud object that is raining is at least 10% greater when RH below 3 km is above 75% compared to environments with RH 50% or below.

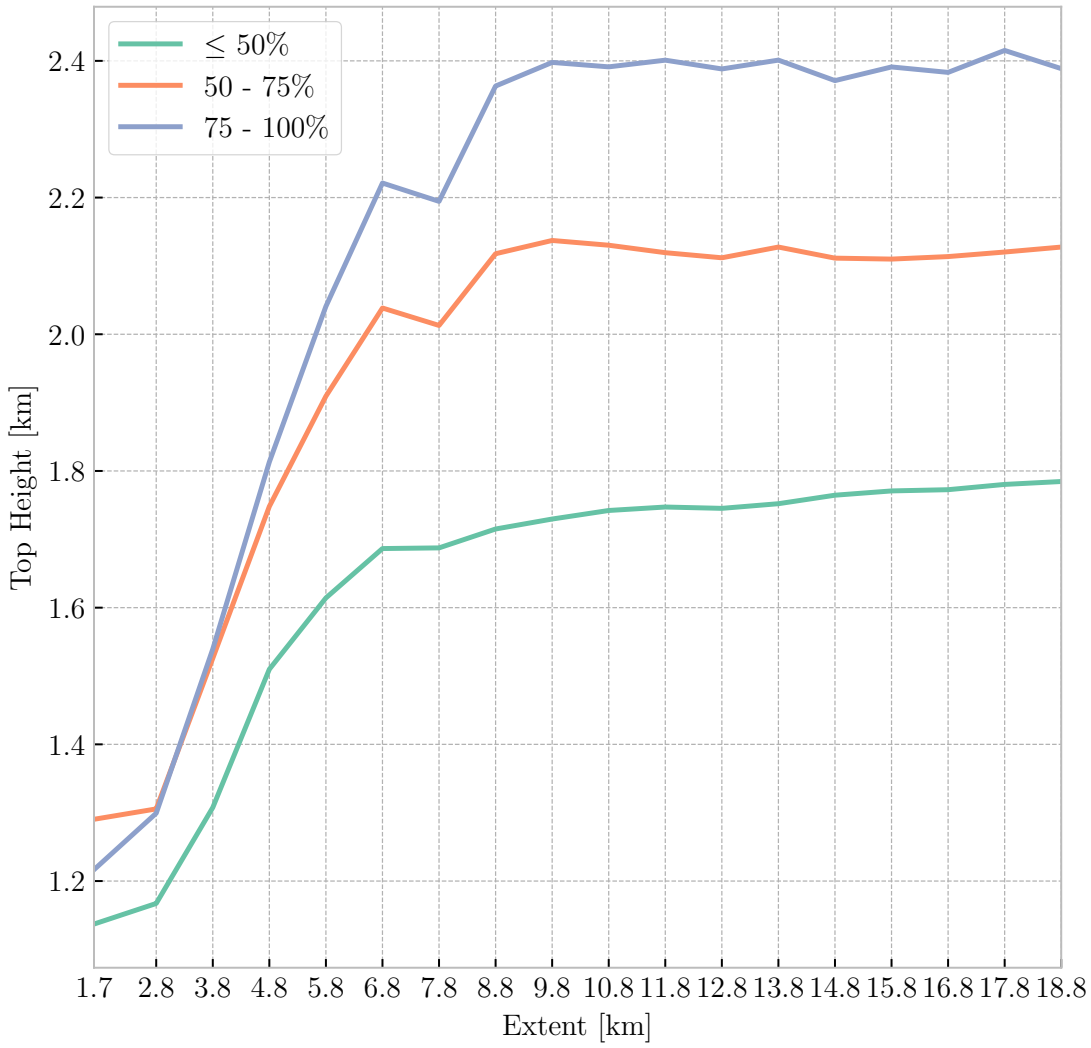

Figure 2.9: The median top height for raining shallow cumulus cloud objects with a given extent is shown. The different line colors separate cloud objects by environmental moisture (defined using relative humidity below 3 km). Reprinted from Smalley and Rapp (2020b).

This also suggests that cloud updrafts are less impacted by cloud edge mixing and may result in more vigorous updrafts, resulting in a higher rain likelihood, and a larger raining cloud fraction, when the environment is moist.

Figure 2.10: The median fraction of pixels within cloud objects of a given extent producing rain is shown. The different line colors separate cloud objects by environmental moisture (defined using relative humidity below 3 km). Reprinted from Smalley and Rapp (2020b).

2.5 Limitations

While we have attempted to mitigate as many limitations as possible, some limitations in the shallow cumulus identification scheme and precipitation identification scheme that could impact

the results may still be present. The cloud object identification scheme used by this study is limited by the 1.7 km along-track spatial resolution of CloudSat. As a result, the smallest cloud objects this study can sample have a minimum cloud extent of 1.7 km. There are likely raining cloud objects smaller than this threshold. However, this limitation is unavoidable given CloudSat's resolution.

Previous studies have used ground-based cloud radars to analyze shallow cumulus at a spatial resolution as high as 30 m (e.g., Kollias et al., 2003). Considering raining clouds may not always be large enough to fill CloudSat's footprint, raining cloud objects may be missed if they lack a sufficient size and intensity necessary to trigger a rain detection by CloudSat. To test this, we performed sensitivity tests by setting a 0.1 x 0.1 km grid within CloudSat's footprint and assigning each subpixel reflectivity values ranging from clear to cloud to different rain intensities. We assumed a gaussian shaped gain function and calculated the reflectivity that would be measured by CloudSat for varying subpixel reflectivities and rain fractions to determine the fraction of raining subpixels at a given intensity that will reach CloudSat's thresholds for rain certain, rain possible and rain probable (Table 2.3). At the rain certain threshold of 0 dBZ, Table 3 shows that the rain rate must be $\geq$ 0.05 mm hr^{-1}, and a rain shaft producing 0.05 mm hr^{-1} rain rates must be the entire size of CloudSat's footprint (2.38 km^2) to trigger a rain detection. As rain rate increases, the minimum rain shaft size for a CloudSat rain detection decreases. Table 2.3 shows a similar pattern at both the rain probable and possible thresholds; however, any shallow cumulus cloud producing rainfall at rates $>$ 0.50 mm hr^{-1} only needs to be 0.01 km^2. (equivalent to one subpixel) to reach the rain possible threshold of -15 dBZ. These results suggest potential beam-filling problems may impact our results and could contribute to the rapid increase in rain likelihood for the smallest cloud objects. Many previous studies, some of which use higher resolution ground-based radar observations, showing similar double power-law relationships as cloud objects grow larger and scale breaks that occur at similar sizes (e.g., Benner and Curry, 1998; Trivej and Stevens, 2010) lends some confidence that our rain likelihood distributions are not purely due to sampling limitations. Another consideration is any shallow cumulus cloud objects identified by CALIPSO within the ground clutter region of CPR are missed in the rain likelihood statistics. However, Rapp et al. (2013) estimated that around

0.6% of shallow clutter clouds may produce precipitation, suggesting relatively small impacts on our findings.

Table 2.3: Fractional area of raining subpixels (100 x 100 m) within CloudSat's footprint that satisfy the rain certain, probable, or possible flags. Reprinted from Smalley and Rapp (2020b).

Average Reflectivity of Raining Subpixels	**Rain Rate**	**Certain**	**Probable**	**Possible**
-10 dBZ	0.01 mm hr^{-1}	NA	NA	0.76 km^2
0 dBZ	0.05 mm hr^{-1}	2.38 km^2	0.43 km^2	0.08 km^2
4 dBZ	0.10 mm hr^{-1}	0.95 km^2	0.17 km^2	0.03 km^2
13 dBZ	0.50 mm hr^{-1}	0.12 km^2	0.03 km^2	0.01 km^2
17 dBZ	1.00 mm hr^{-1}	0.05 km^2	0.01 km^2	0.01 km^2
24 dBZ	5.00 mm hr^{-1}	0.01 km^2	0.01 km^2	0.01 km^2

There are 238 total (0.1 x 0.1 km) subpixels, each with an area of 0.01 km^2, within CloudSat's footprint (1.4 x 1.7 km), which has an area of 2.38 km^2. Fractional areas where CloudSat will not detect rain at the specified rain rate are labeled as NA. The rain rates are determined from the average reflectivity values, and listed in Lebsock and L'Ecuyer (2011a). CloudSat's rain detection reflectivity thresholds at rain certain, probable, and possible are 0 dBZ, -7.5 dBZ, and -15 dBZ, respectively.

It is well established that as shallow cumulus grow they can modify the surrounding local environment through the vertical transport of latent heat. This can act to both increase environmental moisture and reduce LTS, allowing for subsequent growth and potentially rain (Johnson et al., 1999). Because we use ECMWF RH and LTS to classify the large-scale environment, cloud-scale modulation of the local environment is not considered. This limitation is unavoidable from a purely observational standpoint.

Additionally, the environmental thresholds used here to classify shallow cumulus and stratocumulus cloud objects were initially developed using monthly averaged data. This may be why the environmental separation scheme identifies cloud objects larger than the typical cumulus cloud (e.g., Rauber et al., 2007). As mentioned earlier, the largest 5% of shallow cumulus cloud object sizes are removed from this analysis, although this has little impact on our overall findings.

2.6 Summary and Discussion

Earlier studies have used cloud and LES models, constrained using field study data at select sites, to investigate the impact of shallow cumulus size on rain production. These studies concluded that as shallow cumulus clouds grow larger, the likelihood of rainfall increases. This was attributed to the influence of entrainment on larger shallow cumulus clouds decreasing which allows for stronger updrafts. Given that global observations of shallow cumulus clouds are limited, it is essential that simulated clouds be compared to observations. This not only helps constrain shallow cumulus and their impacts on climate models but also our general understanding of warm rain production. This study developed a large global cloud object dataset from CloudSat/CALIPSO observations to analyze the influence of cloud extent on rain likelihood. We then used LTS to identify shallow cumulus cloud objects. This approach allows us to not only analyze shallow cumulus cloud object characteristics, but identify any relationship between cloud size, rain likelihood, and the environment.

By binning the shallow cumulus cloud object data set onto a 2.5° x 2.5° grid, results show that most shallow cumulus cloud objects (both precipitating and non-precipitating) are observed over the trade wind regions. These regions are generally associated with a weakly stable boundary layer and weak large-scale subsidence. As a result, the boundary layer can deepen and decouple from the surface creating a favorable environment for shallow cumulus.

Most shallow cumulus cloud objects have cloud-top heights on the order of 1 km; however, raining shallow cumulus are generally about two times taller, with the tallest occurring over equatorial regions. SSTs over these regions tend to be warm resulting in a wetter environment and deeper boundary layer, both of which are shown to enhance the likelihood of precipitation.

Generally, shallow cumulus cloud objects are small with a cloud extent typically less than 5 km, but raining shallow cumulus cloud objects tend to be about three times larger than non-raining, lending support to the hypothesis that larger clouds are more likely to produce rainfall. Spatially, the largest shallow cumulus cloud objects tend to occur in the eastern ocean basins, while the smallest shallow cumulus cloud objects tend to occur over the west Pacific warm pool and the Indian Ocean.

Similar trends are seen in the spatial distribution of raining cloud extent. Over regions with large shallow cumulus cloud objects, prior studies concluded that both a stronger inversion and stronger boundary layer winds result in cloud objects with larger cloud extents (e.g., Ghate et al., 2016).

To identify the relationship between cloud extent and rain likelihood, we constrained shallow cumulus cloud objects using cloud-top height and environmental moisture. For a fixed shallow cumulus cloud object depth, the two main conclusions are that cloud objects with a larger extent are more likely to rain and as environmental moisture increases rain likelihood becomes larger for smaller cloud objects.

For shallow cumulus cloud objects with top heights $<$ 1.5 km, the change in rain likelihood increases approximately linearly with cloud object size, with the slope dependent on the environmental relative humidity. One possible explanation is that the shallow cumulus cloud objects sampled with cloud-top heights $<$ 1.5 km are developing cumulus that have not yet reached the top of the boundary layer. For shallow cumulus cloud objects taller than 1.5 km, the change in rain likelihood shows a double power-law distribution with one scaling at extent values $<$ 7 - 8 km that breaks down and flattens into another scaling distribution at extent values $>$ 8 km. Trivej and Stevens (2010) show that the mean reflectivity as a function of cloud size also has this double power-law scaling which explains why rain likelihood (based here on reflectivity thresholds) follows this distribution. Similar behavior is shown for the relationship between cloud top height and extent and the raining fraction of clouds and extent, with the break occurring at different top heights in different environmental regimes.

The shift in scaling of the rain likelihood distribution may be attributed to an environmental regime shift (Trivej and Stevens, 2010). Small cloud objects are trade inversion limited and rapidly grow deeper and larger following the 2 to 1 size to height aspect ratios shown in earlier studies (e.g., Benner and Curry, 1998) up to the capping inversion. As they grow larger, rain likelihood increases, suggesting that as cloud size increases they are less affected by entrainment and supporting the hypothesis that shallow cumulus become better protected from mixing as they grow larger (e.g., Heus et al., 2009; Burnet and Brenguier, 2010).

Previous studies (i.e., Trivej and Stevens, 2010) suggest that the breakpoint in the double power-law distribution is related to a shift in meteorological controls on convection, specifically changes in environmental moisture. Past the breakpoint, rain likelihood with cloud size increases more slowly but the rain likelihood at which the breakpoint occurs depends on the environmental RH. The same size cloud is more likely to produce precipitation in higher RH regimes, and the fraction of the cloud producing precipitation also increases. Both provide observational support for the idea that because of decreased evaporation at cloud edges, shallow cumulus updrafts are not as harmed by mixing in a humid environment. As a result, they can sustain larger droplets longer that may eventually fall out as rain.

Other potentially important factors important for the rain likelihood distribution with cloud size that were not examined here are the role of organization and aerosols. Our results suggest that aerosols near the coastlines likely play a role in limiting rain likelihood. However, Minor et al. (2011), found that spatial organization was more important than giant CCN concentration. Consistent with the suggested importance of spatial organization, Trivej and Stevens (2010) found that increasing shallow cumulus cloud size in precipitating shallow cumulus was coupled to an increase in cloud area fraction, which they attributed a moister environment more conducive to vertical and horizontal development. Precipitation in the trade regions has often been linked to convective organization (e.g., Zuidema et al., 2012; Seifert and Heus, 2013; Stevens et al., 2019), with cold pools formed by previous convection initiating new shallow cumulus that can grow deeper and become more likely to rain. The break in the rain likelihood distribution with cloud size shown here could be related to a shift toward more spatially organized convection. We are currently expanding our cloud object dataset to include additional metrics for cloud spacing and expect to use this dataset in the future to investigate the importance of shallow cumulus organization to precipitation likelihood.

Our results provide global observational support for previous modeling and limited field campaign studies hypothesizing that larger clouds or clouds in a more humid environment can protect their updrafts from entrainment and increase the likelihood of warm rain. Our results are encouraging; however, we cannot directly estimate entrainment using these observations. As a result, we

can only speculate that larger shallow cumulus cloud objects are more likely to rain because their updrafts more protected from entrainment. Luo et al. (2010) identified a methodology that can be used to estimate entrainment in deep convective clouds using satellite data. This methodology uses estimates of moist static energy profiles throughout the depth of the cloud to estimate the entrainment rate. Future work could focus on developing similar satellite-based methodologies to estimate the entrainment rate in shallow cumulus clouds.

3. A-TRAIN ESTIMATES OF THE SENSITIVITY OF WARM RAIN LIKELIHOOD AND EFFICIENCY TO CLOUD SIZE, ENVIRONMENTAL MOISTURE, AND AEROSOLS*

3.1 Abstract

Precipitation efficiency has been found to play an important role in constraining the sensitivity of the climate through its role in controlling cloud cover, yet understanding of its controls are not fully understood. Here we use CloudSat observations to identify individual contiguous shallow cumulus cloud objects and compute the ratio of W_C to rain water path as a proxy for WRE. Cloud objects are then conditionally sampled by cloud-top height, relative humidity, and aerosol optical depth (AOD) to analyze changes in WRE as a function of cloud size (extent). For a fixed cloud-top height, WRE increases with extent and environmental humidity following a double power-law distribution, as a function of extent. Similarly, WRE increases holding environmental moisture constant. There is surprisingly little relationship between WRE and AOD when conditioned by cloud-top height, suggesting that once raindrop formation begins, aerosols may not be as important for WRE as cloud size and depth. Consistent with prior studies, results show an increase in WRE with sea surface temperature. However, for a given depth and sea-surface temperature (SST), WRE is also dependent on cloud size and becomes larger as cloud size increases. Given that larger objects become more frequent with increasing SST, these results imply that increasing precipitation efficiencies with SST are due not only to deeper clouds with greater cloud water contents, but also the propensity for larger clouds which may have more protected updrafts.

3.2 Introduction

Low cloud cover continues to be a dominant source of uncertainty in projecting future climate (e.g. Bony and Dufresne, 2005; Dufresne and Bony, 2008; Vial et al., 2013), with variations in shallow cumulus distributions explaining much of the differences in climate model-derived estimates

*Reprinted with permission from "A-Train estimates of the sensitivity of warm rain likelihood and efficiency to cloud size, environmental moisture, and aerosols" by Kevin M. Smalley and Anita D. Rapp, 2020. *Atmospheric Chemistry and Physics Discussions*, NA, NA–NA, Copyright [12 August 2020] by the European Geosciences Union.

of climate sensitivity (e.g. Wyant et al., 2006; Medeiros and Stevens, 2011; Nam et al., 2012). This stems from climate models' inability to simulate shallow cumulus and their impacts, due in part to the low temporal and spatial resolution of these models (e.g. Stevens et al., 2002), as well as the fact that small-scale processes important for cloud development, including turbulence and convection, must be parameterized (e.g. Tiedtke, 1989; Zhang and McFarlane, 1995; Bretherton et al., 2004). Studies have shown precipitation efficiency is a key parameter used to constrain cloud parameterizations within climate models (Rennó et al., 1994; Del Genio et al., 2005; Zhao, 2014; Lutsko and Cronin, 2018). Nam et al. (2012) hypothesized that climate models produce shallow clouds that are too reflective possibly because model precipitation efficiencies are too weak, resulting in excess cloud water which increases cloud optical depth and shallow cumulus reflectance. Prior observational and modeling studies found the precipitation efficiency of shallow cumulus increases as sea-surface temperature (SST) increases in response to climate change (Lau and Wu, 2003; Bailey et al., 2015; Lutsko and Cronin, 2018). Factors including environmental moisture (e.g. Heus and Jonker, 2008; Schmeissner et al., 2015), entrainment (e.g. Korolev et al., 2016; Pinsky et al., 2016b,a), and aerosols (e.g. Koren et al., 2014; Dagan et al., 2016; Jung et al., 2016b,a) help regulate both thermodynamic and dynamical processes that promote favorable conditions important to not only warm rain production, but also the efficiency of the conversion of cloud water to precipitation. To better constrain cloud parameterizations of these processes and subsequently climate sensitivity to low cloud cover, more observation-based studies analyzing physical processes influencing warm rain efficiencies are needed.

In an ideal shallow cumulus cloud, liquid water content increases adiabatically from cloud base to top. However, liquid water content is generally only 50% - 80% of the adiabatic values due to entrainment (Gerber et al., 2008). Evaporation induced by cloud-edge mixing not only impacts shallow cumulus updraft strength, but also the number and size of droplets within a cloud (Lu et al., 2012), with increased evaporation potentially reducing the number and size of available droplets. Using a LES, Moser and Lasher-Trapp (2017) found the influence of entrainment decreases from cloud-edge to center of individual shallow cumulus as they grow larger. This results in liquid water

content at cloud center being closer to adiabatic in larger clouds because fewer droplets evaporate away at cloud-center. This implies that the collision-coalescence process is more efficient at cloud center because there is more cloud water available to be collected by large droplets. At cloud edge, there are not only fewer droplets but also smaller droplets, potentially reducing collision-coalescence efficiencies there. This is consistent with other LES results that found shallow cumulus updrafts are more insulated from entrainment as they become larger (e.g. Heus and Jonker, 2008; Burnet and Brenguier, 2010; Tian and Kuang, 2016). LES and limited field-campaign observational studies have shown that cloud updrafts not only become more protected as cloud size increases but also as environmental moisture increases (Heus and Jonker, 2008; Schmeissner et al., 2015; Hernandez-Deckers and Sherwood, 2018). Using a cloud model, Romps (2014) found that precipitation efficiency decreases as relative humidity decreases because precipitation evaporates more readily in a drier environment. Considering environmental moisture scales with temperature, this is consistent with results found by Lau and Wu (2003) which show the efficiency of warm rain production increases as SSTs increase using TRMM satellite observations. Given LES results showing that shallow cumulus updrafts are more protected as clouds grow in size and/or environmental moisture increases, *we hypothesize larger droplets will be evident closer to the cloud base and increase WRE in larger cloud objects because the cloud-core of larger cloud objects is more protected from entrainment*.

While perhaps not as important as organization (Minor et al., 2011) or cloud size (Jiang and Feingold, 2006), it is widely understood that aerosol concentrations act to suppress warm rain production (Twomey, 1974; Albrecht, 1989) by increasing the cloud droplet concentration and reducing cloud droplet sizes (Squires, 1958). Albrecht (1989) found that increasing precipitation efficiency within a model is equivalent to decreasing the amount of CCN, which reduces the amount of cloud water. Similarly, Saleeby et al. (2015) used a cloud model to recently find both cloud water and raindrop concentration decreases as cloud concentration nuclei increases. Lebsock and L'Ecuyer (2011a) used CloudSat and Moderate Resolution Imaging Spectroradiometer (MODIS) observations to show that as drop size decreases, the ratio of rain water to cloud water also de-

creases. Together, these studies suggest the number of large droplets able to fall at sufficient terminal velocities to initiate collision-coalescence and continue growing to large enough sizes to fall out as rain decreases with increasing aerosol concentrations, which would reduce warm rain efficiency (WRE).

Observationally, prior studies have used satellite observations to infer the relationship between precipitation efficiency and both sea-surface temperature (Lau and Wu, 2003) and drop size (Lebsock and L'Ecuyer, 2011a). However, the relationship between cloud water and precipitation as shallow cumulus grows larger, environmental moisture increases, and/or aerosol loading has only been investigated using cloud models (e.g. Moser and Lasher-Trapp, 2017) and limited field-campaign observations (e.g. Gerber et al., 2008). While these case and model studies provide insight into the physical processes, it is unclear how well they represent the shallow cumulus clouds observed globally. Satellites can observe a large enough sample size of shallow cumulus over different regions and during different stages of their lifecycle to gain a more holistic view of this relationship. Prior studies have used TRMM and Global GPM observations to analyze warm rain production and efficiency (e.g. Lau and Wu, 2003). Unfortunately, TRMM and GPM are precipitation radars operating at the Ku- and Ka-bands not capable of observing the non-raining portions of clouds or light precipitation. Building off work in Smalley and Rapp (2020b) that analyzed the relationship between rain likelihood and cloud size, this study uses the higher sensitivity radar of CloudSat in addition to MODIS observations to test the hypothesis that *WRE is higher in larger shallow cumulus and is modulated by environmental moisture and aerosol loading*.

3.3 Data and Methods

To determine if larger shallow cumulus clouds are more efficient at producing warm rainfall, this study uses the CloudSat Cloud Profiling Radar (CPR; Tanelli et al., 2008) to identify individual contiguous shallow cumulus cloud objects. The CPR is a near-nadir pointing 94-GHz radar that measures backscattered radiation from cloud particles and is used to analyze the vertical and horizontal distribution of clouds. The CPR has a 1.4 x 1.8 km horizontal resolution and 480 m pulse

length oversampled by a factor of two, giving a vertical resolution of 240 m.

Contiguous cloudy regions are initially identified using the 2B-GEOPROF (Marchand et al., 2008) cloud mask confidence values ≥ 20, which removes orbit elements that may be influenced by ground clutter (Marchand et al., 2008). Before identifying cloud objects, 2C-RAIN-PROFILE (Lebsock and L'Ecuyer, 2011b) modeled reflectivity is mapped onto the two-dimensional cloud mask field. As outlined by L'Ecuyer and Stephens (2002), Mitrescu et al. (2010), and Lebsock and L'Ecuyer (2011b), modeled reflectivity adjusts the raw reflectivity for multi-scattering and attenuation when it is raining. As described by Smalley and Rapp (2020b), we use a lower-tropospheric stability threshold of 18.55 K to separate cloud objects occurring in environments favoring stratocumulus development from those occurring in environments favoring shallow cumulus development. Shallow cumulus cloud objects are then identified using the methodology described by Smalley and Rapp (2020b) using the combined two-dimensional reflectivity field, with only single-layer cloud objects included. This study uses 2C-RAIN-PROFILE integrated $W_P > 0$ to identify raining cloud objects and does not consider non-raining objects. We then store the median cloud-top height and maximum along-track extent (hereby extent) of each cloud object for later analysis.

Although CloudSat 2B-CWC-RVOD (Austin et al., 2009) does provide a W_C product, the rain drop size distribution used in 2B-CWC-RVOD is not the same as that used in 2C-RAIN-PROFILE. Additionally, Christensen et al. (2013) found that the 2B-CWC-RVOD algorithm struggles to filter out precipitation sized droplets in the presence of light precipitation and drizzle, which results in an overestimation of cloud water. This, coupled with differences in assumed drop size distributions by 2B-CWC-RVOD and 2C-RAIN-PROFILE, makes 2B-CWC-RVOD W_C not ideal for this study, so we instead use MODIS W_C. While there are biases in MODIS shallow cumulus W_C, prior studies have found them to be small in comparison to other satellite retrievals (e.g. Lebsock and Su, 2014). W_C is then calculated for each CloudSat pixel by averaging the nearest nine MOD-06-1KM (Platnick et al., 2003) pixels, which have been previously matched to the CloudSat track in the MOD-06-1KM product (Cronk and Partain, 2018). We then store and analyze the median W_C associated with each cloud object.

WRE of each shallow cumulus cloud object is calculated as $\frac{W_P}{W_C}$. Note, this is a proxy for true WRE, because the mass flux of water in and out of a cloud cannot be determined without a model, however prior observational studies have used this ratio to analyze the amount of cloud water converted to rain water (e.g. Lebsock and L'Ecuyer, 2011a).

Considering reflectivity is a function of the drop size distribution to the sixth power, it is expected that the maximum reflectivity in non-raining cloud objects will occur near cloud-top, then shift downward as a cloud transitions from non-raining to raining. Wang et al. (2017) used the vertical reflectivity gradient (VGZ) to investigate warm rain onset. They found VGZ(positive down) reverses sign (positive to negative) when clouds transition from non-raining to raining. Given previous studies and results shown in Smalley and Rapp (2020b) finding rain is more likely as clouds grow larger in extent, it is hypothesized that the negative VGZwithin individual raining cloud objects will increase in magnitude as cloud objects increase in extent. The methodology described in Wang et al. (2017) is applied to find the VGZfor each pixel within every shallow cumulus cloud object. VGZ at cloud object center pixel (VGZ_{CP}) will then be compared to VGZ at cloud object edge pixel (VGZ_{CP}) to infer the impact of mixing on cloud object cores as a function of cloud size and environmental moisture.

The influence of aerosols on the relationship between WRE and cloud object extent are determined using Aqua MODIS level-3 daily 550 nm aerosol optical depth (AOD) (Ruiz-Arias et al., 2013). Each cloud object is matched to the nearest 1°x1° gridbox AOD value. Note, this study does not consider the type of aerosol present in each environment, however, this may also factor into the WRE.

Similar to Smalley and Rapp (2020b), analysis is constrained to only marine shallow cumulus between 60 N and 60 S. Measurements are constricted to June 2006 and December 2010 because CloudSat stopped taking night time measurements after 2010 due to a battery anomaly (Witkowski et al., 2012). Environmental moisture is classified using 6-hourly ECMWF-AUX (Cronk and Partain, 2017) average relative humidity below 3 km matched to each cloud object. Cloud-top height, environmental moisture, VGZ, and AOD are used as control variables to analyze the relationship

between WRE and cloud object extent.

3.4 Warm rain relationship to extent

We analyze the spatial distribution of W_P, W_C, WRE, AOD, and extent of raining shallow cumulus cloud objects by binning them to a 2.5° x 2.5° global grid.

Figure 3.1a shows the spatial distribution of W_P over the global ocean basins, with W_P increasing equatorward. This is consistent with prior literature that found raining shallow cumulus are most frequent within the tropics (e.g. Smalley and Rapp, 2020b). W_P is largest near the ITCZ, ITCZ, and tropical warm pool, with values exceeding 45 g m^{-2}. Deep convection is more frequent here (e.g. Waliser and Gautier, 1993), so some objects may be transitioning from raining shallow cumulus to deeper convection. The results likely include a mix of frequently occurring tropical raining shallow cumulus and the early stages of developing deep convection possibly resulting in large W_P over the tropics.

Spatial patterns in W_C (Figure 3.1b) within the tropics generally follow W_P, with values ranging between 110 g m^{-2} and 150 g m^{-2} in the tropics. Considering the tropics are more humid than the mid-latitude and polar regions, this is consistent with modeling studies that found less cloud water evaporates away in wetter environments (e.g. Hernandez-Deckers and Sherwood, 2018). Considering boundary layer depth scales with SST (e.g. Wood and Bretherton, 2004a), the boundary layer is generally deeper over the tropical oceans than the sub-tropical oceans. This supports deeper clouds (e.g. Short and Nakamura, 2000; Rauber et al., 2007; Smalley and Rapp, 2020b) and could also help explain why W_C and WP are largest in the tropics.

Figure 3.1c shows the spatial patterns in WRE follow spatial patterns in W_P, with values increasing equatorward. Shallow cumulus cloud object WRE is largest within the ITCZ, ITCZ, and tropical warm pool, with values > 0.35. This is consistent with Lau and Wu (2003), who found precipitation efficiency is positively correlated with SST (e.g. Lau and Wu, 2003), and implies that WRE is higher in wetter environments.

Patterns in spatial extent shown in Figure 3.1d are similar to those found by Smalley and Rapp

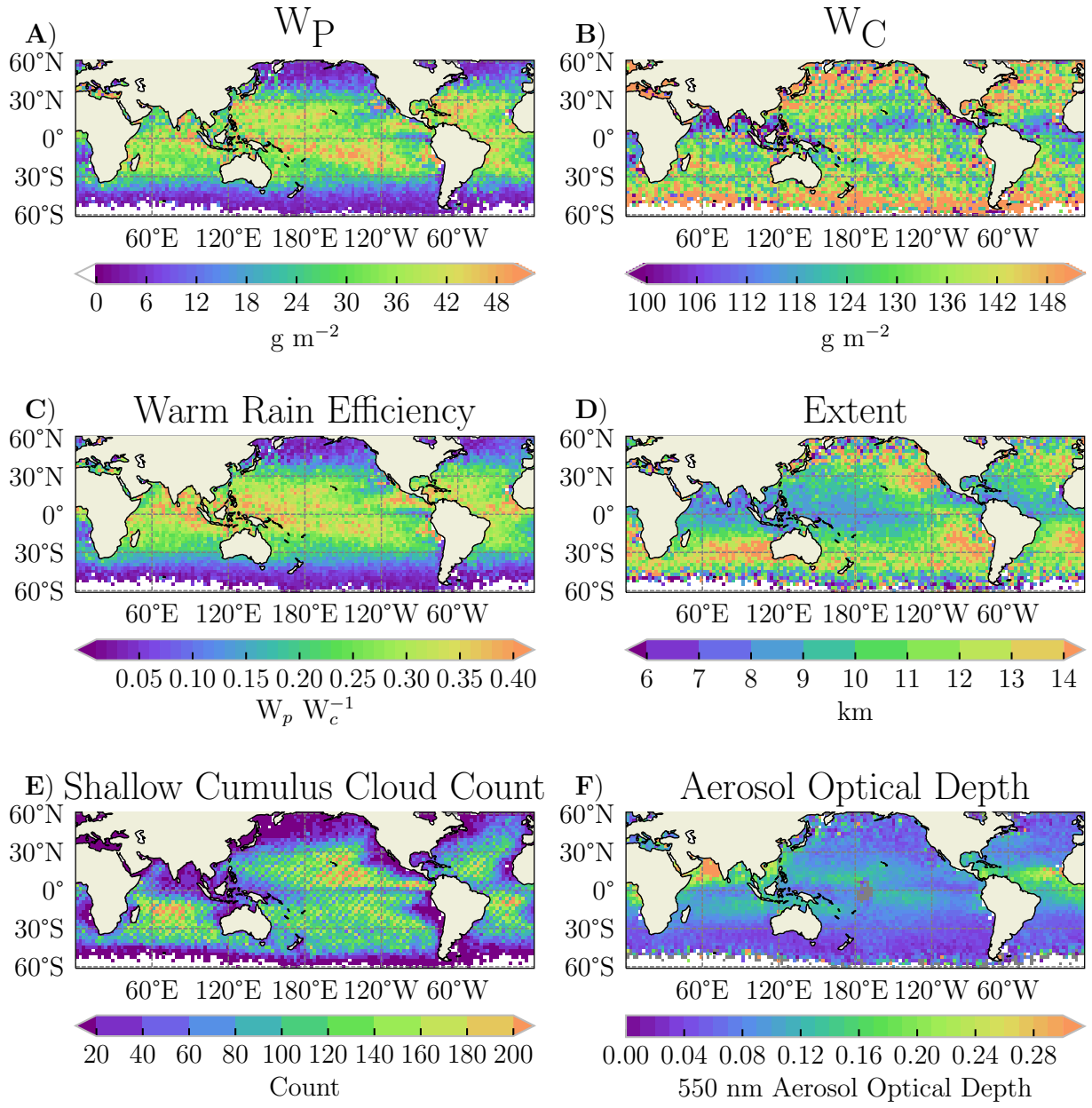

Figure 3.1: The spatial distribution of integrated W_P, W_C, warm rain efficiency, extent, number of shallow cumulus cloud objects, and aerosol optical depth are shown in panels A), B), C), D), E), and F) respectively. Cloud objects are binned onto a 2.5° x 2.5° spatial grid, and any grid box containing no data is white. Reprinted from Smalley and Rapp (2020a).

(2020b), who used combined CloudSat/CALIPSO to define extent, with extent decreasing from the stratocumulus regions east into the trade cumulus regions and north into the ITCZ. Interestingly, Figure 3.1c shows WRE also peaks in the southeast Pacific stratocumulus region, implying that

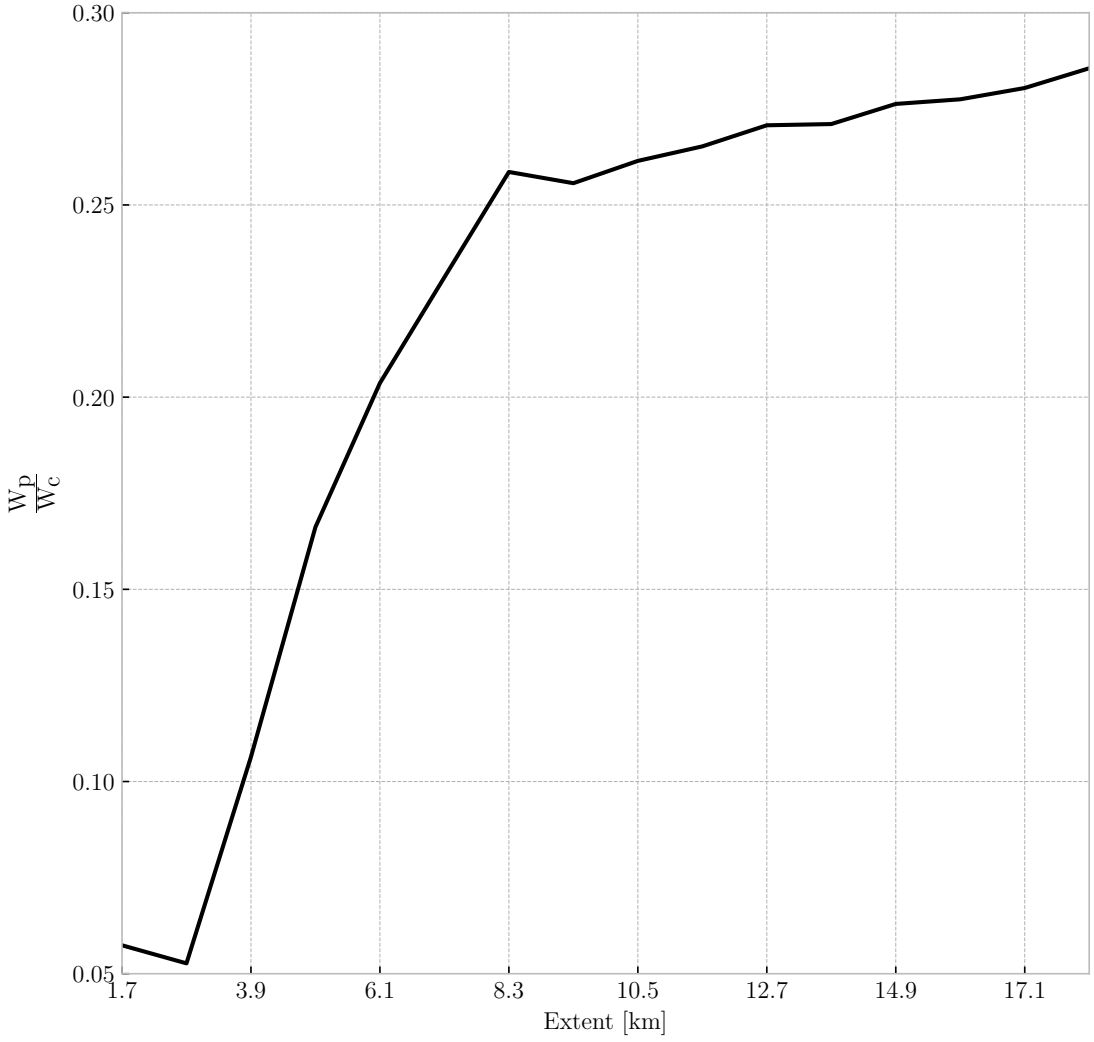

Figure 3.2: The median warm rain efficiency $\left(\frac{W_p}{W_c}\right)$ at a given median size (extent). Reprinted from Smalley and Rapp (2020a).

WRE is high in regions with relatively low SST. However, Figure 3.1e shows that fewer than 40 shallow cumulus objects are observed in a given gridbox over this region in four years, reducing confidence in WRE here. Together, Figures 3.1c and 3.1d indicate that the relationship between WRE and extent is complicated and potentially depends on cloud depth (which increases in the

tropics) and on environmental conditions including environmental moisture and aerosol loading.

To determine how WRE depends on cloud size, Figure 3.2 shows WRE as a function of cloud object extent. WRE follows a double power-law relationship, with WRE < 0.25 for cloud objects < 8.3 km and approaching 0.3 for cloud objects > 8.3 km. Similar to these results, earlier studies have shown a double power-law distribution in shallow cumulus size (e.g. Benner and Curry, 1998; Trivej and Stevens, 2010), which will be discussed in further detail later.

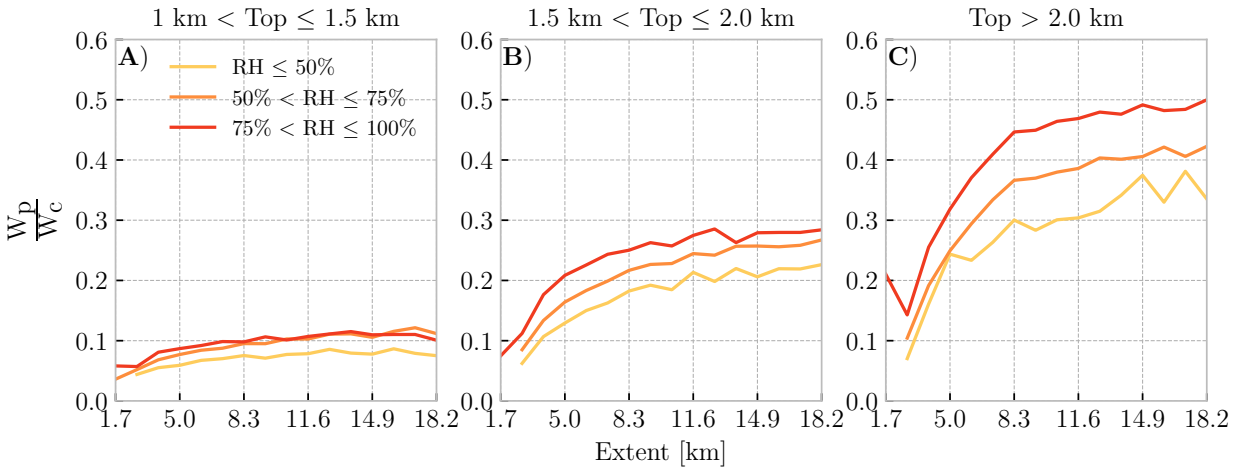

Figure 3.3: The median warm rain efficiency $\left(\frac{W_p}{W_c}\right)$ at a given median size (extent). The different line colors represent cloud objects separated by environmental moisture (< 3 km relative humidity). Reprinted from Smalley and Rapp (2020a).

To address the impact of environmental moisture and cloud depth on WRE, Figure 3.3 shows the relationship between WRE and cloud object extent conditioned using cloud-top height and < 3 km relative humidity. Holding environmental moisture constant, WRE depends strongly on cloud-top height with WRE nearly doubling for each 0.5km increase in cloud top height for a given extent. For a given RH and top height, there is also an increase in WRE with extent. Holding top height constant, there is also an increase in WRE with increasing environmental moisture; however, increases in WRE are dominated by changing cloud size (depth and extent).

To support the hypothesis that larger shallow cumulus can sustain a larger droplet field within

their cores to increase the precipitation efficiency, the variation in the VGZacross individual cloud objects is examined. We expect that VGZwill be a larger negative value near cloud center than cloud edge, especially as cloud size increases. As an example, Figure 3.4a shows the change in median VGZ_{CP} to VGZ_{CP} for cloud objects with an extent of 10.2 km. VGZ decreases from 10 dBZ km^1 at cloud object edge to approximately -20 dBZ km^1 at cloud object center. This demonstrates that larger droplets are present near cloud base near cloud object center compared to the edge. This implies, at least for extents of 10.5 km, drops grow larger near cloud object centers and may be more protected from mixing.

Figure 3.4b shows the relationship between VGZ_{CP} and VGZ_{CP} as a function of extent and top height. For a constant cloud-top height, VGZ_{CP} again follows a double power-law distribution. Specifically, the magnitude of the VGZ_{CP} rapidly increases from approximately 10 dBZ km^{-1} to 20 dBZ km^{-1} as extent approaches 8.3 km, while it plateaus around 20 dBZ km^{-1} for extents $>$ 8.3 km. Conversely, VGZ_{CP} decreases in magnitude, approaching 0 dBZ km^{-1} for the largest cloud object extents. However, it does not decrease as fast as VGZ_{CP}, implying that the change in vertical reflectivity gradient in the center of cloud is driving changes in differences from center to edge. Figure 3.4b also shows that the change in VGZ_{CP} depends on cloud-top height, with larger magnitudes for the tallest clouds. This is consistent with previous modeling studies that found larger shallow cumulus are more protected from entrainment (e.g. Burnet and Brenguier, 2010; Hernandez-Deckers and Sherwood, 2018), resulting in larger droplets (e.g. Moser and Lasher-Trapp, 2017) and a higher probability of rainfall (e.g. Smalley and Rapp, 2020b) in observations.

To determine how VGZ_{CP} influences the relationship between WRE and extent, Figure 3.4c shows WRE as a function of extent conditioned by top height and VGZ_{CP}, with WRE increasing as the magnitude of VGZ_{CP} increases. This, coupled with Figure 3.4b, illustrates that as shallow cumulus grows deeper and wider, drops at the center of the cloud can grow larger and scavenge more available cloud water. This is consistent with larger shallow cumulus being more efficient at producing rainfall, perhaps in part because they are less influenced by environmental mixing.

Until this point, this paper has focused on the impact of cloud size and environmental moisture

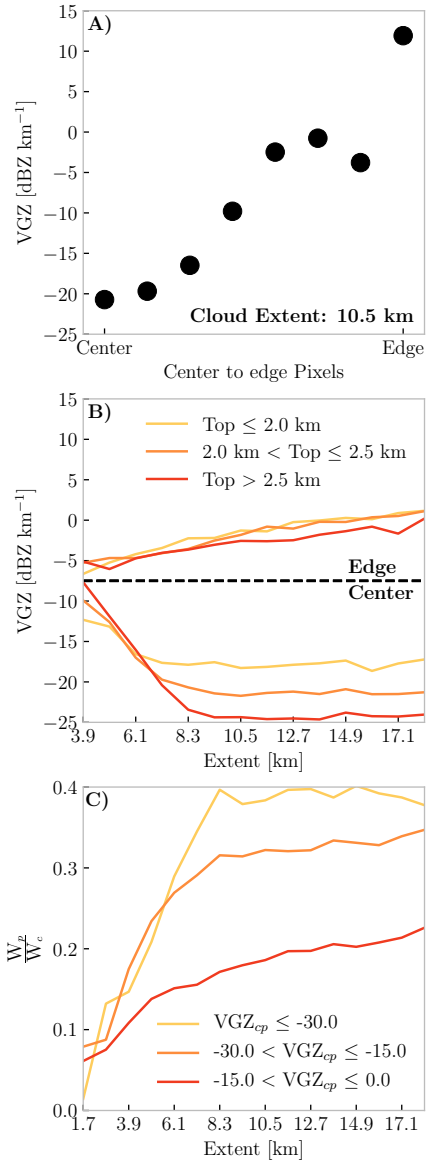

Figure 3.4: Panel A) shows the median change in the vertical reflectivity (VGZ) from the center to edge of all cloud objects with an extent of 10.5 km. Panel B) shows the median VGZ at the center (red) and edge (blue) of different sized (extent) raining cloud objects. Different lines represent cloud objects separated by top height. Panel C) shows the median warm rain efficiency ($\frac{W_P}{W_C}$) at a given median size (extent). The different line colors represent cloud objects separated by the vertical reflectivity gradient on the center pixel (VGZ_{cp}) of all cloud objects. Reprinted from Smalley and Rapp (2020a).

on WRE. However, it is also understood that aerosol concentrations influence both the number and size of droplets within a cloud, with larger aerosol concentrations resulting in a greater number of smaller droplets (e.g. Twomey, 1974; Albrecht, 1989). As a result, we hypothesize increasing

aerosol concentrations, which vary regionally (Figure 3.1f), increase the ratio of cloud droplets to raindrops, thus reducing WRE.

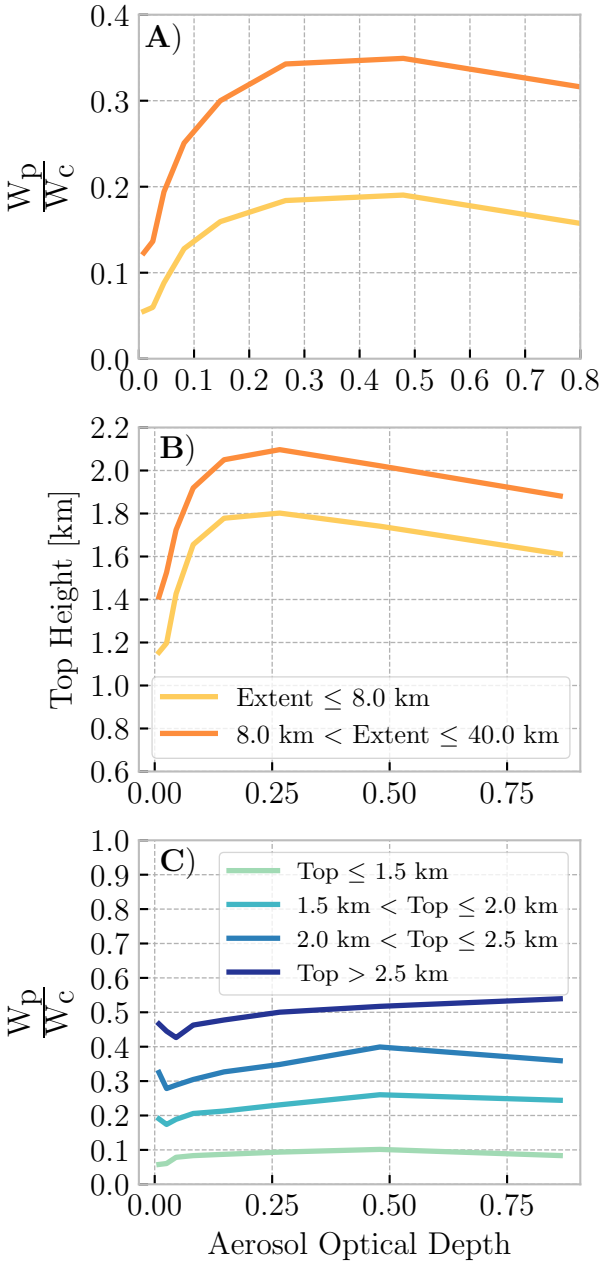

Figure 3.5: Panel A) shows the relationship between median warm rain efficiency as MODIS 550 nm aerosol optical depth. Panel B) shows the relationship between median cloud-top height and aerosol optical depth. Panel C) shows the relationship between warm rain efficiency $\left(\frac{W_p}{W_c}\right)$ and aerosol optical depth. Line colors in panels A) and B) represent cloud objects separated by extent, while line colors in panel C) represent cloud objects separated by top height. Reprinted from Smalley and Rapp (2020a).

Figure 3.5a shows the relationship between WRE and AOD, conditioned by top height. At first glance, it appears that WRE increases as a function of AOD, which contradicts the expectation of a shift in drop size distribution towards fewer large drops to initiate collision-coalescence which would reduce the amount of cloud water converted to rain water. However, disentangling aerosol-cloud interactions from other meteorological variables is quite difficult, as increasing aerosol concentrations are often correlated with other environmental variables (e.g. Koren et al., 2014).

Given the strong dependence of WRE on top height, we further examine the relationship between AOD and top height (Figure 3.5b), conditioned by extent. The curves shown in Figure 3.5a look similar to those shown in Figure 3.5b, suggesting the positive correlation between aerosols and top height are responsible for the observed relationship between AOD and WRE. Indeed, Figure 3.5c further supports this assertion. When conditioned by top height, WRE shows little dependence on AOD and suggests that the conversion from W_C to W_P is more sensitive to cloud depth than aerosols. While these results seem counterintuitive, this analysis examines clouds in which precipitation has been detected. Examination of the likelihood of precipitation shows the expected decrease with increasing AOD (not shown). These results imply that once the condensation-coalescence is initiated, aerosol loading has a smaller impact on the conversion of cloud water to rain than other cloud or environmental characteristics.

3.5 Summary and Discussion

This study uses the methodology described by Smalley and Rapp (2020b) to classify a large global shallow cumulus cloud object dataset from CloudSat and determine the relationship between WRE, cloud extent, environmental moisture, and aerosol loading. We find that WRE increases as a function of cloud size (top height and extent) and environmental moisture. Benner and Curry (1998) found a double-power law distribution in shallow cumulus thickness as a function of cloud diameter, and Trivej and Stevens (2010) hypothesized that the shift from one power-law distribution to another results from small shallow cumulus that can rapidly grow in size until reaching the trade inversion. We find a similar relationship between WRE and extent, showing that one distri-

bution exists with WRE increasing faster for extents < 8.3 km then slowly increasing above this breakpoint. Trivej and Stevens (2010) also found that environmental factors, particularly environmental moisture, become important once cloud-top height reaches the trade inversion. Our results show that WRE is most sensitive to environmental moisture above an extent of 8.3 km, which we assume represents the average extent where cloud objects reach the trade inversion.

Unexpectedly, we find that for a fixed cloud depth, WRE is fairly insensitive to AOD. One explanation may be that, although high AOD values do occur over the global ocean basins, the majority of cloud objects being sampled still form in relatively clean air, so the minority of cloud objects occurring over polluted regions have a small impact on the overall statistics. Another explanation may be that this analysis only includes precipitating clouds, so once collision-coalescence is initiated, the amount of cloud water converted to rain water is less influenced by aerosol concentrations.

Past studies conclude that precipitation efficiency increases as SST increases (Lau and Wu, 2003; Bailey et al., 2015; Lutsko and Cronin, 2018). Considering warmer SSTs tend to result in deeper clouds (e.g. Wood and Bretherton, 2004b) and more humid environments (e.g. Chen and Liu, 2016), it is reasonable to expect that WRE would increase in response (e.g. Lau and Wu, 2003). Our results show that WRE is highest near the equator where SSTs are warmest. However, the general relationship between cloud size (depth and extent), environmental moisture, and WRE suggests that WRE is more sensitive to cloud size than environmental moisture. To directly address the SST dependence, Figure 3.6 shows the frequency distribution of extents and the median WRE, both as a function of cloud-top height and SST. For a given cloud-top height, WRE does increase as a function of SST. However, for a fixed SST, WRE also increases as extent increases. Additionally, Figure 3.6 shows that the frequency distribution of cloud object sizes shifts toward more frequent larger extents with increasing SST. Together, these suggest that increasing WRE with SST shown in past studies not only results from the deepening clouds but also the shift towards more frequent larger clouds.

Prior literature has shown that modeled shallow cumulus cores become more adiabatic as they

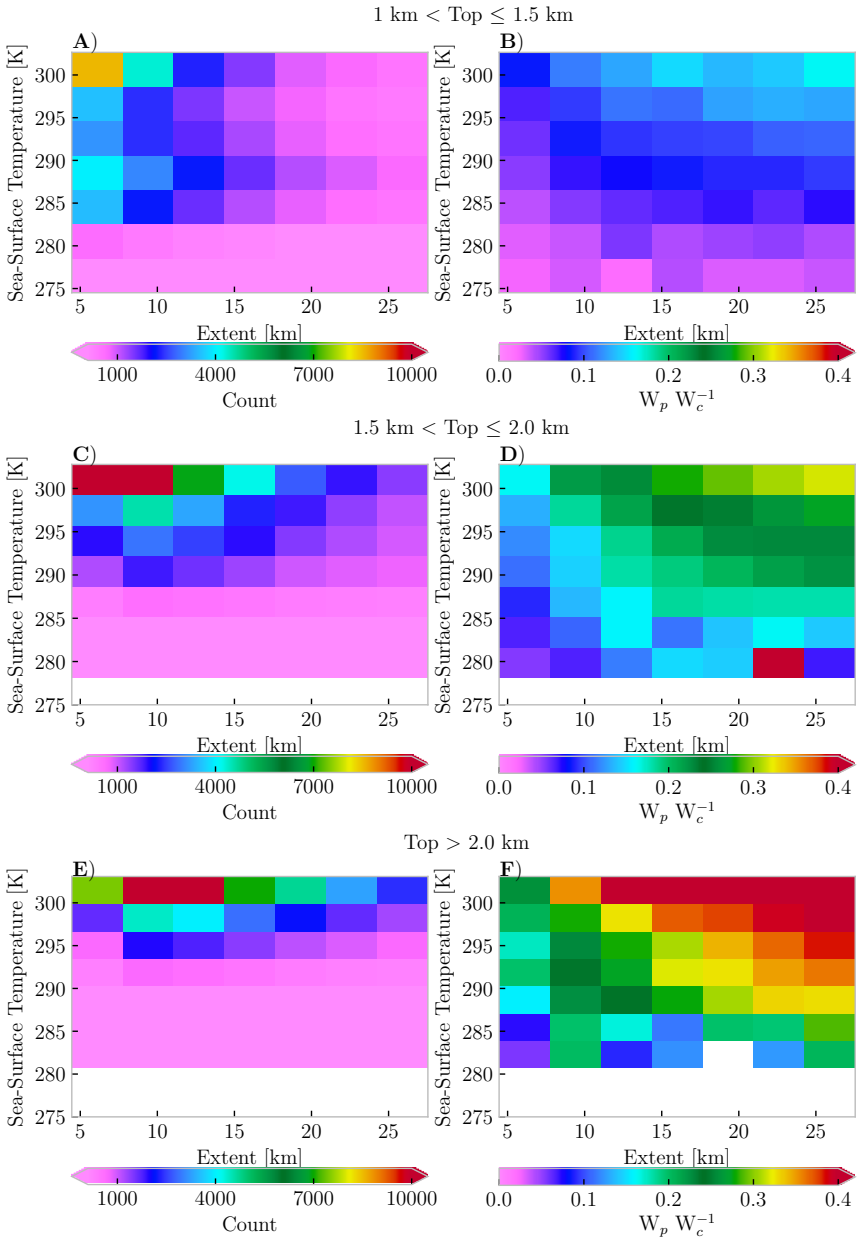

Figure 3.6: The two-dimensional distribution of extent as a function of sea-surface temperature, conditioned by cloud-top height, is shown in panels A), C), and E) respectively. The median warm rain efficiency (W_p W_c^{-1}) as a function of Extent and sea-surface temperature are shown in panels B), D), and F) respectively. Reprinted from Smalley and Rapp (2020a).

grow larger (Moser and Lasher-Trapp, 2017), potentially resulting in larger drops. Figure 3.6 and our analysis of the relationship between VGZ_{CP}, extent, and WRE suggest drop growth is being enhanced near the base at the center of larger cloud objects, potentially resulting in more cloud

water being scavenged by larger droplets and more efficient autoconversion and accretion processes. Most climate models parameterize autoconversion and accretion as functions of cloud and precipitation properties (e.g. Lohmann and Roeckner, 1996; Liu and Daum, 2004; Morrison et al., 2005; Lim and Hong, 2010; Lee and Baik, 2017), but recently enhancement factors that depend on variations and covariations in WC and WP have been introduced to correct for biases due to subgrid-scale Wc and Wp inhomogeneity (e.g. Lebsock et al., 2013; Boutle et al., 2014; Witte et al., 2019). Presumably, the dependence of these enhancement factors on Wc variability would capture the increase in WRE with cloud depth shown here, however it is unclear if these enhancement factors, which are based on the variance in Wc and Wp, capture the effects of cloud extent on WC and WP, and subsequently WRE. Our dataset provides an opportunity for a future analysis that could focus on investigating the relationship between subgrid-scale variability in WC, WP, WRE, and extent, which could help improve our understanding and simulation of precipitating shallow cloud processes in climate models.

4. THE IMPACT OF RAIN RATE, RAINING PATCH SIZE, AND SPACING ON SOUTHEASTERN PACIFIC CLOUD FRACTION TRANSITIONS

4.1 Abstract

Rain-induced cold pools are one mechanism by which transitions in cloud fraction in marine stratocumulus over the southeast Pacific occur. We use CloudSat/CALIPSO to identify raining patches within stratocumulus over the southeast Pacific, and then calculate the cloud fraction surrounding each raining patch, spacing, mean rain rate, and raining patch size (extent). The spatial patterns show that as cloud fraction decreases and rain rate increases from east to west, a minimum in spacing exists between 80°W-100°W, but the maximum extent occurs further west. Holding spacing constant, cloud fraction decreases with rain rate but increases with extent. Additionally, cloud fraction is generally lower between 80°W-100°W when cells are large. We attribute this behavior to the heavier rainfall associated with larger cells, which may result in possible cold pool interactions that could drive lower cloud fractions around the largest cells producing the most intense rainfall.

4.2 Introduction

Just off the west coasts of the major continents, large stratocumulus cloud decks that gradually transition from contiguous cloud layers to broken-cell trade cumulus toward the equator are common. These large cloud decks have a pronounced cooling effect on the surface (e.g. Hartmann et al., 1992), therefore it is important to understand how the extent of these clouds may change in response to climate change (e.g. Vial et al., 2013). Historically, the advection of humid sub-tropical air to warmer waters east of the major stratocumulus regions which results in a deeper boundary layer, has been viewed as a primary driver of stratocumulus transitions (e.g. Albrecht et al., 1995; Wyant et al., 1997; Bretherton and Wyant, 1997; Stevens, 2000; Wood and Bretherton, 2004b). As cool moist air is advected westward, it travels over progressively warmer water and regions with weaker subsidence aloft. Below the cloud layer, more stable air coupled with deeper and more

unstable air within the cloud layer decouples the surface from the cloud layer, allowing more vigorous updrafts to form within the cloud layer. These updrafts are able to penetrate the top of the boundary layer and mix drier air into the cloud layer, helping to break it apart (e.g. Wyant et al., 1997).

Modeling and regional observational-based studies have also hypothesized that rainfall can drive the development of closed to open cell transitions within stratocumulus decks. Rainfall induced transitions can occur by two mechanisms: 1) by removing cloud water from the cloud layer (Austin et al., 1995) and 2) by cold pool collisions (Comstock et al., 2005; Stevens et al., 2005; vanZanten and Stevens, 2005; Feingold et al., 2010; Yamaguchi and Feingold, 2015). Focusing on the second mechanism, the evaporation of drizzle and light rainfall induces downdrafts which spread out at the surface as cold pools. These cold pools may then collide and mechanically produce more intense updrafts that can induce turbulence at cloud top which mixes drier air down into the cloud layer from above the boundary layer helping to thin it out (e.g. Comstock et al., 2005).

During the VAMOS Ocean-Cloud-Atmosphere-Land Study (VOCALS) Regional Experiment over the southeast Pacific, Terai and Wood (2013) used aircraft observations to show that measurable cold pools typically do not form until rain rates exceed 1 mm day^{-1}. However, Yamaguchi and Feingold (2015) found that single raining patches producing locally heavy rainfall are insufficient in driving transitions in a cloud model. Specifically, Yamaguchi and Feingold (2015) found the distance between raining patches of stratocumulus important in determining if a transition to open-cell stratocumulus will occur. Observational cold pool horizontal sizes in this region are typically smaller than 50 km and rarely exceed 100 km (Terai and Wood, 2013). This implies that raining patches must typically be closer than 100 km for cold pool interactions that may drive transitions to occur. If spacing between cells is large, Yamaguchi and Feingold (2015) found that transitions occur slower, but only if the raining patches are producing heavy enough rainfall and/or raining patches are large enough for cold pool interactions to occur.

Most studies have used either cloud models (e.g. Feingold et al., 2010; Yamaguchi and Feingold, 2015; McGibbon and Bretherton, 2017) or field-campaign observations (e.g. Bretherton et al.,

2004; Terai and Wood, 2013; Abel et al., 2017; Cadeddu et al., 2020) to analyze the influence of rainfall on stratocumulus transitions. Although modeling and field-campaign studies may be better for investigating individual physical processes driving transitions, this limits analyses to specific regions and short time frames and may not be representative of climatological transitions. Satellites observations can provide a large enough sample size over a long enough time frame to analyze variability between raining patch characteristics and cloud fraction transitions over the southeast Pacific stratocumulus to shallow cumulus climatological transition region. CloudSat, in particular, is highly sensitive to the light precipitation produced by these clouds, and in conjunction with CALIPSO can provide a more holistic view of total cloud fraction over this region. Rapp (2016) used CloudSat and CALIPSO observations to investigate the influence of rainfall on these transitions and found cloud fraction changes faster around raining clouds than non-raining clouds within the southeast Pacific transition region. However, the relationship between raining patch size, spacing, intensity, and these cloud fraction transitions was not investigated. To fill these gaps, this study will use CloudSat and CALIPSO observations to test the hypothesis that *raining cell spacing minima, raining patch size maxima, or rain intensity maxima are present across a stratocumulus to shallow cumulus cloud fraction transition over the southeast Pacific.*

4.3 Data and Methods

CloudSat and CALIPSO are used to identify contiguous cloudy regions over the stratocumulus cloud fraction transition region in the southeast Pacific. CloudSat carries a near-nadir pointing 94-GHz radar (CPR; Tanelli et al., 2008) with a 1.7 x 1.4 km horizontal resolution and a 480 m pulse-length oversampled by a factor of 2 giving a vertical resolution of 240 m. The CPR is sensitive to both cloud and rain droplets, however, ground clutter in the nearest three bins (Tanelli et al., 2008) to the surface limit its usefulness closest to the ground. CALIPSO carries a lidar that has a higher resolution than CloudSat in the lowest 8 km, with a horizontal resolution of 333 m. CALIPSO is highly sensitive to small cloud droplets that would otherwise be missed by CPR and can sense droplets in the lowest part of the atmosphere that occurs in the ground clutter region. Using both

CloudSat and CALIPSO to identify cloudy regions gives a more holistic view of where clouds are occurring at any given time. We use the layer-top and layer-base products from 2B-GEOPROF-LIDAR (Mace and Zhang, 2014) to identify contiguous cloudy regions. This product stores up to 5 cloud-layers on any given pixel, but we only include single-layer clouds in this analysis, and we do consider a single-cloudy bin as contiguous.

Once we identify contiguous cloudy regions, we further subset the data into contiguous raining regions by only including regions where 2C-RAIN-PROFILE (Lebsock and L'Ecuyer, 2011b) rain rates are > 0 mm hr^{-1}. Contiguous raining regions must both be entirely below the freezing level and over the ocean. This is done by matching cloud-top height to the freezing level identified using ECMWF (Owens and Hewson, 2018) temperatures matched to CloudSat's track, which is stored in 2C-PRECIP-COLUMN (Haynes et al., 2009), and matching the navigation flag from 2B-GEOPROF (Marchand et al., 2008) to each pixel for the separation between land and ocean. Each contiguous raining region is stored as individual raining patches along with the mesoscale cloud fraction, rain patch along-track size (extent), and maximum rain rate for each raining patch. spacing is defined as the minimum nearest neighbor distance from one raining patch edge to the nearest other raining patch edge along CloudSat's orbit. The mesoscale cloud fraction surrounding the center pixel of each raining patch is calculated by averaging the ratio of cloudy pixels to the total number of pixels within a window between the raining patch edge and the nearest raining patch edge on either side. Raining patch extent is defined as the number of contiguous raining pixels multiplied by CloudSat's along-track resolution of 1.4 km.

As shown in Figure 4.1, this study focuses on the southeast Pacific between longitudes of 80°W and 120°W and latitudes between 10°S and 25°S. Analysis of stratocumulus transitions over the southeast Pacific has been investigated extensively by prior literature (e.g. Klein and Hartmann, 1993; Albrecht et al., 1995; Davis et al., 1996; Stevens et al., 2005; Wood, 2012; Rapp, 2016). Measurements are constrained to June 2006 - December 2010 because CloudSat stopped taking nighttime measurements after 2010 due to a battery anomaly (Witkowski et al., 2012).

4.4 Results

4.4.1 Entire Southeastern Pacific Domain

To analyze spatial patterns in the distribution of mean cloud fraction, mean rain rate, mean spacing, and mean size, raining patches are binned to a 2.5° x 2.5° grid over the southeast Pacific. Figure 4.1a shows that the number of raining patches sharply increases from the South American coast through 80°W, increasing from below 100 samples to $>$ 500 samples, with the largest number of raining patches occurring between longitudes of 80°W - 120°W and latitudes of 5°S - 25°S, before gradually tapering off towards the trade cumulus region. Focusing on cloud fraction, Figure 4.1b shows that cloud fraction decreases from east to west, with cloud fraction surrounding each raining patch $>$ 0.9 closest to the coast decreasing to values $<$ 0.7 west of 120°W. As shown in Figure 4.1c, the gradient in rain rates is aligned with the gradient in cloud fraction, however, the magnitude of rain rate increases from east to west with rain rate exceeding 1 mm hr^{-1} east of 105°W. Figure 4.1d shows that there is a minima in cell spacing between 80°W and 110°W and north of 25°, with values $<$ 50 km. Figure 4.1e shows small variations in size with the largest values approaching 7 km west of 105°W and then decreasing again to the west. The local minima in cell spacing across the climatological cloud fraction transition is consistent with our hypothesis; however, the local maxima in extent is east relative to the largest cloud fraction gradient.

The location of the local maxima in extent (Figure 4.1e) also appears to be co-located with the spatial maxima in rain rate. To identify any relationship between rain rate and extent, Figure 4.2a shows median rain rate as a function of extent. We find that rain rate and extent are positively correlated, with a correlation coefficient of 0.39. As a result, rain rates are generally below 0.02 mm hr^{-1} when raining patches are smaller than the median size (4.2 km), and rain rate does not exceed 0.5 mm hr^{-1} until raining patches reach a size of approximately 8.4 km. Overall, this result shows that rain rate is not independent of extent, and it is reasonable to expect that a larger raining patch will produce more intense rainfall.

Even though rain rate and extent are related, that does not necessarily mean that they both

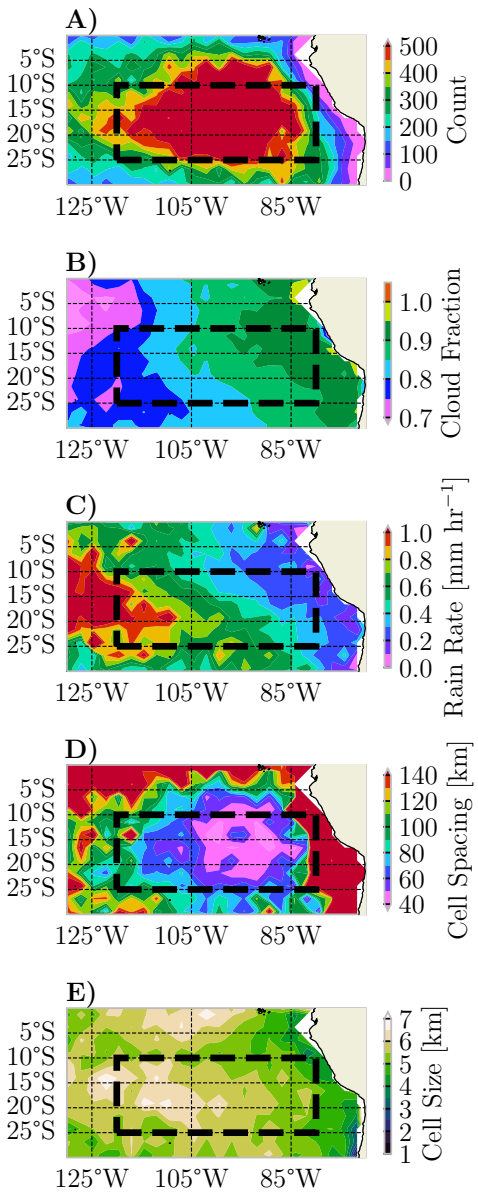

Figure 4.1: The spatial distribution of number of samples, cloud fraction, rain rate, raining patch spacing, and raining patch size are shown in panels A), B), C), D), and E) respectively. The dashed box represents the bounds of this analysis domain (10°S-25°S; 80°W-120°W).

influence cloud fraction in the same way. To test this, Figure 4.2b shows median cloud fraction as a function of rain rate, conditioned by extent. Opposite from what is expected if raining extent were important for cloud fraction transitions, cloud fraction increases around the raining cells when they are larger. However, cloud fraction decreases with increasing rain rate for all patch sizes, although

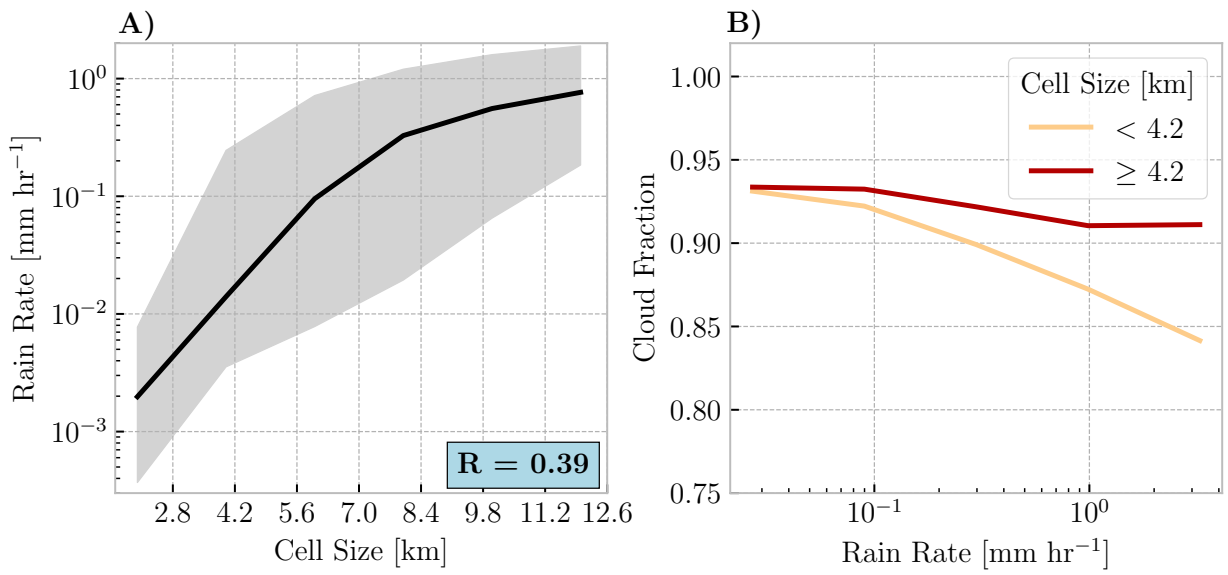

Figure 4.2: The median rain rate at a given raining patch size is shown in panel A). The gray region in panel A) represents the interquartile of rain rate as a function of raining patch size. Median cloud fraction at a given rain rate is shown in panel B), and the different line colors represent raining patches separated by raining patch size.

the effects appear to be larger for the smaller patch sizes. These figures imply that the intensity of precipitation may be more related to the surrounding cloud fraction than the patch size, despite the positive correlation between the two.

To further test the relative importance of patch size versus intensity, we calculate cloud fraction anomalies relative to the climatological mean surrounding a rain cell within each 2.5°x2.5° gridbox. We then average the anomalies for raining patches above and below the median patch size. Figure 4.3a shows the mean cloud fraction anomalies are negative between 80°W-100°W and 10°S-25°S, while anomalies are positive west of 100°W when raining patches are above the median size. The region of negative anomalies is generally co-located with the region of the closest raining patches (Figure 4.1d). Figure 4.3b shows that, even though mean rain rates are generally > 0.4 mm hr^{-1} spatially over the entire domain when raining patches are larger than the median size, the region of negative cloud fraction anomalies are generally aligned with the sharpest gradient in rain rate. Figure 4.3c shows opposite patterns in mean cloud fraction anomalies to those shown in Figure

4.3a when raining patches are smaller than the median size. However, Figure 4.3d shows rain rates are relatively constant from the coast to 105°W with values generally below 0.1 mm hr^{-1}. These results suggest that over the eastern portion of the domain, rain rate may be more related to the surrounding cloud fraction than extent because we would expect positive cloud fraction anomalies over this region when raining patches are largest if extent is driving the relationship.

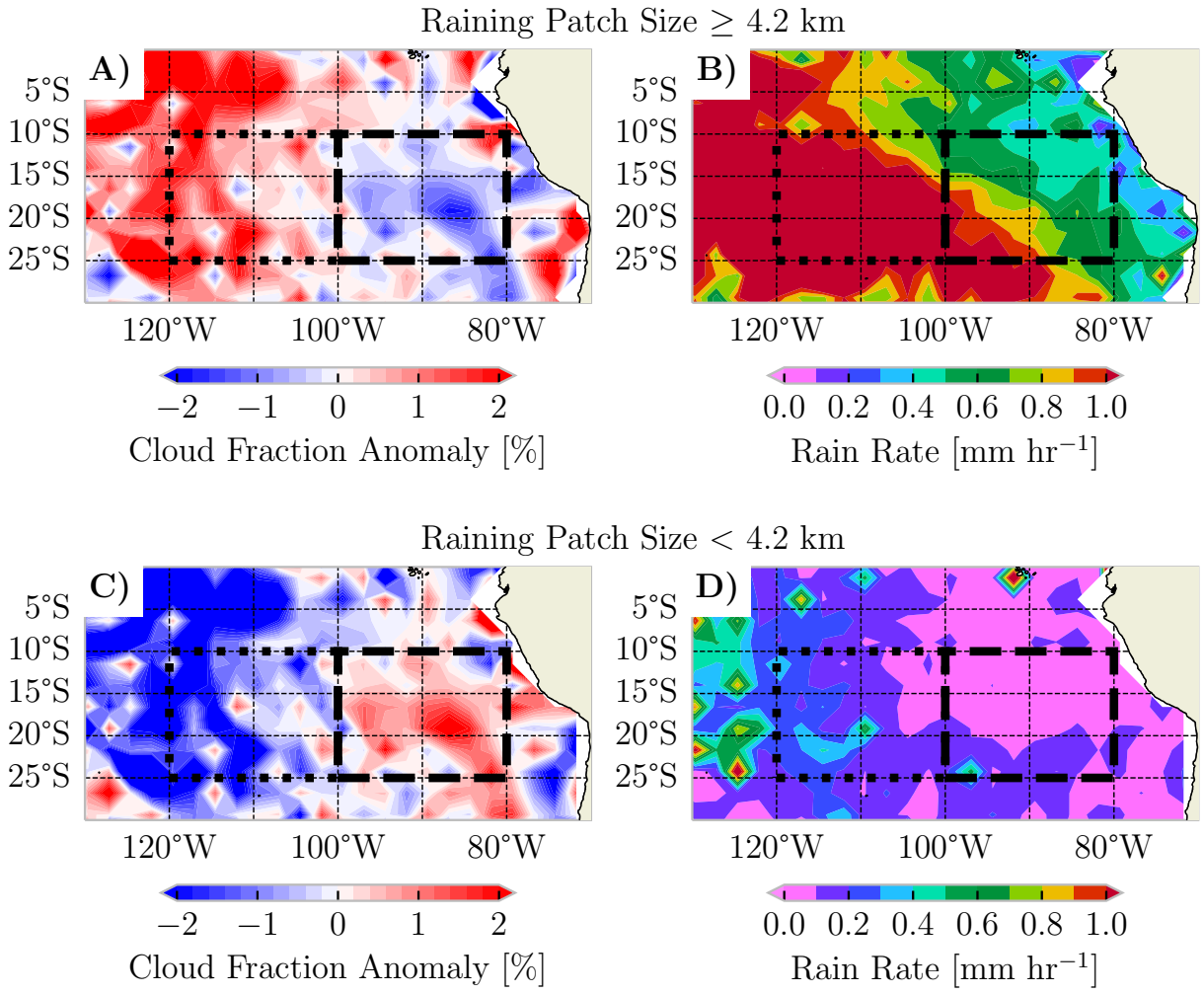

Figure 4.3: The spatial distribution of mean cloud fraction anomalies within each 2.5°x2.5° gridbox for raining patches ≥ km and those less than km are shown in panels A) and C) respectively. The spatial distribution of mean rain rate within each 2.5°x2.5° gridbox for raining patches ≥ km and those less than km are shown in panels B) and D) respectively. The dashed box represents the eastern region (10°S-25°S; 80°W-100°W), while the dotted line represents the western region (10°S-25°S; 100°W-120°W).

4.4.2 Eastern and Western Southeastern Pacific Regions

Figure 4.2b establishes that extent and rain rate have opposite relationships with cloud fraction across the southeast Pacific domain, and cloud fraction anomalies shown in Figures 4.3a and c suggest that rain rate may be more related to changes in surrounding cloud fraction east of 100°W than extent. To further analyze regional importance of extent and rain rate to changes in cloud fraction, the remainder of this analysis focuses on two subregions, an eastern domain (80°W and 100°W; 10°S and 25°S) and a western domain (100°W and 120°W; 10°S and 25°S).

To isolate the relative importance of rain rate to changes in cloud fraction over both regions, Figure 4.4 shows median cloud fraction as a function of spacing conditioned by extent (Figures 4.4a and b) and rain rate (Figures 4.4c and d). Over the western region, Figure 4.4a shows that cloud fraction decreases with spacing but varies little with extent. The relationship between cloud fraction and spacing found in Figure 4.4a is consistent between both the eastern and western regions and is not surprising because cloud fraction is calculated using the nearest-neighbor distances to the nearest two other raining patches. Conversely, over the eastern region, Figure 4.4b shows cloud fraction decreases faster with increasing spacing when raining patches are larger than the median size than it does when they are smaller, with cloud fraction differences approaching 3% as spacing approaches 100 km. Figure 4.4c shows the relationship between cloud fraction and spacing is relatively independent of rain rate, with cloud fraction decreasing at approximately the same rate during the most and least intense rainfall over the western region. Over the eastern region, Figure 4.4d shows cloud fraction decreases faster with spacing during the most intense rainfall, with differences of approximately 5 % between cloud fraction surrounding raining patches producing the most and least intense rainfall. The curves shown in Figures 4.4a and b look similar to those shown in Figures 4.4c and d. This suggests that decreases in cloud fraction with extent at given spacing over both regions are actually masking the importance of rain intensity, because of the positive correlation between rain rate and extent (Figure 4.2a) and the opposite influences of rain rate and extent on cloud fraction (Figure 4.2b).

Until this point, we have not made any inferences about the relative importance of the spacing

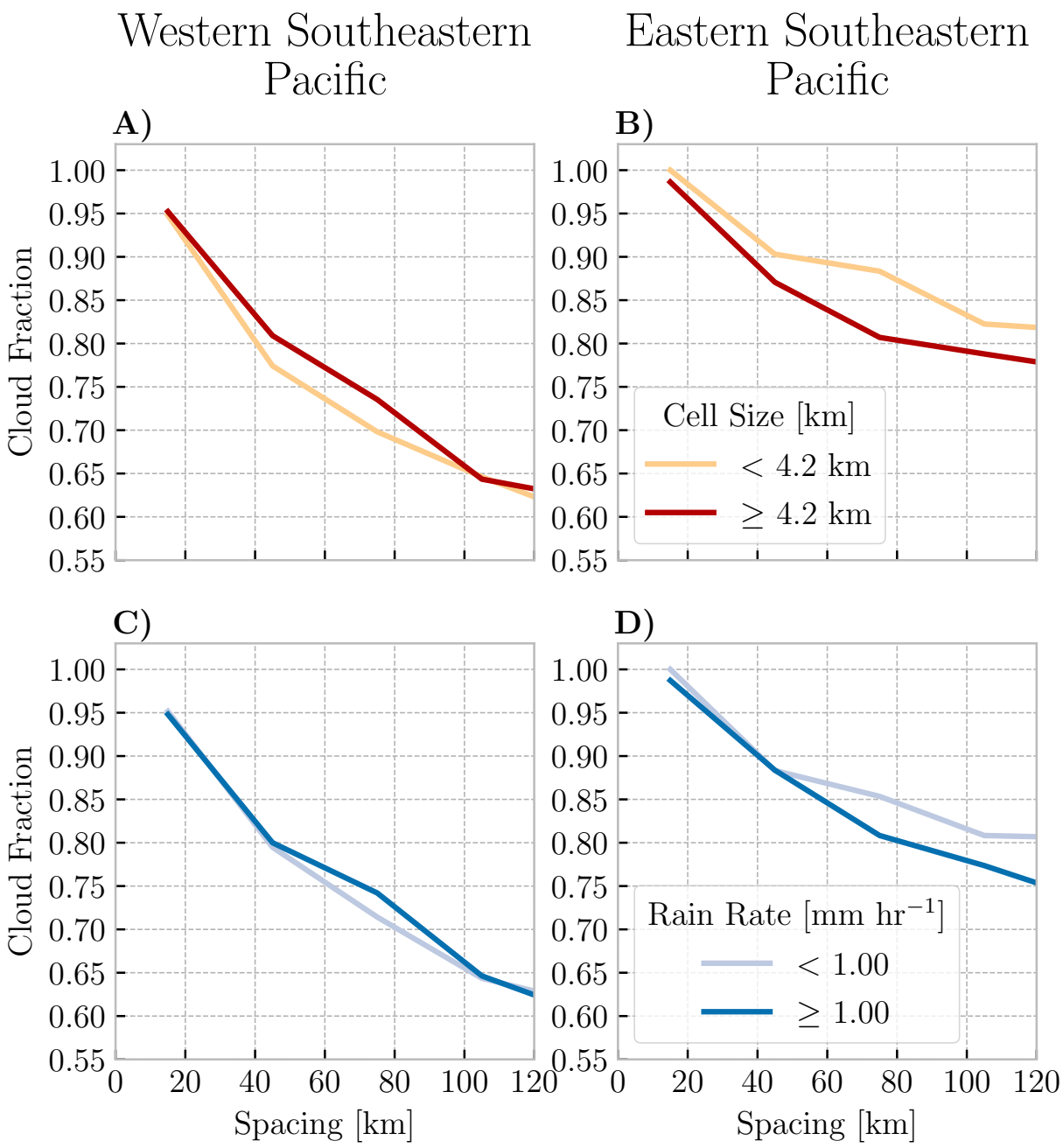

Figure 4.4: Median cloud fraction as a function of spacing over the eastern (80°-100°) portion of the southeast pacific are shown in panels A) and C). Median cloud fraction as a function of spacing western (100°-120°) portion of the southeast Pacific domain are shown in panels B) and D). Shades of red represent raining patches that are separated by size, while shades of blue represent raining patches that are separated by rain rate.

between raining patches to surrounding cloud fraction. Figure 4.5a and b show the joint relative frequency distributions of raining patches at a given spacing and rain rate over the western and eastern regions respectively. Over the eastern region, Figure 4.5b shows that raining patches most frequently produce either very light drizzle, with values below 0.02 mm hr^{-1}, or moderately heavy rainfall, with rain rates between 0.1 and 1.1 mm hr^{-1}, and are most frequently spaced within 100 km of each other. Relating this to cloud fraction, Figure 4.4d shows that cloud fraction decreases at approximately the same rate for rain intensities above and below 1 mm hr^{-1} until spacing reaches approximately 45 km, and once spacing exceeds 45 km, cloud fraction decreases faster when rain rate is highest. If we assume that cold pools typically do not develop until rain rates exceed 1 mm hr^{-1} and cold pool sizes generally range between 10 and 100 km (Terai and Wood, 2013), Figure 4.5b suggests that raining patches may be close enough together for cold pool interactions to occur (Yamaguchi and Feingold, 2015) over the eastern region, which may help explain the cloud fraction differences between the least and most intense rainfall shown in Figure 4.4d once spacing exceeds 45 km.

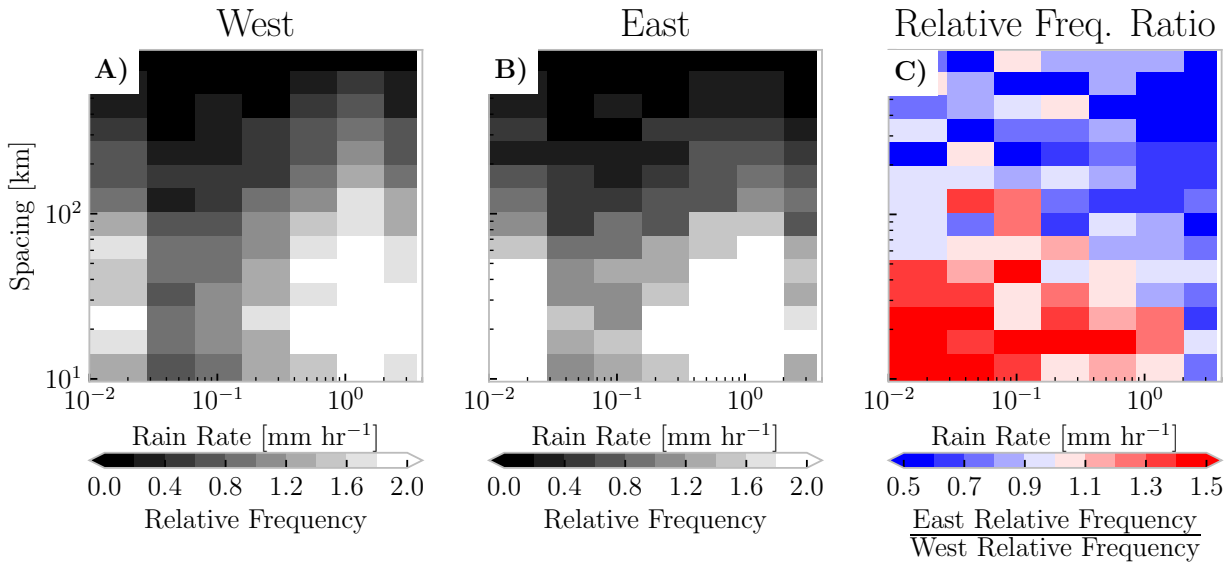

Figure 4.5: The relative frequencies of rain rate as a function of spacing over the western (100°-120°) and eastern (80°-100°) portions of the southeast Pacific domain are shown in panels A) and B). The ratio of the relative frequency over the eastern region to that over the western region is shown in panel C).

Figure 4.5a shows that most raining patches are within 100 km of each other over the western region as well. If this is the case, why are patterns shown in Figure 4.4c and d inconsistent? To address this, Figure 4.4c shows that cloud fraction is generally lower for any given spacing than that over the eastern region (Figure 4.4d). For raining patches within 100 km of each other, this implies that rain rate may not be as important to changes in cloud fraction because cloud fraction is lower, which may mean that the raining patches are simply too far apart for cold pool interactions to occur or stratocumulus transitions have already occurred.

Even though most raining patches are within 100 km of each other over the western region, Figure 4.5a shows that a larger fraction of raining patches are further than 100 km apart than over the eastern region (Figure 4.5b). To directly compare subregions, Figure 4.5c shows the ratio of relative frequency over the eastern to western regions. It shows more raining patches over the western region produce rain rates > 1 mm hr^{-1} than over the eastern region, but they tend to be further than 100 km apart. This implies that, although rain rates tend to be higher, raining patches are also more likely to be too far apart for any potential cold pool interactions to occur over the western region (Yamaguchi and Feingold, 2015).

4.5 Summary and Discussion

To test the hypothesis that *raining cell spacing minima, raining patch size maxima, or rain intensity maxima are present across a stratocumulus to shallow cumulus cloud fraction transition over the southeast Pacific.*, we identify and analyze individual contiguous raining patches along CloudSat/CALIPSO's orbit. We then calculate the cloud fraction surrounding each raining patch, minimum spacing, extent, and mean rain rate and analyze the relationships between them. Contrary to our hypothesis that increasing rain extent would be related to regions with lower cloud fractions, cloud fraction increases with extent; however, it does decrease with increasing rain rate. This decrease in cloud fraction with rain rate was also shown in Rapp (2016) with the cloud fraction surrounding raining CloudSat pixels being approximately 5% lower when rain rate is highest than when it is the lowest.

As hypothesized, a local minimum in raining patch spacing exists between 80°W and 110°W with raining patches generally < 50 km apart, which falls within the typical size range of cold pools of 10 - 100 km (Terai and Wood, 2013). Additionally, the sharpest gradient in rain rate is co-located with the minima in cell spacing. This, coupled with raining patches closer than 100 km together, suggests that cold pool collisions could occur in this region which may promote stratocumulus transitions (Yamaguchi and Feingold, 2015). Unlike spacing, extent remains relatively constant across the cloud transition region. This may be partially because most raining patches are smaller than 8.4 km, and Cloudsat cannot resolve fine enough horizontal scales to adequately capture the small-scale variability in extent due to its along-track resolution of 1.4 km.

Wood and Hartmann (2006) used a neural network to classify the mesoscale organization of cellular convection into closed, open, and organized, and they found that cellular organization transitioned from closed cell stratocumulus closest to the coast to organized open pockets of shallow cumulus between 85°W and 100°W to unorganized shallow cumulus west of 100°W over the southeast pacific. Rapp (2016) and Smalley and L'Ecuyer (2015) identified a similar region west of the South American coast between 80°W and 100°W where cloud fraction surrounding raining CloudSat pixels decreases faster than cloud fraction surrounding non-raining pixels. We found anomalously low cloud fraction surrounding larger raining patches occur in a similar region to that shown by these studies, and Rapp (2016) hypothesized that, between the regions of organized closed stratocumulus and unorganized shallow cumulus (Wood and Hartmann, 2006), precipitation is intense enough, raining patches are large enough, and/or raining patches are close enough together for cold pools to interact and cloud fraction transitions to occur. Focusing on the relationship between rain rate and extent, we find that cloud fraction anomalies are negative here and co-located and oriented with the gradient in rain rate when raining patches are large. Given the positive correlation between extent and rain rate, this suggests that rain rate may be more important to changes in cloud fraction because rain rate is positively correlated with extent, and we would expect rain rate to drive cold pool strength (Terai and Wood, 2013). If rain rate is driving transitions, our results imply that cold pool interactions do not begin until raining patches are approximately

40 km apart, which is within the typical range of cold pool sizes found by Terai and Wood (2013). We speculate that CloudSat's limited nadir-only observations and its orbit orientation relative to the climatological wind trajectories (Sandu et al., 2010) may not effectively sample spacings below 40 km across this cloud fraction transition.

We also find that cloud fraction differences between the raining patch subsets producing the least and most intense rainfall do not become noticeably different until spacing exceeds 80 km, or within the upper range of cold pool sizes (Terai and Wood, 2013). Terai and Wood (2013) speculated that large cold pools are often associated with cold pool clusters, but Yamaguchi and Feingold (2015) hypothesized that rain cell extent becomes important for cloud fraction transitions to occur if the distance between raining patches is large. Our results are more consistent with Yamaguchi and Feingold (2015), because larger raining patches are more likely to produce more intense rainfall which may drive more intense cold pools that could travel further distances (Terai and Wood, 2013).

Over the western region, cloud fraction anomalies are almost always positive when raining patches are large, even though rain rates are on average higher than the eastern region. Not only are cloud fractions typically lower but distances between raining patches are larger here, this implies that cold pool interactions are less likely to occur (Yamaguchi and Feingold, 2015). As a result, it is more likely that lower cloud fractions result from the boundary layer decoupling from the surface due to daytime heating (Burleyson et al., 2013) west of 100°W, which would be correlated with both more intense rainfall and lower cloud fractions (e.g. Wyant et al., 1997).

Considering extensive literature has shown that both cloud fraction and rain rate have a seasonal (e.g. Klein and Hartmann, 1993; Lin et al., 2009; Rapp et al., 2013) dependence, it is reasonable to expect similar seasonal patterns in our results. Cloud fraction is highest with the furthest westward extent during southern hemispheric winter (Klein and Hartmann, 1993), while rainfall is most frequently closest to the coast (Rapp et al., 2013). Further analysis is needed to analyze the seasonal differences in rain rate, extent, and spacing; however, it will need to be cleverly designed to minimize CloudSat/CALIPSO sampling issues or will need to rely on another dataset.

Similar to the seasonal variability in cloud fraction and rain rates, earlier studies found a pronounced diurnal cycle in stratocumulus (e.g. Bretherton et al., 2004; Burleyson et al., 2013; Burleyson and Yuter, 2015), with larger cloud fractions and most intense rainfall occurring over a much wider area during the night (Rapp et al., 2013; Burleyson et al., 2013; Burleyson and Yuter, 2015). The highest cloud fractions recede toward the coast and rain rates recede towards the western portion of the region during the day. Any analysis of precipitation induced transitions is more difficult during the day because daytime heating also acts to uncouple the boundary layer (Burleyson et al., 2013) which can thin stratocumulus but also lead to deeper, more intense raining patches. During the night, it is easier to isolate the influence of rainfall on transitions due to the lack of solar heating. It is more difficult to do a similar analysis for day and night due to sampling limitations, but we do not think that day/night differences influenced our results since most raining patches were sampled during the night.

Stratocumulus transitions remain difficult to represent within climate models (e.g Teixeira et al., 2011). Recent studies have improved parameterizations to better capture stratocumulus transitions in response to changes in temperature and boundary layer depth which have been applied to climate models (Bogenschutz and Krueger, 2013; Guo et al., 2015), however, climate models struggle to simulate the impact of mesoscale organization on transitions due to inadequate parameterizations of sub-scale features responsible (e.g. Pawlowska and Brenguier, 2003; Bretherton and Blossey, 2014). Our study adds to prior observational work suggesting that organization of precipitation, specifically the relationship between rain intensity and spacing between raining patches, is important to cloud fraction transitions (e.g. Wood and Hartmann, 2006; Smalley and L'Ecuyer, 2015; Rapp, 2016). As a result, we speculate that climate model parameterization representations of subgrid scale mesoscale organization in response to precipitation must be improved to better represent its influence on cloud fraction transitions.

5. CONCLUSIONS

The characteristics of raining shallow and stratocumulus have primarily been investigated using LES models and regional ground and air-based observations (e.g., Zuidema et al., 2012; Dagan et al., 2016; Jung et al., 2016b,a; Korolev et al., 2016; Pinsky et al., 2016b,a). LES models have been used to analyze the influence of factors including entrainment, environmental moisture, aerosols, and organization on warm rain. While these types of studies are important to understanding small-scale cloud processes, they may not completely represent the real-world observations. Most observational-based studies that have been conducted that look into the influence of these factors on warm rain production are constrained regionally and temporally. This dissertation addresses these issues by analyzing the characteristics of raining low clouds using global CloudSat/CALIPSO satellite observations. This allows us to sample clouds producing light precipitation below sensor limits of other platforms as well as over a long time frame and globally.

Initial work (Chapter 2) focuses on the first hypothesis stating that *larger marine shallow cumulus and/or shallow cumulus occurring in a wetter environment are more likely to produce warm rain*. This is tested by identifying individual marine shallow cumulus cloud objects along CloudSat/CALIPSO's orbit between 2006 and 2010. We then analyzed the likelihood of warm rain as a function of extent and conditioned that relationship by environmental moisture. In general, we found that warm rain likelihood increases as a function of extent. Holding extent and top height constant, we found rain likelihood increases with environmental moisture, and, holding extent and environmental moisture constant, we found rain likelihood increases with cloud-top height. These results are consistent with prior modeling studies that found as shallow cumulus grow larger and/or environmental moisture increases, their updrafts become more protected from entrainment and they become more likely to produce precipitation (e.g., Heus et al., 2009; Burnet and Brenguier, 2010). To improve the representation of shallow cumulus precipitation in climate models, our results imply that shallow cumulus horizontal size may be important for constraining the influence of entrainment on updraft strength and subsequently rainfall production.

If warm rain likelihood is increasing partially because shallow cumulus updraft cores are less likely to experience environmental mixing, this suggests that cloud cores within larger shallow cumulus are potentially more adiabatic and may have more efficient rainfall production. This led us to test the hypothesis (Chapter 3) that *WRE is higher in larger shallow cumulus and is modulated by environmental moisture and aerosol loading*. We tested this by identifying raining shallow cumulus cloud objects using only CloudSat and then computing the ratio of cloud water to rain water as WRE. We then conditionally sampled the cloud objects by cloud-top height, environmental moisture, AOD, and SST to analyze the relationship between WRE and extent. In general, we found that WRE increases with extent, and it also increases with both cloud-top height and environmental moisture. Surprisingly, we found that WRE does not change much with AOD. We speculate that this may be because once drop formation begins, aerosols may not be as important as cloud depth or environmental moisture to WRE. As found by other studies, we found that WRE increases with SST. Considering, WRE is dependent on cloud-top height, extent, SST, and that larger cloud objects are more frequent when SSTs are higher, our results suggest that higher WRE with increasing SSTs are not only due to deeper clouds, but also an increasing frequency of larger clouds which may have more protected updrafts. This suggests that to improve representations of autoconversion and accretion in climate models, model parameterizations not only need to account for cloud depth but may need to account for cloud size as well.

The final part of this dissertation (Chapter 4) focuses on the impacts of the mesoscale organization of raining cells on stratocumulus to shallow cumulus transitions in the southeastern Pacific. Given prior studies that found rain intensity, raining patch size, and the spacing between raining patches are important to cloud fraction transitions in the formation of open pockets of shallow cumulus (Comstock et al., 2005; Stevens et al., 2005; vanZanten and Stevens, 2005; Feingold et al., 2010; Yamaguchi and Feingold, 2015), we tested the hypothesis that *raining cell spacing minima, raining patch size maxima, or rain intensity maxima are present across a stratocumulus to shallow cumulus cloud fraction transition over the southeast Pacific.*. This was accomplished by identifying individual contiguous raining patches along CloudSat/CALIPSO's orbit within the southeast Pa-

cific, then by calculating the mean cloud fraction surrounding each raining patch, nearest-neighbor spacing to the closest other raining patch, and raining patch size to analyze any potential influences of rainfall on cloud fraction transitions. We find that cloud fraction decreases but rain rate increases from east to west across the southeast Pacific. Between 80°W-100°W, there is a minimum in spacing, but the maximum in raining patch size occurs further west. Holding spacing constant, we find that cloud fraction decreases with rain rate but increases with raining patch size. Co-located with the minima in spacing and maximum gradient in rain rate, cloud fraction is generally lower in the presence of larger raining patches. We attribute this to the most intense rainfall generally being associated with larger raining patches. Considering cold pool sizes over this region typically range from 10-100 km Terai and Wood (2013), we speculate that cold pool interactions driven by the heaviest rainfall are possibly contributing to differences in cloud fraction. This adds to prior observational findings that show precipitation is important for stratocumulus transitions (e.g. Wood and Hartmann, 2006; Smalley and L'Ecuyer, 2015; Rapp, 2016), and implies that the effects of mesoscale organization of rainfall may be important for parameterizations in climate models to better capture changes in subtropical low cloud fraction.

Even though satellites cannot be used to analyze the actual cloud processes that may affect warm rain production, this dissertation research demonstrates that they can be used to look at cloud characteristics globally and for relatively long time-periods, which can provide insight into potential factors important to warm rain production and its effects including entrainment, environmental moisture, aerosols, and organization.

REFERENCES

Abel, S. J., and Coauthors, 2017: The Role of Precipitation in Controlling the Transition from Stratocumulus to Cumulus Clouds in a Northern Hemisphere Cold-Air Outbreak. *Journal of the Atmospheric Sciences*, **74 (7)**, 2293–2314, doi:10.1175/JAS-D-16-0362.1, URL https://doi.org/10.1175/JAS-D-16-0362.1, https://journals.ametsoc.org/jas/article-pdf/74/7/2293/4764242/jas-d-16-0362_1.pdf.

Albrecht, B. A., 1989: Aerosols, cloud microphysics, and fractional cloudiness. *Science*, **245 (4923)**, 1227–1230, doi:10.1126/science.245.4923.1227, URL https://science.sciencemag.org/content/245/4923/1227, https://science.sciencemag.org/content/245/4923/1227.full.pdf.

Albrecht, B. A., C. S. Bretherton, D. Johnson, W. H. Scubert, and A. S. Frisch, 1995: The Atlantic Stratocumulus Transition Experiment—ASTEX. *Bulletin of the American Meteorological Society*, **76 (6)**, 889–904, doi:10.1175/1520-0477(1995)076<0889:TASTE>2.0.CO;2, URL https://doi.org/10.1175/1520-0477(1995)076<0889:TASTE>2.0.CO;2, https://journals.ametsoc.org/bams/article-pdf/76/6/889/3727921/1520-0477(1995)076_0889_taste_2_0_co_2.pdf.

Anselmo, T., and Coauthors, 2007: Cloud-aerosol lidar infrared pathfinder satellite observations (calipso). Tech. Rep. PC-SCI-503, Langley Research Center, Hampton, Virginia.

Austin, P., Y. Wang, V. Kujala, and R. Pincus, 1995: Precipitation in Stratocumulus Clouds: Observational and Modeling Results. *Journal of the Atmospheric Sciences*, **52 (13)**, 2329–2352, doi:10.1175/1520-0469(1995)052<2329:PISCOA>2.0.CO;2, URL https://doi.org/10.1175/1520-0469(1995)052<2329:PISCOA>2.0.CO;2, https://journals.ametsoc.org/jas/article-pdf/52/13/2329/3427434/1520-0469(1995)052_2329_piscoa_2_0_co_2.pdf.

Austin, R. T., A. J. Heymsfield, and G. L. Stephens, 2009: Retrieval of ice cloud microphysical parameters using the cloudsat millimeter-wave radar and temperature. *Journal of Geophysical Research: Atmospheres*, **114 (D8)**, doi:10.1029/2008JD010049, URL https://agupubs.onlinelibrary.wiley.com/doi/abs/10.1029/2008JD010049, https://agupubs.onlinelibrary.wiley.com/doi/pdf/10.1029/2008JD010049.

Bailey, A., J. Nusbaumer, and D. Noone, 2015: Precipitation efficiency derived from isotope ratios in water vapor distinguishes dynamical and microphysical influences on subtropical atmospheric constituents. *Journal of Geophysical Research: Atmospheres*, **120 (18)**, 9119–9137, doi:10.1002/2015JD023403, URL https://agupubs.onlinelibrary.wiley.com/doi/abs/10.1002/2015JD023403, https://agupubs.onlinelibrary.wiley.com/doi/pdf/10.1002/2015JD023403.

Beard, K. V., and H. T. Ochs, 1993: Warm-rain initiation: An overview of microphysical mechanisms. *Journal of Applied Meteorology*, **32 (4)**, 608–625, doi:10.1175/1520-0450(1993)032<0608:WRIAOO>2.0.CO;2, URL https://doi.org/10.1175/1520-0450(1993)032<0608:WRIAOO>2.0.CO;2, https://doi.org/10.1175/1520-0450(1993)032<0608:WRIAOO>2.0.CO;2.

Behrangi, A., Y. Tian, B. H. Lambrigtsen, and G. L. Stephens, 2014: What does CloudSat reveal about global land precipitation detection by other spaceborne sensors? *Water Resources Research*, **50 (6)**, 4893–4905, doi:10.1002/2013wr014566, URL https://doi.org/10.1002%2F2013wr014566.

Benner, T. C., and J. A. Curry, 1998: Characteristics of small tropical cumulus clouds and their impact on the environment. *Journal of Geophysical Research: Atmospheres*, **103 (D22)**, 28 753–28 767, doi:10.1029/98JD02579, URL https://agupubs.onlinelibrary.wiley.com/doi/abs/10.1029/98JD02579, https://agupubs.onlinelibrary.wiley.com/doi/pdf/10.1029/98JD02579.

Bogenschutz, P. A., and S. K. Krueger, 2013: A simplified pdf parameterization of subgrid-scale clouds and turbulence for cloud-resolving models. *Journal of Advances in Modeling Earth Systems*, **5 (2)**, 195–211, doi:10.1002/jame.20018, URL https://agupubs.onlinelibrary.wiley.com/doi/abs/10.1002/jame.20018, https://agupubs.onlinelibrary.wiley.com/doi/pdf/10.1002/jame.20018.

Bony, S., and J.-L. Dufresne, 2005: Marine boundary layer clouds at the heart of tropical cloud feedback uncertainties in climate models. *Geophysical Research Letters*, **32 (20)**, doi:10.1029/2005GL023851, URL https://agupubs.onlinelibrary.wiley.com/doi/abs/10.1029/2005GL023851, https://agupubs.onlinelibrary.wiley.com/doi/pdf/10.1029/2005GL023851.

Boutle, I. A., S. J. Abel, P. G. Hill, and C. J. Morcrette, 2014: Spatial variability of liquid cloud and rain: observations and microphysical effects. *Quarterly Journal of the Royal Meteorological Society*, **140 (679)**, 583–594, doi:10.1002/qj.2140, URL https://rmets.onlinelibrary.wiley.com/doi/abs/10.1002/qj.2140, https://rmets.onlinelibrary.wiley.com/doi/pdf/10.1002/qj.2140.

Bretherton, C. S., and P. N. Blossey, 2014: Low cloud reduction in a greenhouse-warmed climate: Results from lagrangian les of a subtropical marine cloudiness transition. *Journal of Advances in Modeling Earth Systems*, **6 (1)**, 91–114, doi:10.1002/2013MS000250, URL https://agupubs.onlinelibrary.wiley.com/doi/abs/10.1002/2013MS000250, https://agupubs.onlinelibrary.wiley.com/doi/pdf/10.1002/2013MS000250.

Bretherton, C. S., J. R. McCaa, and H. Grenier, 2004: A new parameterization for shallow cumulus convection and its application to marine subtropical cloud-topped boundary layers. part i: Description and 1d results. *Monthly Weather Review*, **132 (4)**, 864–882, doi:10.1175/1520-0493(2004)132<0864:ANPFSC>2.0.CO;2, URL https://doi.org/10.1175/1520-0493(2004)132<0864:ANPFSC>2.0.CO;2, https://doi.org/10.1175/1520-0493(2004)132<0864:ANPFSC>2.0.CO;2.

Bretherton, C. S., and M. C. Wyant, 1997: Moisture transport, lower-tropospheric stability, and decoupling of cloud-topped boundary layers. *Journal of the Atmospheric Sciences*, **54 (1)**, 148–167, doi:10.1175/1520-0469(1997)054<0148:MTLTSA>2.0.CO;2, URL https://doi.org/10.1175/1520-0469(1997)054<0148:MTLTSA>2.0.CO;2, https://doi.org/10.1175/1520-0469(1997)054<0148:MTLTSA>2.0.CO;2.

Burleyson, C. D., S. P. de Szoeke, S. E. Yuter, M. Wilbanks, and W. A. Brewer, 2013: Ship-Based Observations of the Diurnal Cycle of Southeast Pacific Marine Stratocumulus Clouds and Precipitation. *Journal of the Atmospheric Sciences*, **70 (12)**, 3876–3894, doi:10.1175/JAS-D-13-01.1, URL https://doi.org/10.1175/JAS-D-13-01.1, https://journals.ametsoc.org/jas/article-pdf/70/12/3876/3924077/jas-d-13-01_1.pdf.

Burleyson, C. D., and S. E. Yuter, 2015: Patterns of Diurnal Marine Stratocumulus Cloud Fraction Variability*. *Journal of Applied Meteorology and Climatology*, **54 (4)**, 847–866, doi:10.

1175/JAMC-D-14-0178.1, URL https://doi.org/10.1175/JAMC-D-14-0178.1, https://journals.ametsoc.org/jamc/article-pdf/54/4/847/3581713/jamc-d-14-0178_1.pdf.

Burnet, F., and J.-L. Brenguier, 2010: The onset of precipitation in warm cumulus clouds: An observational case-study. *Quarterly Journal of the Royal Meteorological Society*, n/a–n/a, doi:10.1002/qj.552, URL https://doi.org/10.1002%2Fqj.552.

Cadeddu, M. P., V. P. Ghate, and M. Mech, 2020: Ground-based observations of cloud and drizzle liquid water path in stratocumulus clouds. *Atmospheric Measurement Techniques*, **13 (3)**, 1485–1499, doi:10.5194/amt-13-1485-2020, URL https://amt.copernicus.org/articles/13/1485/2020/.

Chen, B., and C. Liu, 2016: Warm organized rain systems over the tropical eastern pacific. *Journal of Climate*, **29 (9)**, 3403–3422, doi:10.1175/jcli-d-15-0177.1, URL https://doi.org/10.1175%2Fjcli-d-15-0177.1.

Christensen, M. W., G. L. Stephens, and M. D. Lebsock, 2013: Exposing biases in retrieved low cloud properties from CloudSat: A guide for evaluating observations and climate data. *Journal of Geophysical Research: Atmospheres*, **118 (21)**, 12,120–12,131, doi:10.1002/2013jd020224, URL https://doi.org/10.1002%2F2013jd020224.

Comstock, K. K., C. S. Bretherton, and S. E. Yuter, 2005: Mesoscale Variability and Drizzle in Southeast Pacific Stratocumulus. *Journal of the Atmospheric Sciences*, **62 (10)**, 3792–3807, doi:10.1175/JAS3567.1, URL https://doi.org/10.1175/JAS3567.1, https://journals.ametsoc.org/jas/article-pdf/62/10/3792/3478264/jas3567_1.pdf.

Cooper, W. A., S. G. Lasher-Trapp, and A. M. Blyth, 2013: The influence of entrainment and mixing on the initial formation of rain in a warm cumulus cloud. *Journal of the Atmospheric Sciences*, **70 (6)**, 1727–1743, doi:10.1175/jas-d-12-0128.1, URL https://doi.org/10.1175%2Fjas-d-12-0128.1.

Cronk, H., and P. Partain, 2017: Cloudsat ecmwf-aux auxillary data product process description and interface control document. Tech. rep., Colorado State University.

Cronk, H., and P. Partain, 2018: Cloudsat mod06-aux auxiliary data process description and interface control document. Tech. rep., Colorado State University.

Dagan, G., I. Koren, and O. Altaratz, 2018: Quantifying the effect of aerosol on vertical velocity and effective terminal velocity in warm convective clouds. *Atmospheric Chemistry and Physics*, **18 (9)**, 6761–6769, doi:10.5194/acp-18-6761-2018, URL https://doi.org/10.5194%2Facp-18-6761-2018.

Dagan, G., I. Koren, O. Altaratz, and R. H. Heiblum, 2016: Aerosol effect on the evolution of the thermodynamic properties of warm convective cloud fields. *Scientific Reports*, **6 (1)**, doi:10.1038/srep38769, URL https://doi.org/10.1038%2Fsrep38769.

Davis, A., A. Marshak, W. Wiscombe, and R. Cahalan, 1996: Scale Invariance of Liquid Water Distributions in Marine Stratocumulus. Part I: Spectral Properties and Stationarity Issues. *Journal of the Atmospheric Sciences*, **53 (11)**, 1538–1558, doi:10.1175/1520-0469(1996)053<1538:SIOLWD>2.0.CO;2, URL https://doi.org/10.1175/1520-0469(1996)053<1538:SIOLWD>2.0.CO;2, https://journals.ametsoc.org/jas/article-pdf/53/11/1538/3427938/1520-0469(1996)053_1538_siolwd_2_0_co_2.pdf.

Del Genio, A. D., W. Kovari, M.-S. Yao, and J. Jonas, 2005: Cumulus microphysics and climate sensitivity. *Journal of Climate*, **18 (13)**, 2376–2387, doi:10.1175/JCLI3413.1, URL https://doi.org/10.1175/JCLI3413.1, https://doi.org/10.1175/JCLI3413.1.

Derksen, J. W. B., G.-J. H. Roelofs, and T. RÃ¶ckmann, 2009: Influence of entrainment of CCN on microphysical properties of warm cumulus. *Atmospheric Chemistry and Physics*, **9 (16)**, 6005–6015, doi:10.5194/acp-9-6005-2009, URL https://doi.org/10.5194%2Facp-9-6005-2009.

Dufresne, J.-L., and S. Bony, 2008: An assessment of the primary sources of spread of global warming estimates from coupled atmosphere–ocean models. *Journal of Climate*, **21 (19)**, 5135–5144, doi:10.1175/2008JCLI2239.1, URL https://doi.org/10.1175/2008JCLI2239.1, https://doi.org/10.1175/2008JCLI2239.1.

Eastman, R., S. G. Warren, and C. J. Hahn, 2011: Variations in cloud cover and cloud types over the ocean from surface observations, 1954?2008. *Journal of Climate*, **24 (22)**, 5914–5934, doi:10.1175/2011JCLI3972.1, URL https://doi.org/10.1175/2011JCLI3972.1, https://doi.org/10.1175/2011JCLI3972.1.

Feingold, G., I. Koren, H. Wang, H. Xue, and W. A. Brewer, 2010: Precipitation-generated oscillations in open cellular cloud fields. *Nature*, **466 (7308)**, 849–852, doi:10.1038/nature09314, URL https://doi.org/10.1038/nature09314.

George, D., and P. Mallery, 2009: *SPSS for Windows Step by Step: A Simple Study Guide and Reference, 17.0 Update*. 10th ed., Allyn & Bacon, Inc., Needham Heights, MA, USA.

Gerber, H. E., G. M. Frick, J. B. Jensen, and J. G. Hudson, 2008: Entrainment, mixing, and microphysics in trade-wind cumulus. *Journal of the Meteorological Society of Japan. Ser. II*, **86A**, 87–106, doi:10.2151/jmsj.86A.87.

Ghate, V. P., M. A. Miller, and P. Zhu, 2016: Differences between nonprecipitating tropical and trade wind marine shallow cumuli. *Monthly Weather Review*, **144 (2)**, 681–701, doi:10.1175/mwr-d-15-0110.1, URL https://doi.org/10.1175%2Fmwr-d-15-0110.1.

Guillaume, A., B. H. Kahn, Q. Yue, E. J. Fetzer, S. Wong, G. J. Manipon, H. Hua, and B. D. Wilson, 2018: Horizontal and vertical scaling of cloud geometry inferred from CloudSat data. *Journal of the Atmospheric Sciences*, **75 (7)**, 2187–2197, doi:10.1175/jas-d-17-0111.1, URL https://doi.org/10.1175%2Fjas-d-17-0111.1.

Guo, H., J.-C. Golaz, L. J. Donner, B. Wyman, M. Zhao, and P. Ginoux, 2015: Clubb as a unified cloud parameterization: Opportunities and challenges. *Geophysical Research Letters*, **42 (11)**, 4540–4547, doi:10.1002/2015GL063672, URL https://agupubs.onlinelibrary.wiley.com/doi/abs/10.1002/2015GL063672, https://agupubs.onlinelibrary.wiley.com/doi/pdf/10.1002/2015GL063672.

Hartmann, D. L., M. E. Ockert-Bell, and M. L. Michelsen, 1992: The Effect of Cloud Type on Earth's Energy Balance: Global Analysis. *Journal of Climate*, **5 (11)**, 1281–1304, doi:10.1175/1520-0442(1992)005<1281:TEOCTO>2.0.CO;2, URL https://doi.org/10.1175/1520-0442(1992)005<1281:TEOCTO>2.0.CO;2, https://journals.ametsoc.org/jcli/article-pdf/5/11/1281/4679899/1520-0442(1992)005_1281_teocto_2_0_co_2.pdf.

Haynes, J. M., T. S. LEcuyer, G. L. Stephens, S. D. Miller, C. Mitrescu, N. B. Wood, and S. Tanelli, 2009: Rainfall retrieval over the ocean with spaceborne w-band radar. *Journal of Geophysical*

Research, **114**, doi:10.1029/2008jd009973, URL https://doi.org/10.1029%2F2008jd009973.

Hernandez-Deckers, D., and S. C. Sherwood, 2018: On the role of entrainment in the fate of cumulus thermals. *Journal of the Atmospheric Sciences*, **75 (11)**, 3911–3924, doi:10.1175/jas-d-18-0077.1, URL https://doi.org/10.1175%2Fjas-d-18-0077.1.

Heus, T., and H. J. J. Jonker, 2008: Subsiding shells around shallow cumulus clouds. *Journal of the Atmospheric Sciences*, **65 (3)**, 1003–1018, doi:10.1175/2007jas2322.1, URL https://doi.org/10.1175%2F2007jas2322.1.

Heus, T., C. F. J. Pols, H. J. J. Jonker, H. E. A. V. den Akker, and D. H. Lenschow, 2009: Observational validation of the compensating mass flux through the shell around cumulus clouds. *Quarterly Journal of the Royal Meteorological Society*, **135 (638)**, 101–112, doi:10.1002/qj.358, URL https://doi.org/10.1002%2Fqj.358.

Jiang, H., and G. Feingold, 2006: Effect of aerosol on warm convective clouds: Aerosol-cloud-surface flux feedbacks in a new coupled large eddy model. *Journal of Geophysical Research*, **111 (D1)**, doi:10.1029/2005jd006138, URL https://doi.org/10.1029%2F2005jd006138.

Jiang, H., G. Feingold, and A. Sorooshian, 2010: Effect of aerosol on the susceptibility and efficiency of precipitation in warm trade cumulus clouds. *Journal of the Atmospheric Sciences*, **67 (11)**, 3525–3540, doi:10.1175/2010jas3484.1, URL https://doi.org/10.1175%2F2010jas3484.1.

Johnson, R. H., T. M. Rickenbach, S. A. Rutledge, P. E. Ciesielski, and W. H. Schubert, 1999: Trimodal characteristics of tropical convection. *Journal of Climate*, **12 (8)**, 2397–2418, doi:10.1175/1520-0442(1999)012<2397:TCOTC>2.0.CO;2, URL https://doi.org/10.1175/1520-0442(1999)012<2397:TCOTC>2.0.CO;2, https://doi.org/10.1175/1520-0442(1999)012<2397:TCOTC>2.0.CO;2.

Jung, E., B. A. Albrecht, G. Feingold, H. H. Jonsson, P. Chuang, and S. L. Donaher, 2016a: Aerosols, clouds, and precipitation in the north atlantic trades observed during the barbados aerosol cloud experiment – part 1: Distributions and variability. *Atmospheric Chemistry and Physics*, **16 (13)**, 8643–8666, doi:10.5194/acp-16-8643-2016, URL https://doi.org/10.5194%

2Facp-16-8643-2016.

Jung, E., B. A. Albrecht, A. Sorooshian, P. Zuidema, and H. H. Jonsson, 2016b: Precipitation susceptibility in marine stratocumulus and shallow cumulus from airborne measurements. *Atmospheric Chemistry and Physics*, **16 (17)**, 11 395–11 413, doi:10.5194/acp-16-11395-2016, URL https://doi.org/10.5194%2Facp-16-11395-2016.

JÃ¤hn, M., D. Muñoz-Esparza, F. Chouza, O. Reitebuch, O. Knoth, M. Haarig, and A. Ansmann, 2016: Investigations of boundary layer structure, cloud characteristics and vertical mixing of aerosols at barbados with large eddy simulations. *Atmospheric Chemistry and Physics*, **16 (2)**, 651–674, doi:10.5194/acp-16-651-2016, URL https://doi.org/10.5194%2Facp-16-651-2016.

Kirshbaum, D. J., and A. L. M. Grant, 2012: Invigoration of cumulus cloud fields by mesoscale ascent. *Quarterly Journal of the Royal Meteorological Society*, **138 (669)**, 2136–2150, doi:10.1002/qj.1954, URL https://doi.org/10.1002%2Fqj.1954.

Klein, S. A., and D. L. Hartmann, 1993: The seasonal cycle of low stratiform clouds. *Journal of Climate*, **6 (8)**, 1587–1606, doi:10.1175/1520-0442(1993)006<1587:TSCOLS>2.0.CO;2, URL https://doi.org/10.1175/1520-0442(1993)006<1587:TSCOLS>2.0.CO;2, https://doi.org/10.1175/1520-0442(1993)006<1587:TSCOLS>2.0.CO;2.

Kollias, P., B. A. Albrecht, and F. D. Marks Jr., 2003: Cloud radar observations of vertical drafts and microphysics in convective rain. *Journal of Geophysical Research: Atmospheres*, **108 (D2)**, doi:10.1029/2001JD002033, URL https://agupubs.onlinelibrary.wiley.com/doi/abs/10.1029/2001JD002033, https://agupubs.onlinelibrary.wiley.com/doi/pdf/10.1029/2001JD002033.

Koren, I., G. Dagan, and O. Altaratz, 2014: From aerosol-limited to invigoration of warm convective clouds. *Science*, **344 (6188)**, 1143–1146, doi:10.1126/science.1252595, URL https://science.sciencemag.org/content/344/6188/1143, https://science.sciencemag.org/content/344/6188/1143.full.pdf.

Korolev, A., A. Khain, M. Pinsky, and J. French, 2016: Theoretical study of mixing in liquid clouds – part 1: Classical concepts. *Atmospheric Chemistry and Physics*, **16 (14)**, 9235–9254, doi:10.5194/acp-16-9235-2016, URL https://doi.org/10.5194%2Facp-16-9235-2016.

Kuo, K.-S., R. M. Welch, R. C. Weger, M. A. Engelstad, and S. K. Sengupta, 1993: The three-dimensional structure of cumulus clouds over the ocean: 1. structural analysis. *Journal of Geophysical Research: Atmospheres*, **98 (D11)**, 20 685–20 711, doi:10.1029/93JD02331, URL https://agupubs.onlinelibrary.wiley.com/doi/abs/10.1029/93JD02331, https://agupubs.onlinelibrary.wiley.com/doi/pdf/10.1029/93JD02331.

Lamer, K., P. Kollias, and L. Nuijens, 2015: Observations of the variability of shallow trade wind cumulus cloudiness and mass flux. *Journal of Geophysical Research: Atmospheres*, **120 (12)**, 6161–6178, doi:10.1002/2014jd022950, URL https://doi.org/10.1002%2F2014jd022950.

Lau, K. M., and H. T. Wu, 2003: Warm rain processes over tropical oceans and climate implications. *Geophysical Research Letters*, **30 (24)**, doi:10.1029/2003gl018567, URL https://doi.org/10.1029%2F2003gl018567.

Lebsock, M., H. Morrison, and A. Gettelman, 2013: Microphysical implications of cloud-precipitation covariance derived from satellite remote sensing. *Journal of Geophysical Research: Atmospheres*, **118 (12)**, 6521–6533, doi:10.1002/jgrd.50347, URL https://agupubs.onlinelibrary.wiley.com/doi/abs/10.1002/jgrd.50347, https://agupubs.onlinelibrary.wiley.com/doi/pdf/10.1002/jgrd.50347.

Lebsock, M., and H. Su, 2014: Application of active spaceborne remote sensing for understanding biases between passive cloud water path retrievals. *Journal of Geophysical Research: Atmospheres*, **119 (14)**, 8962–8979, doi:10.1002/2014JD021568, URL https://agupubs.onlinelibrary.wiley.com/doi/abs/10.1002/2014JD021568, https://agupubs.onlinelibrary.wiley.com/doi/pdf/10.1002/2014JD021568.

Lebsock, M. D., and T. S. L'Ecuyer, 2011a: The retrieval of warm rain from cloudsat. *Journal of Geophysical Research: Atmospheres*, **116 (D20)**, doi:10.1029/2011JD016076, URL https://agupubs.onlinelibrary.wiley.com/doi/abs/10.1029/2011JD016076, https://agupubs.onlinelibrary.wiley.com/doi/pdf/10.1029/2011JD016076.

Lebsock, M. D., and T. S. L'Ecuyer, 2011b: The retrieval of warm rain from cloudsat. *Journal of Geophysical Research: Atmospheres*, **116 (D20)**, doi:10.1029/2011JD016076,

URL https://agupubs.onlinelibrary.wiley.com/doi/abs/10.1029/2011JD016076, https://agupubs.onlinelibrary.wiley.com/doi/pdf/10.1029/2011JD016076.

L'Ecuyer, T. S., and G. L. Stephens, 2002: An estimation-based precipitation retrieval algorithm for attenuating radars. *Journal of Applied Meteorology*, **41 (3)**, 272–285, doi:10.1175/1520-0450(2002)041<0272:AEBPRA>2.0.CO;2, URL https://doi.org/10.1175/1520-0450(2002)041<0272:AEBPRA>2.0.CO;2, https://doi.org/10.1175/1520-0450(2002)041<0272:AEBPRA>2.0.CO;2.

Lee, H., and J.-J. Baik, 2017: A Physically Based Autoconversion Parameterization. *Journal of the Atmospheric Sciences*, **74 (5)**, 1599–1616, doi:10.1175/JAS-D-16-0207.1, URL https://doi.org/10.1175/JAS-D-16-0207.1, https://journals.ametsoc.org/jas/article-pdf/74/5/1599/3872353/jas-d-16-0207_1.pdf.

Leon, D. C., Z. Wang, and D. Liu, 2008: Climatology of drizzle in marine boundary layer clouds based on 1 year of data from CloudSat and cloud-aerosol lidar and infrared pathfinder satellite observations (CALIPSO). *Journal of Geophysical Research*, **113**, doi:10.1029/2008jd009835, URL https://doi.org/10.1029%2F2008jd009835.

Li, Z., P. Zuidema, and P. Zhu, 2014: Simulated convective invigoration processes at trade wind cumulus cold pool boundaries. *Journal of the Atmospheric Sciences*, **71 (8)**, 2823–2841, doi:10.1175/jas-d-13-0184.1, URL https://doi.org/10.1175%2Fjas-d-13-0184.1.

Lim, K.-S. S., and S.-Y. Hong, 2010: Development of an Effective Double-Moment Cloud Microphysics Scheme with Prognostic Cloud Condensation Nuclei (CCN) for Weather and Climate Models. *Monthly Weather Review*, **138 (5)**, 1587–1612, doi:10.1175/2009MWR2968.1, URL https://doi.org/10.1175/2009MWR2968.1, https://journals.ametsoc.org/mwr/article-pdf/138/5/1587/4257009/2009mwr2968_1.pdf.

Lin, W., M. Zhang, and N. G. Loeb, 2009: Seasonal Variation of the Physical Properties of Marine Boundary Layer Clouds off the California Coast. *Journal of Climate*, **22 (10)**, 2624–2638, doi:10.1175/2008JCLI2478.1, URL https://doi.org/10.1175/2008JCLI2478.1, https://journals.ametsoc.org/jcli/article-pdf/22/10/2624/3950446/2008jcli2478_1.pdf.

Liu, C., and E. J. Zipser, 2009: "warm rain" in the tropics: Seasonal and regional distributions based on 9 yr of TRMM data. *Journal of Climate*, **22 (3)**, 767–779, doi:10.1175/2008jcli2641.1, URL https://doi.org/10.1175%2F2008jcli2641.1.

Liu, Y., and P. H. Daum, 2004: Parameterization of the autoconversion process.part i: Analytical formulation of the kessler-type parameterizations. *Journal of the Atmospheric Sciences*, **61 (13)**, 1539–1548, doi:10.1175/1520-0469(2004)061<1539:POTAPI>2.0.CO;2, URL https://doi.org/10.1175/1520-0469(2004)061<1539:POTAPI>2.0.CO;2, https://doi.org/10.1175/1520-0469(2004)061<1539:POTAPI>2.0.CO;2.

Lohmann, U., and E. Roeckner, 1996: Design and performance of a new cloud microphysics scheme developed for the echam general circulation model. *Climate Dynamics*, **12 (8)**, 557–572, doi:10.1007/BF00207939, URL https://doi.org/10.1007/BF00207939.

Lu, C., Y. Liu, S. Niu, and A. M. Vogelmann, 2012: Lateral entrainment rate in shallow cumuli: Dependence on dry air sources and probability density functions. *Geophysical Research Letters*, **39 (20)**, doi:10.1029/2012gl053646, URL https://doi.org/10.1029%2F2012gl053646.

Luo, Z. J., G. Y. Liu, and G. L. Stephens, 2010: Use of a-train data to estimate convective buoyancy and entrainment rate. *Geophysical Research Letters*, **37 (9)**, n/a–n/a, doi:10.1029/2010gl042904, URL https://doi.org/10.1029%2F2010gl042904.

Lutsko, N. J., and T. W. Cronin, 2018: Increase in precipitation efficiency with surface warming in radiative-convective equilibrium. *Journal of Advances in Modeling Earth Systems*, **10 (11)**, 2992–3010, doi:10.1029/2018MS001482, URL https://agupubs.onlinelibrary.wiley.com/doi/abs/10.1029/2018MS001482, https://agupubs.onlinelibrary.wiley.com/doi/pdf/10.1029/2018MS001482.

Mace, G. G., and Q. Zhang, 2014: The CloudSat radar-lidar geometrical profile product (RL-GeoProf): Updates, improvements, and selected results. *Journal of Geophysical Research: Atmospheres*, **119 (15)**, 9441–9462, doi:10.1002/2013jd021374, URL https://doi.org/10.1002%2F2013jd021374.

Marchand, R., G. G. Mace, T. Ackerman, and G. Stephens, 2008: Hydrometeor detection

UsingCloudsat—an earth-orbiting 94-GHz cloud radar. *Journal of Atmospheric and Oceanic Technology*, **25 (4)**, 519–533, doi:10.1175/2007jtecha1006.1, URL https://doi.org/10.1175%2F2007jtecha1006.1.

McGibbon, J., and C. S. Bretherton, 2017: Skill of ship-following large-eddy simulations in reproducing magic observations across the northeast pacific stratocumulus to cumulus transition region. *Journal of Advances in Modeling Earth Systems*, **9 (2)**, 810–831, doi:10.1002/2017MS000924, URL https://agupubs.onlinelibrary.wiley.com/doi/abs/10.1002/2017MS000924, https://agupubs.onlinelibrary.wiley.com/doi/pdf/10.1002/2017MS000924.

Medeiros, B., and L. Nuijens, 2016: Clouds at barbados are representative of clouds across the trade wind regions in observations and climate models. *Proceedings of the National Academy of Sciences*, **113 (22)**, E3062–E3070, doi:10.1073/pnas.1521494113, URL https://doi.org/10.1073%2Fpnas.1521494113.

Medeiros, B., and B. Stevens, 2011: Revealing differences in gcm representations of low clouds. *Climate Dynamics*, **36 (1)**, 385–399, doi:10.1007/s00382-009-0694-5, URL https://doi.org/10.1007/s00382-009-0694-5.

Medeiros, B., B. Stevens, and S. Bony, 2014: Using aquaplanets to understand the robust responses of comprehensive climate models to forcing. *Climate Dynamics*, **44 (7-8)**, 1957–1977, doi:10.1007/s00382-014-2138-0, URL https://doi.org/10.1007%2Fs00382-014-2138-0.

Minor, H. A., R. M. Rauber, S. GÃ¶ke, and L. Di Girolamo, 2011: Trade wind cloud evolution observed by polarization radar: Relationship to giant condensation nuclei concentrations and cloud organization. *Journal of the Atmospheric Sciences*, **68 (5)**, 1075–1096, doi:10.1175/2010JAS3675.1, URL https://doi.org/10.1175/2010JAS3675.1, https://doi.org/10.1175/2010JAS3675.1.

Mitrescu, C., T. L'Ecuyer, J. Haynes, S. Miller, and J. Turk, 2010: Cloudsat precipitation profiling algorithm—model description. *Journal of Applied Meteorology and Climatology*, **49 (5)**, 991–1003, doi:10.1175/2009JAMC2181.1, URL https://doi.org/10.1175/2009JAMC2181.1, https://doi.org/10.1175/2009JAMC2181.1.

Morrison, H., J. A. Curry, and V. I. Khvorostyanov, 2005: A New Double-Moment Microphysics Parameterization for Application in Cloud and Climate Models. Part I: Description. *Journal of the Atmospheric Sciences*, **62 (6)**, 1665–1677, doi:10.1175/JAS3446.1, URL https://doi.org/10.1175/JAS3446.1, https://journals.ametsoc.org/jas/article-pdf/62/6/1665/3604275/jas3446_1.pdf.

Moser, D. H., and S. Lasher-Trapp, 2017: The influence of successive thermals on entrainment and dilution in a simulated cumulus congestus. *Journal of the Atmospheric Sciences*, **74 (2)**, 375–392, doi:10.1175/JAS-D-16-0144.1, URL https://doi.org/10.1175/JAS-D-16-0144.1, https://doi.org/10.1175/JAS-D-16-0144.1.

Nam, C., S. Bony, J.-L. Dufresne, and H. Chepfer, 2012: The 'too few, too bright' tropical low-cloud problem in CMIP5 models. *Geophysical Research Letters*, **39 (21)**, n/a–n/a, doi:10.1029/2012gl053421, URL https://doi.org/10.1029%2F2012gl053421.

Neggers, R. A. J., P. J. Griewank, and T. Heus, 2019: Power-law scaling in the internal variability of cumulus cloud size distributions due to subsampling and spatial organization. *Journal of the Atmospheric Sciences*, **76 (6)**, 1489–1503, doi:10.1175/JAS-D-18-0194.1, URL https://doi.org/10.1175/JAS-D-18-0194.1, https://doi.org/10.1175/JAS-D-18-0194.1.

Neggers, R. A. J., H. J. J. Jonker, and A. P. Siebesma, 2003: Size statistics of cumulus cloud populations in large-eddy simulations. *Journal of the Atmospheric Sciences*, **60 (8)**, 1060–1074, doi:10.1175/1520-0469(2003)60<1060:SSOCCP>2.0.CO;2, URL https://doi.org/10.1175/1520-0469(2003)60<1060:SSOCCP>2.0.CO;2, https://doi.org/10.1175/1520-0469(2003)60<1060:SSOCCP>2.0.CO;2.

Norris, J. R., 1998: Low cloud type over the ocean from surface observations. part ii: Geographical and seasonal variations. *Journal of Climate*, **11 (3)**, 383–403, doi:10.1175/1520-0442(1998)011<0383:LCTOTO>2.0.CO;2, URL https://doi.org/10.1175/1520-0442(1998)011<0383:LCTOTO>2.0.CO;2, https://doi.org/10.1175/1520-0442(1998)011<0383:LCTOTO>2.0.CO;2.

Nuijens, L., K. Emanuel, H. Masunaga, and T. L'Ecuyer, 2017: Implications of warm rain in shallow cumulus and congestus clouds for large-scale circulations. *Surveys in Geo-*

physics, **38 (6)**, 1257–1282, doi:10.1007/s10712-017-9429-z, URL https://doi.org/10.1007%2Fs10712-017-9429-z.

Owens, R. G., and T. Hewson, 2018: Ecmwf forecast user guide. Tech. rep., European Centre for Medium-Range Weather Forecasts, Reading. doi:10.21957/m1cs7h, URL https://www.ecmwf.int/node/16559, replaces previous editions that were available as PDF documents.

Park, S., and C. S. Bretherton, 2009: The university of washington shallow convection and moist turbulence schemes and their impact on climate simulations with the community atmosphere model. *Journal of Climate*, **22 (12)**, 3449–3469, doi:10.1175/2008jcli2557.1, URL https://doi.org/10.1175%2F2008jcli2557.1.

Pawlowska, H., and J.-L. Brenguier, 2003: An observational study of drizzle formation in stratocumulus clouds for general circulation model (gcm) parameterizations. *Journal of Geophysical Research: Atmospheres*, **108 (D15)**, doi:10.1029/2002JD002679, URL https://agupubs.onlinelibrary.wiley.com/doi/abs/10.1029/2002JD002679, https://agupubs.onlinelibrary.wiley.com/doi/pdf/10.1029/2002JD002679.

Pinsky, M., A. Khain, and A. Korolev, 2016a: Theoretical analysis of mixing in liquid clouds – part 3: Inhomogeneous mixing. *Atmospheric Chemistry and Physics*, **16 (14)**, 9273–9297, doi:10.5194/acp-16-9273-2016, URL https://doi.org/10.5194%2Facp-16-9273-2016.

Pinsky, M., A. Khain, A. Korolev, and L. Magaritz-Ronen, 2016b: Theoretical investigation of mixing in warm clouds – part 2: Homogeneous mixing. *Atmospheric Chemistry and Physics*, **16 (14)**, 9255–9272, doi:10.5194/acp-16-9255-2016, URL https://doi.org/10.5194%2Facp-16-9255-2016.

Platnick, S., M. D. King, S. A. Ackerman, W. P. Menzel, B. A. Baum, J. C. Riedi, and R. A. Frey, 2003: The modis cloud products: algorithms and examples from terra. *IEEE Transactions on Geoscience and Remote Sensing*, **41 (2)**, 459–473.

Rapp, A. D., 2016: Observational evidence linking precipitation and mesoscale cloud fraction in the southeast pacific. *Geophysical Research Letters*, **43 (13)**, 7267–7273, doi:10.1002/2016GL069906, URL https://agupubs.onlinelibrary.wiley.com/doi/abs/10.1002/

2016GL069906, https://agupubs.onlinelibrary.wiley.com/doi/pdf/10.1002/2016GL069906.

Rapp, A. D., M. Lebsock, and T. L'Ecuyer, 2013: Low cloud precipitation climatology in the southeastern pacific marine stratocumulus region using CloudSat. *Environmental Research Letters*, **8 (1)**, 014 027, doi:10.1088/1748-9326/8/1/014027, URL https://doi.org/10.1088%2F1748-9326%2F8%2F1%2F014027.

Rauber, R. M., and Coauthors, 2007: Rain in shallow cumulus over the ocean: The RICO campaign. *Bulletin of the American Meteorological Society*, **88 (12)**, 1912–1928, doi:10.1175/bams-88-12-1912, URL https://doi.org/10.1175%2Fbams-88-12-1912.

Rennó, N. O., K. A. Emanuel, and P. H. Stone, 1994: Radiative-convective model with an explicit hydrologic cycle: 1. formulation and sensitivity to model parameters. *Journal of Geophysical Research: Atmospheres*, **99 (D7)**, 14 429–14 441, doi:10.1029/94JD00020, URL https://agupubs.onlinelibrary.wiley.com/doi/abs/10.1029/94JD00020, https://agupubs.onlinelibrary.wiley.com/doi/pdf/10.1029/94JD00020.

Romps, D. M., 2014: An analytical model for tropical relative humidity. *Journal of Climate*, **27 (19)**, 7432–7449, doi:10.1175/JCLI-D-14-00255.1, URL https://doi.org/10.1175/JCLI-D-14-00255.1, https://doi.org/10.1175/JCLI-D-14-00255.1.

Rosenfeld, D., 2000: Suppression of rain and snow by urban and industrial air pollution. *Science*, **287 (5459)**, 1793–1796, doi:10.1126/science.287.5459.1793, URL https://science.sciencemag.org/content/287/5459/1793, https://science.sciencemag.org/content/287/5459/1793.full.pdf.

Ruiz-Arias, J. A., J. Dudhia, C. A. Gueymard, and D. Pozo-Vázquez, 2013: Assessment of the level-3 modis daily aerosol optical depth in the context of surface solar radiation and numerical weather modeling. *Atmospheric Chemistry and Physics*, **13 (2)**, 675–692, doi:10.5194/acp-13-675-2013, URL https://www.atmos-chem-phys.net/13/675/2013/.

Saleeby, S. M., S. R. Herbener, S. C. van den Heever, and T. L'Ecuyer, 2015: Impacts of cloud droplet–nucleating aerosols on shallow tropical convection. *Journal of the Atmospheric Sciences*, **72 (4)**, 1369–1385, doi:10.1175/JAS-D-14-0153.1, URL https://doi.org/10.1175/JAS-D-14-0153.1, https://doi.org/10.1175/JAS-D-14-0153.1.

Sandu, I., B. Stevens, and R. Pincus, 2010: On the transitions in marine boundary layer cloudiness. *Atmospheric Chemistry and Physics*, **10 (5)**, 2377–2391, doi:10.5194/acp-10-2377-2010, URL https://acp.copernicus.org/articles/10/2377/2010/.

Sassen, K., and Z. Wang, 2008: Classifying clouds around the globe with the CloudSat radar: 1-year of results. *Geophysical Research Letters*, **35 (4)**, doi:10.1029/2007gl032591, URL https://doi.org/10.1029%2F2007gl032591.

Schmeissner, T., R. A. Shaw, J. Ditas, F. Stratmann, M. Wendisch, and H. Siebert, 2015: Turbulent mixing in shallow trade wind cumuli: Dependence on cloud life cycle. *Journal of the Atmospheric Sciences*, **72 (4)**, 1447–1465, doi:10.1175/jas-d-14-0230.1, URL https://doi.org/10.1175%2Fjas-d-14-0230.1.

Schoeberl, M. R., 2002: The afternoon constellation: a formation of earth observing systems for the atmosphere and hydrosphere. *IEEE International Geoscience and Remote Sensing Symposium*, Vol. 1, 354–356 vol.1.

Schumacher, C., and R. A. Houze, 2003: The trmm precipitation radar's view of shallow, isolated rain. *Journal of Applied Meteorology*, **42 (10)**, 1519–1524, doi:10.1175/1520-0450(2003)042<1519:TTPRVO>2.0.CO;2, URL https://doi.org/10.1175/1520-0450(2003)042<1519:TTPRVO>2.0.CO;2, https://doi.org/10.1175/1520-0450(2003)042<1519:TTPRVO>2.0.CO;2.

Seifert, A., and T. Heus, 2013: Large-eddy simulation of organized precipitating trade wind cumulus clouds. *Atmospheric Chemistry and Physics*, **13 (11)**, 5631–5645, doi:10.5194/acp-13-5631-2013, URL https://doi.org/10.5194%2Facp-13-5631-2013.

Short, D. A., and K. Nakamura, 2000: Trmm radar observations of shallow precipitation over the tropical oceans. *Journal of Climate*, **13 (23)**, 4107–4124, doi:10.1175/1520-0442(2000)013<4107:TROOSP>2.0.CO;2, URL https://doi.org/10.1175/1520-0442(2000)013<4107:TROOSP>2.0.CO;2, https://doi.org/10.1175/1520-0442(2000)013<4107:TROOSP>2.0.CO;2.

Slingo, J. M., 2007: The development and verification of a cloud prediction scheme for the ecmwf model. *Quarterly Journal of the Royal Meteorological Society*, **113 (477)**, 899–927, doi:10.1002/qj.49711347710, URL https://doi.org/10.1002%2Fqj.49711347710.

Smalley, K. M., and A. D. Rapp, 2020a: A-train estimates of the sensitivity of warm rain likelihood and efficiency to cloud size, environmental moisture, and aerosols. *Atmospheric Chemistry and Physics Discussions*, **2020**, 1–19, doi:10.5194/acp-2020-754, URL https://acp.copernicus.org/preprints/acp-2020-754/.

Smalley, K. M., and A. D. Rapp, 2020b: The Role of Cloud Size and Environmental Moisture in Shallow Cumulus Precipitation. *Journal of Applied Meteorology and Climatology*, **59 (3)**, 535–550, doi:10.1175/JAMC-D-19-0145.1, URL https://doi.org/10.1175/JAMC-D-19-0145.1, https://journals.ametsoc.org/jamc/article-pdf/59/3/535/4921344/jamcd190145.pdf.

Smalley, M., and T. L'Ecuyer, 2015: A Global Assessment of the Spatial Distribution of Precipitation Occurrence. *Journal of Applied Meteorology and Climatology*, **54 (11)**, 2179–2197, doi:10.1175/JAMC-D-15-0019.1, URL https://doi.org/10.1175/JAMC-D-15-0019.1, https://journals.ametsoc.org/jamc/article-pdf/54/11/2179/3579513/jamc-d-15-0019_1.pdf.

Snodgrass, E. R., L. D. Girolamo, and R. M. Rauber, 2009: Precipitation characteristics of trade wind clouds during RICO derived from radar, satellite, and aircraft measurements. *Journal of Applied Meteorology and Climatology*, **48 (3)**, 464–483, doi:10.1175/2008jamc1946.1, URL https://doi.org/10.1175%2F2008jamc1946.1.

Squires, P., 1958: The microstructure and colloidal stability of warm clouds. *Tellus*, **10 (2)**, 256–261, doi:10.1111/j.2153-3490.1958.tb02011.x, URL https://onlinelibrary.wiley.com/doi/abs/10.1111/j.2153-3490.1958.tb02011.x, https://onlinelibrary.wiley.com/doi/pdf/10.1111/j.2153-3490.1958.tb02011.x.

Stevens, B., 2000: Cloud transitions and decoupling in shear-free stratocumulus-topped boundary layers. *Geophysical Research Letters*, **27 (16)**, 2557–2560, doi:10.1029/1999GL011257, URL https://agupubs.onlinelibrary.wiley.com/doi/abs/10.1029/1999GL011257, https://agupubs.onlinelibrary.wiley.com/doi/pdf/10.1029/1999GL011257.

Stevens, B., W. R. Cotton, G. Feingold, and C.-H. Moeng, 1998: Large-eddy simulations of strongly precipitating, shallow, stratocumulus-topped boundary layers. *Journal of the Atmospheric Sciences*, **55 (24)**, 3616–3638, doi:10.1175/1520-0469(1998)055<3616:LESOSP>2.0.

CO;2, URL https://doi.org/10.1175/1520-0469(1998)055<3616:LESOSP>2.0.CO;2.

Stevens, B., G. Vali, K. Comstock, R. Wood, M. C. van Zanten, P. H. Austin, C. S. Bretherton, and D. H. Lenschow, 2005: POCKETS OF OPEN CELLS AND DRIZZLE IN MARINE STRATOCUMULUS. *Bulletin of the American Meteorological Society*, **86 (1)**, 51–58, doi:10.1175/BAMS-86-1-51, URL https://doi.org/10.1175/BAMS-86-1-51, https://journals.ametsoc.org/bams/article-pdf/86/1/51/3735050/bams-86-1-51.pdf.

Stevens, B., and Coauthors, 2019: Sugar, gravel, fish, and flowers: Mesoscale cloud patterns in the tradewinds. *Quarterly Journal of the Royal Meteorological Society*, **0 (ja)**, doi:10.1002/qj.3662, URL https://rmets.onlinelibrary.wiley.com/doi/abs/10.1002/qj.3662, https://rmets.onlinelibrary.wiley.com/doi/pdf/10.1002/qj.3662.

Stevens, D. E., A. S. Ackerman, and C. S. Bretherton, 2002: Effects of domain size and numerical resolution on the simulation of shallow cumulus convection. *Journal of the Atmospheric Sciences*, **59 (23)**, 3285–3301, doi:10.1175/1520-0469(2002)059<3285:EODSAN>2.0.CO;2, URL https://doi.org/10.1175/1520-0469(2002)059<3285:EODSAN>2.0.CO;2, https://doi.org/10.1175/1520-0469(2002)059<3285:EODSAN>2.0.CO;2.

Tanelli, S., S. L. Durden, E. Im, K. S. Pak, D. G. Reinke, P. Partain, J. M. Haynes, and R. T. Marchand, 2008: Cloudsat's cloud profiling radar after two years in orbit: Performance, calibration, and processing. *IEEE Transactions on Geoscience and Remote Sensing*, **46 (11)**, 3560–3573, doi:10.1109/TGRS.2008.2002030.

Teixeira, J., and Coauthors, 2011: Tropical and Subtropical Cloud Transitions in Weather and Climate Prediction Models: The GCSS/WGNE Pacific Cross-Section Intercomparison (GPCI). *Journal of Climate*, **24 (20)**, 5223–5256, doi:10.1175/2011JCLI3672.1, URL https://doi.org/10.1175/2011JCLI3672.1, https://journals.ametsoc.org/jcli/article-pdf/24/20/5223/3983884/2011jcli3672_1.pdf.

Terai, C. R., and R. Wood, 2013: Aircraft observations of cold pools under marine stratocumulus. *Atmospheric Chemistry and Physics*, **13 (19)**, 9899–9914, doi:10.5194/acp-13-9899-2013, URL https://acp.copernicus.org/articles/13/9899/2013/.

Tian, Y., and Z. Kuang, 2016: Dependence of entrainment in shallow cumulus convection on vertical velocity and distance to cloud edge. *Geophysical Research Letters*, **43 (8)**, 4056–4065, doi:10.1002/2016gl069005, URL https://doi.org/10.1002%2F2016gl069005.

Tiedtke, M., 1989: A comprehensive mass flux scheme for cumulus parameterization in large-scale models. *Monthly Weather Review*, **117 (8)**, 1779–1800, doi:10.1175/1520-0493(1989)117<1779:ACMFSF>2.0.CO;2, URL https://doi.org/10.1175/1520-0493(1989)117<1779:ACMFSF>2.0.CO;2, https://doi.org/10.1175/1520-0493(1989)117<1779:ACMFSF>2.0.CO;2.

Trivej, P., and B. Stevens, 2010: The echo size distribution of precipitating shallow cumuli. *Journal of the Atmospheric Sciences*, **67 (3)**, 788–804, doi:10.1175/2009JAS3178.1, URL https://doi.org/10.1175/2009JAS3178.1, https://doi.org/10.1175/2009JAS3178.1.

Twomey, S., 1974: Pollution and the planetary albedo. *Atmospheric Environment*, **8 (12)**, 1251 – 1256, doi:https://doi.org/10.1016/0004-6981(74)90004-3, URL http://www.sciencedirect.com/science/article/pii/0004698174900043.

vanZanten, M. C., and B. Stevens, 2005: Observations of the Structure of Heavily Precipitating Marine Stratocumulus. *Journal of the Atmospheric Sciences*, **62 (12)**, 4327–4342, doi:10.1175/JAS3611.1, URL https://doi.org/10.1175/JAS3611.1, https://journals.ametsoc.org/jas/article-pdf/62/12/4327/3478805/jas3611_1.pdf.

Vial, J., J.-L. Dufresne, and S. Bony, 2013: On the interpretation of inter-model spread in cmip5 climate sensitivity estimates. *Climate Dynamics*, **41 (11)**, 3339–3362, doi:10.1007/s00382-013-1725-9, URL https://doi.org/10.1007/s00382-013-1725-9.

Waliser, D. E., and C. Gautier, 1993: A satellite-derived climatology of the itcz. *Journal of Climate*, **6 (11)**, 2162–2174, doi:10.1175/1520-0442(1993)006<2162:ASDCOT>2.0.CO;2, URL https://doi.org/10.1175/1520-0442(1993)006<2162:ASDCOT>2.0.CO;2, https://doi.org/10.1175/1520-0442(1993)006<2162:ASDCOT>2.0.CO;2.

Wang, Y., Y. Chen, Y. Fu, and G. Liu, 2017: Identification of precipitation onset based on cloudsat observations. *Journal of Quantitative Spectroscopy and Radiative Transfer*, **188**, 142 – 147, doi:https://doi.org/10.1016/j.jqsrt.2016.06.028, URL http://www.sciencedirect.com/science/article/

pii/S0022407315301886, advances in Atmospheric Light Scattering: Theory and Remote Sensing Techniques.

Warner, C., J. Simpson, D. W. Martin, D. Suchman, F. R. Mosher, and R. F. Reinking, 1979: Shallow convection on day 261 of gate/ mesoscale arcs. *Monthly Weather Review*, **107 (12)**, 1617–1635, doi:10.1175/1520-0493(1979)107<1617:SCODOG>2.0.CO;2, URL https://doi.org/10.1175/1520-0493(1979)107<1617:SCODOG>2.0.CO;2, https://doi.org/10.1175/1520-0493(1979)107<1617:SCODOG>2.0.CO;2.

Watson, C. D., R. B. Smith, and A. D. Nugent, 2015: Processes controlling precipitation in shallow, orographic, trade wind convection. *Journal of the Atmospheric Sciences*, **72 (8)**, 3051–3072, doi:10.1175/jas-d-14-0333.1, URL https://doi.org/10.1175%2Fjas-d-14-0333.1.

Witkowski, M., and Coauthors, 2012: Cloudsat anomaly recovery and operational lessons learned. Tech. rep., Jet Propulsion Laboratory, National Aeronautics and Space Administration.

Witte, M. K., H. Morrison, J. B. Jensen, A. Bansemer, and A. Gettelman, 2019: On the Covariability of Cloud and Rain Water as a Function of Length Scale. *Journal of the Atmospheric Sciences*, **76 (8)**, 2295–2308, doi:10.1175/JAS-D-19-0048.1, URL https://doi.org/10.1175/JAS-D-19-0048.1, https://journals.ametsoc.org/jas/article-pdf/76/8/2295/4876704/jas-d-19-0048_1.pdf.

Wood, R., 2012: Stratocumulus Clouds. *Monthly Weather Review*, **140 (8)**, 2373–2423, doi:10.1175/MWR-D-11-00121.1, URL https://doi.org/10.1175/MWR-D-11-00121.1, https://journals.ametsoc.org/mwr/article-pdf/140/8/2373/4279106/mwr-d-11-00121_1.pdf.

Wood, R., and C. S. Bretherton, 2004a: Boundary layer depth, entrainment, and decoupling in the cloud-capped subtropical and tropical marine boundary layer. *Journal of Climate*, **17 (18)**, 3576–3588, doi:10.1175/1520-0442(2004)017<3576:BLDEAD>2.0.CO;2, URL https://doi.org/10.1175/1520-0442(2004)017<3576:BLDEAD>2.0.CO;2, https://doi.org/10.1175/1520-0442(2004)017<3576:BLDEAD>2.0.CO;2.

Wood, R., and C. S. Bretherton, 2004b: Boundary Layer Depth, Entrainment, and Decoupling in the Cloud-Capped Subtropical and Tropical Marine Boundary Layer. *Journal of Climate*,

17 (18), 3576–3588, doi:10.1175/1520-0442(2004)017<3576:BLDEAD>2.0.CO;2, URL https://doi.org/10.1175/1520-0442(2004)017<3576:BLDEAD>2.0.CO;2, https://journals.ametsoc.org/jcli/article-pdf/17/18/3576/3786757/1520-0442(2004)017_3576_bldead_2_0_co_2.pdf.

Wood, R., and C. S. Bretherton, 2006: On the relationship between stratiform low cloud cover and lower-tropospheric stability. *Journal of Climate*, **19 (24)**, 6425–6432, doi:10.1175/jcli3988.1, URL https://doi.org/10.1175%2Fjcli3988.1.

Wood, R., and P. R. Field, 2011: The distribution of cloud horizontal sizes. *Journal of Climate*, **24 (18)**, 4800–4816, doi:10.1175/2011jcli4056.1, URL https://doi.org/10.1175%2F2011jcli4056.1.

Wood, R., and D. L. Hartmann, 2006: Spatial Variability of Liquid Water Path in Marine Low Cloud: The Importance of Mesoscale Cellular Convection. *Journal of Climate*, **19 (9)**, 1748–1764, doi:10.1175/JCLI3702.1, URL https://doi.org/10.1175/JCLI3702.1, https://journals.ametsoc.org/jcli/article-pdf/19/9/1748/3803447/jcli3702_1.pdf.

Wood, R., T. L. Kubar, and D. L. Hartmann, 2009: Understanding the importance of microphysics and macrophysics for warm rain in marine low clouds. part II: Heuristic models of rain formation. *Journal of the Atmospheric Sciences*, **66 (10)**, 2973–2990, doi:10.1175/2009jas3072.1, URL https://doi.org/10.1175%2F2009jas3072.1.

Wyant, M. C., C. S. Bretherton, H. A. Rand, and D. E. Stevens, 1997: Numerical Simulations and a Conceptual Model of the Stratocumulus to Trade Cumulus Transition. *Journal of the Atmospheric Sciences*, **54 (1)**, 168–192, doi:10.1175/1520-0469(1997)054<0168:NSAACM>2.0.CO;2, URL https://doi.org/10.1175/1520-0469(1997)054<0168:NSAACM>2.0.CO;2, https://journals.ametsoc.org/jas/article-pdf/54/1/168/3429040/1520-0469(1997)054_0168_nsaacm_2_0_co_2.pdf.

Wyant, M. C., M. Khairoutdinov, and C. S. Bretherton, 2006: Climate sensitivity and cloud response of a gcm with a superparameterization. *Geophysical Research Letters*, **33 (6)**, doi:10.1029/2005GL025464, URL https://agupubs.onlinelibrary.wiley.com/doi/abs/10.1029/2005GL025464, https://agupubs.onlinelibrary.wiley.com/doi/pdf/10.1029/2005GL025464.

Yamaguchi, T., and G. Feingold, 2015: On the relationship between open cellular convective cloud patterns and the spatial distribution of precipitation. *Atmospheric Chemistry and Physics*, **15 (3)**, 1237–1251, doi:10.5194/acp-15-1237-2015, URL https://www.atmos-chem-phys.net/15/1237/2015/.

You, Y., G. W. Kattawar, P. Yang, Y. X. Hu, and B. A. Baum, 2006: Sensitivity of depolarized lidar signals to cloud and aerosol particle properties. *Journal of Quantitative Spectroscopy and Radiative Transfer*, **100 (1-3)**, 470–482, doi:10.1016/j.jqsrt.2005.11.058, URL https://doi.org/10.1016%2Fj.jqsrt.2005.11.058.

Zeng, X., 2018: Modeling the effect of radiation on warm rain initiation. *Journal of Geophysical Research: Atmospheres*, **123 (13)**, 6896–6906, doi:10.1029/2018jd028354, URL https://doi.org/10.1029%2F2018jd028354.

Zhang, G., and N. A. McFarlane, 1995: Sensitivity of climate simulations to the parameterization of cumulus convection in the canadian climate centre general circulation model. *Atmosphere-Ocean*, **33 (3)**, 407–446, doi:10.1080/07055900.1995.9649539, URL https://doi.org/10.1080%2F07055900.1995.9649539.

Zhao, M., 2014: An investigation of the connections among convection, clouds, and climate sensitivity in a global climate model. *Journal of Climate*, **27 (5)**, 1845–1862, doi:10.1175/JCLI-D-13-00145.1, URL https://doi.org/10.1175/JCLI-D-13-00145.1, https://doi.org/10.1175/JCLI-D-13-00145.1.

Zhou, X., P. Kollias, and E. R. Lewis, 2015: Clouds, precipitation, and marine boundary layer structure during the MAGIC field campaign. *Journal of Climate*, **28 (6)**, 2420–2442, doi:10.1175/jcli-d-14-00320.1, URL https://doi.org/10.1175%2Fjcli-d-14-00320.1.

Zuidema, P., and Coauthors, 2012: On trade wind cumulus cold pools. *Journal of the Atmospheric Sciences*, **69 (1)**, 258–280, doi:10.1175/jas-d-11-0143.1, URL https://doi.org/10.1175%2Fjas-d-11-0143.1.